

คอนฟอร์เมชัน พลังงานและการเกิดสารประกอบเชิงซ้อนระหว่างแอลคาไลแคตไอออนและกรดแอสปาร์ติก



นาย วิเชียร แสงอรุณ

สถาบันวิทยบริการ จุฬาลงกรณ์มหาวิทยาลัย

วิทยานิพนธ์นี้เป็นส่วนหนึ่งของการศึกษาตามหลักสูตรปริญญาวิทยาศาสตรดุษฎีบัณฑิต

สาขาวิชาเคมี ภาควิชาเคมี

คณะวิทยาศาสตร์ จุฬาลงกรณ์มหาวิทยาลัย

ปีการศึกษา 2550

ลิขสิทธิ์ของจุฬาลงกรณ์มหาวิทยาลัย

CONFORMATION, ENERGIES AND COMPLEXATION BETWEEN ALKALI CATIONS AND
ASPARTIC ACID




Mr. Wichien Sang-aroon

สถาบันวิทยบริการ
จุฬาลงกรณ์มหาวิทยาลัย

A Dissertation Submitted in Partial Fulfillment of the Requirements
for the Degree of Doctor of Philosophy Program in Chemistry
Department of Chemistry
Faculty of Science
Chulalongkorn University
Academic year 2007
Copyright of Chulalongkorn University


Thesis Title CONFORMATION, ENERGIES AND COMPLEXATION BETWEEN
ALKALI CATIONS AND ASPARTIC ACID
By Mr. Wichien Sang-aroon
Field of Study Chemistry
Thesis Advisor Associate Professor Vithaya Ruangpornvisuti, Dr.rer.nat.

Accepted by the Faculty of Science, Chulalongkorn University in Partial
Fulfillment of the Requirements for the Doctoral Degree


..... Dean of the Faculty of Science
(Professor Supot Hannongbua, Dr.rer.nat.)


THESIS COMMITTEE


.....Chairman
(Associate Professor Sirirat Kokpol, Ph.D.)


.....Thesis Advisor
(Associate Professor Vithaya Ruangpornvisuti, Dr.rer.nat.)


.....Member
(Professor Jumras Limtrakul, Dr.rer.nat.)


.....Member
(Associate Professor Nuanphun Chantarasiri, Ph.D.)


.....Member
(Associate Professor Tirayut Vilaivan, D.Phil.)


.....Member
(Assistant Professor Pornthep Sompornpisut, Ph.D.)

วิเชียร แสงอรุณ: คอนฟอร์เมชัน พลังงานและการเกิดสารประกอบเชิงซ้อนระหว่างแอลคาไลแคตไอออนและกรดแอสปาร์ติก (CONFORMATION, ENERGIES AND COMPLEXATION BETWEEN ALKALI CATIONS AND ASPARTIC ACID) อ. ที่ปรึกษา : รศ.ดร. วิทยา เรืองพรวิสุทธิ, 127 หน้า

งานวิจัยนี้ใช้การคำนวณแบบวิธีเคนซิติฟังก์ชันโดยแบ่งออกเป็นสามส่วน ส่วนแรกได้คำนวณคอนฟอร์เมชันในสถานะแก๊สของกรดแอสปาร์ติกสปีชีส์ต่างๆ ได้แก่ แคตไอออนิก ทวิตเตอร์ไอออนิก แอนไอออนิก และไดแอนไอออนิก ด้วยวิธีโพเทนเชียลเอนเนอร์จีเซอร์เฟซ ต่อมาได้คำนวณการเกิดสารประกอบเชิงซ้อนระหว่างแอลคาไลแคตไอออนและทวิตเตอร์ไอออนิก แอนไอออนิก และ ไดแอนไอออนิก สปีชีส์ ของกรดแอสปาร์ติก ค่าเมทอลไอออนแอฟฟินิตีของสารประกอบเชิงซ้อนคำนวณได้จากเอนทัลปีของปฏิกิริยาที่ 298.15 เคลวิน สุกท้าย ได้คำนวณค่าคงที่ความเป็นกรด pK_a ของกรดแอสปาร์ติกในสารละลายน้ำ โดยใช้แบบจำลอง PCM ในการคำนวณผลกระทบจากตัวทำละลาย

สถาบันวิทยบริการ
จุฬาลงกรณ์มหาวิทยาลัย

ภาควิชา.....เคมี.....ลายมือชื่อนิสิต.....
สาขาวิชา.....เคมี.....ลายมือชื่ออาจารย์ที่ปรึกษา.....
ปีการศึกษา.....2550.....

4573836023: MAJOR CHEMISTRY.

KEY WORD: ASPARTIC ACID/ POTENTIAL ENERGY SURFACE/ ACIDITY CONSTANT/ COMPLEXATION/ ALKALI METAL/ METAL ION AFFINITY/ DENSITY FUNCTIONAL THEORY

WICHIEEN SANG-AROON: CONFORMATION, ENERGIES AND COMPLEXATION BETWEEN ALKALI CATIONS AND ASPARTIC ACID. THESIS ADVISOR: ASSOC. PROF. VITHAYA RUANGPORNVISUTI, Dr.rer.nat., 127 pp.

This research work is separated into three parts employing density functional calculation. The first part, the gas phase conformations of various aspartic species including cationic (H_3asp^+), zwitterionic (H_2asp), zwitteranionic ($Hasp^-$) and dianionic (asp^{2-}) were explored using potential energy surface (PES) method. Secondly, the complexations between alkali cations; lithium, sodium and potassium and species H_2asp , $Hasp^-$ and asp^{2-} of aspartic acid were investigated. The metal ion affinities in term of reaction enthalpy obtained by vibrational frequency calculation at 298.15 K for all complexes are reported. Finally, acid-dissociation constants, pK_a of aspartic species in aqueous solution were determined using Polarize continuum model (PCM) as solvent-effect calculation.

สถาบันวิทยบริการ
จุฬาลงกรณ์มหาวิทยาลัย

DepartmentChemistry..... Student's signature *W. Sangroon*
Field of study.....Chemistry..... Advisor's signature *Vithaya Ruangpornvisuti*
Academic year..... 2007.....

ACKNOWLEDGEMENTS

The success of this dissertation can be attributed to the extensive support and assistance from my advisor, Assoc. Prof. Dr. Vithaya Ruangpornvisuti. He is never lacking of kindness and support. I deeply thank him for his valuable advice and guidance in this dissertation. In addition, I would like to thank Assoc. Prof. Dr. Sirirat Kokpol, Prof. Dr. Jumras Limtrakul, Assoc. Prof. Dr. Nuanphun Chuntarasiri, Assoc. Prof. Dr. Tirayut Vilaivan and Assist. Prof. Dr. Pornthep Sompornpisut for their valuable suggestion and comments as committee and thesis examiners.

I am very grateful to the Thailand Research Fund for financial support through the Royal Golden Jubilee (RGJ-Ph.D) scholarship. Because of this scholarship, I have got a great opportunity to do research at Laser Chemistry Laboratory, Department of Chemistry, The University of Adelaide, Australia. The people there made my first trip in abroad fully of impression. I would like to thank Assoc. Prof. Dr. Mark A. Buntine, my co-advisor for his suggestion. Special thank would be encourage to the people in the research groups, they are my good friends who take care of me and help me all the time I need when I was in Australia.

The lovely people in Computational Supramolecular Chemistry Research Unit are also being appreciated. Thanks for their spirit and support.

Finally, the big moment in my life that I have been waiting for can not be true without these people. My father, mother, younger brothers and younger sister, they always give me love, care, encouragement, spirit and other assistances throughout my life.

สถาบันวิทยบริการ
จุฬาลงกรณ์มหาวิทยาลัย

CONTENTS

	Page
Abstract in Thai	iv
Abstract in English	v
Acknowledgements	vi
List of Tables	x
List of Figures	xiii
List of Schemes	xvi
List of Abbreviation and symbols	xvii
CHAPTER I INTRODUCTION	1
1.1 Amino acid.....	1
1.1.1 General structure.....	1
1.1.2 Conformation of amino acid and peptide.....	2
1.1.3 Acid-base chemistry of amino acids.....	3
1.1.4 Metal complex of amino acids.....	4
1.2 Aspartic acid.....	4
1.3 Literature review.....	5
1.4 Objectives.....	6
CHAPTER II THEORETICAL METHOD	7
2.1 Introduction to quantum mechanics.....	7
2.2 Solution of the Schrödinger equation of molecular systems.....	7
2.2.1 The Schrödinger equation.....	7
2.2.2 Born-Oppenheimer approximation.....	8
2.2.3 The Hartree-Fock Method.....	9
2.2.4 Basis sets.....	11
2.2.4.1 Minimal basis sets.....	13
2.2.4.2 Scaled orbital by splitting the minimum basis set.....	13
2.2.4.3 Split valence basis sets.....	14
2.2.4.4 Polarized basis sets.....	14

2.2.4.5 Diffuse basis sets.....	15
2.3 Density functional theory (DFT).....	15
2.3.1 The Hohenberg-Khon theory.....	15
2.3.2 The Khon-Sham equation.....	16
2.3.3 DFT exchange and correlations.....	17
2.3.4 Hybrid functions.....	18
2.4 Potential energy surface (PES); minima and transition state.....	19
2.5 Rate constant.....	21
2.6 Thermochemistry.....	22
2.6.1 Partition functions.....	23
2.6.2 Thermodynamic properties.....	24
2.7 Chemical indices and Frontier orbital.....	25
2.8 Polarized continuum solvation model.....	26
2.9 Basis set super position error (BSSE).....	27
CHAPTER III DETAILS OF THE CALCULATIONS.....	29
3.1 Conformation of cationic, zwitterionic and anionic species of aspartic acid and their protonation.....	29
3.1.1 Definitions and Ramachandran map.....	29
3.1.2 Potential energy surface.....	31
3.2 Complexation between alkali cations and aspartic species.....	32
3.2.1 Geometry optimization.....	32
3.2.2 Metal ion affinity (MIA) and Deprotonation energy (DPE).....	32
3.3 Aqueous acid-dissociation constants (pK_a) of aspartic acid.....	33
3.3.1 Quantum chemical and PCM solvation model.....	33
3.3.2 Thermodynamic cycles and acid-dissociation models.....	34
CHAPTER IV RESULTS AND DISCUSSION	36
4.1 Conformation of cationic, zwitterionic and anionic species of aspartic acid and their protonation.....	36

4.1.1 PES of various forms of aspartic acid and their geometrical conformations.....	36
4.1.2 Water-added structures and their protonation.....	41
4.2 Complexation between alkali cations and aspartic species.....	43
4.2.1 Conformational analysis of alkali metal complexes of dianionic species of aspartic acid.....	43
4.2.1.1 Lithium complexes.....	44
4.2.1.2 Sodium complexes.....	47
4.2.1.3 Potassium complexes.....	47
4.2.1.4 Binding energies of aspartate complexes.....	48
4.2.2 Conformational analysis of alkali metal complexes of anionic species of aspartic acid.....	51
4.2.2.1 Lithium complexes.....	52
4.2.2.2 Sodium complexes.....	55
4.2.2.3 Potassium complexes.....	58
4.2.2.4 Comparative reactions of aspartate complexes.....	60
4.2.2.5 Binding mode and ion size effects.....	62
4.2.2.6 Reaction paths to form [Hasp-M] complexes.....	62
4.2.3 Conformational analysis of alkali metal complexes of zwitterionic species of aspartic acid.....	63
4.2.3.1 Lithium complexes.....	64
4.2.3.2 Sodium complexes.....	68
4.2.3.3 Potassium complexes.....	69
4.2.3.4 Comparative reactions of aspartate complexes.....	70
4.2.3.5 Relation between aspartic acid species and their complexes...	71
4.3 Aqueous acid-dissociation constants (pK_a) of aspartic acid.....	73
CHAPTER V CONCLUSIONS.....	79
REFERENCES.....	82
APPENDICES.....	88
APPENDIX A.....	89

APPENDIX B.....	122
VITA.....	127



สถาบันวิทยบริการ
จุฬาลงกรณ์มหาวิทยาลัย

LIST OF TABLES

Table	Page
4.1 The present hydrogen bonding, its type and distance for conformations of the aspartic acid H_3asp^+ species.....	38
4.2 The present hydrogen bonding, its type and distance for conformations of the aspartic acid H_2asp , $Hasp^-$ and asp^{2-} species...	39
4.3 B3LYP/6-31+G(d,p)-optimized conformations of various species of trihydrated and tetrahydrated forms of aspartic acid, their selected geometrical data and total energies.....	40
4.4 B3LYP/6-31+G(d,p)-optimized conformations of various species of aspartic acid in gas phase.....	40
4.5 Stabilization energies of protonation reaction of tri- and tetrahydrated forms of species asp^{2-} , $Hasp^-$ and H_2asp of aspartic acid.....	40
4.6 Relative B3LYP/6-311++G(d,p) energies and MIAs of minima for $[asp-M]^-$ and $[asp-M_2]$ complexes, $M=Li^+$, Na^+ , K^+	40
4.7 Pre-organization energies of aspartate dianion (asp^{2-}) in the formation reaction of the most stable $[asp-M]^-$ and $[asp-M_2]$ complexes.....	49
4.8 Thermodynamic quantities of the formation reaction of the most stable complex conformers for $[asp-M]^-$ and $[asp-M_2]$ complexes.....	49
4.9 The E_{HOMO} , E_{LUMO} and frontier molecular orbital energy gap, $\Delta E_{HOMO-LUMO}$ of free ligand, and various most stable complex conformers for $[asp-M]^-$ and $[asp-M_2]$ complexes.....	50
4.10 Bond distances of alkali metal cations and binding atoms of aspartate ions in the most stable complex conformers $[asp-M]^-$ and $[asp-M_2]$	50
4.11 Relative B3LYP/6-311++G(d,p) energies, MIAs and DPEs of minima for α - $[Hasp-Li]$ and β - $[Hasp-Li]$ complexes.....	54
4.12 Thermodynamic quantities, equilibrium and rate constants of conversion reactions of the $[Hasp-Li]$ complex systems.....	55

4.13	Relative B3LYP/6–311++G(d,p) energies, MIAs and DPEs of minima for α -[Hasp–Na] and β -[Hasp–Na] complexes.....	57
4.14	Thermodynamic quantities, equilibrium and rate constants of conversion reactions of the [Hasp–Na] complex systems.....	58
4.15	Relative B3LYP/6–311++G(d,p) energies, MIAs and DPEs of minima for α -[Hasp–K] and β -[Hasp–K] complexes.....	59
4.16	Thermodynamic quantities, equilibrium and rate constants of conversion reactions of the [Hasp–K] complex systems.....	60
4.17	Quantities for the formation reactions of the most stable conformers for [Hasp–M] complexes and pre–Organization for their aspartate structures.....	61
4.18	The frontier molecular orbital energy gap, $\Delta E_{\text{HOMO-LUMO}}$ and various chemical indices of cations, free ligand, and various most stable complex conformers for [Hasp–M] complexes.....	61
4.19	Bond distances of alkali metal cations and binding atoms of aspartate ions in the most stable conformers of [Hasp–M] complexes.....	62
4.20	Relative energies, MIAs and DPEs of the B3LYP/6–311++G(d,p)–optimized [H ₂ asp–M] ⁺ complex conformers.....	66
4.21	Quantities for the formation reactions of the most stable conformers of salt–bridge and charge–solvated structures for [H ₂ asp–M] ⁺ complexes, and pre–organization for their corresponding aspartic acid structures.....	71
4.22	Gibbs free energy contributions ΔG_{gas} , $\Delta\Delta G_{\text{solv}}$ and ΔG_{aq} (kcal/mol) for the acid dissociation equilibria of aspartic acid in gas phase.....	76
4.23	Gibbs free energy contributions ΔG_{gas} , $\Delta\Delta G_{\text{solv}}$ and ΔG_{aq} (kcal/mol) for the acid dissociation equilibria of aspartic acid of various water–cluster models in gas phase.....	77
4.24	Gibbs free energy contributions ΔG_{gas} , $\Delta\Delta G_{\text{solv}}$ and ΔG_{aq} (kcal/mol) for the acid dissociation equilibria of aspartic acid of bare structure of different water cluster models in gas phase.....	78

LIST OF FIGURES

Figure		Page
1.1	The general structure of amino acid.....	1
1.2	Dipeptide models used in calculations (a) <i>N</i> -acetyl- <i>Xxx-N'</i> -methylamide (b) <i>N</i> -formyl- <i>Xxx-N'</i> -acetamide, R represent side-chain of the amino acid.....	2
1.3	Acid-dissociation equilibria of amino acid.....	3
1.4	pH dependence of four typical species of aspartic acid in aqueous solution and protonation reversible	5
2.1	Potential energy surface describes energy of a molecule in terms of its structure. The minimum corresponds to an equilibrium structure first order saddle point corresponds to a transition state for a reaction a reaction path is the steepest descent path connecting a transition state to minima.	20
2.2	Energy profile E: Potential energy reaction coordinate for A and B via TS $[AB]^\ddagger$	21
2.3	Solvent accessible surface (SAS) traced out by the center of the probe representing a solvent molecule. The solvent excluded surface (SES) is the topological boundary of the union of all possible probes that do not overlap with the molecule.....	27
3.1	Definition of atomic numbering for H_3asp^+ as representative of aspartic acid and definition of dihedral angles ω (H1-O1-C1-C2), ψ (O1-C1-C2-N1), ϕ (H4-N1-C2-C1), χ_1 (N1-C2-C3-C4), χ_2 (C2-C3-C4-O3) and χ_3 (C3-C4-O3-H2).....	30
3.2	Aspartic acid species (a) $H_3asp^+_{-endo-E}$, (b) $H_3asp^+_{-endo-Z}$, (c) $H_3asp^+_{-exo-E}$, (d) $H_3asp^+_{-exo-Z}$, (e) H_2asp_{-endo} , (f) H_2asp_{-exo} , (g) $Hasp^-$ and (h) asp^{2-} species.....	30
3.3	A schematic representation of relation between a backbone (BB) conformation Ramachandran map (top) and a side-chain (SC) conformation map designated by IUPAC convention (bottom). The Ramachandran and IUPAC-SC conformation maps, defined as 'BB[SC]' conformational notation of aspartic acid.....	31

4.1	Classification of the types of internal hydrogen bonding for various species of aspartic acid.....	37
4.2	The B3LYP/6-31+G(d,p) optimized structures of the most stable conformers of four species of aspartic acid as (a) trihydrated and (b) tetrahydrated forms and their protonation scheme. The hydrogen bond distances are in Å.....	41
4.3	Superimpose pictures of the geometrical changes of the most stable conformers of species (a) asp^{2-} , (b) Hasp^- , (c) H_2asp and (d) H_3asp^+ . For clarity, water molecules are not displayed.....	42
4.4	The proposed possible sites for binding mode of interaction between cation and aspartate (asp^{2-}) moiety.....	43
4.5	The most stable conformer of (a) $[\text{asp}-\text{M}]^-$ and (b) $[\text{asp}-\text{M}_2]$ ($\text{M} = \text{Li}^+, \text{Na}^+, \text{K}^+$) complexes. Distances are in Å.....	45
4.6	Plot of complexation free energies of the (a) $[\text{asp}-\text{M}]^-$ (-□-□-□-) and (b) $[\text{asp}-\text{M}_2]$ (-○-○-○-) against sizes of the alkali metal ions M ($\text{M} = \text{Li}^+, \text{Na}^+$ and K^+).....	51
4.7	The possible binding modes of Hasp^- ligand toward cations.....	51
4.8	The most stable conformer of $[\text{Hasp}-\text{Li}]$, $[\text{Hasp}-\text{Na}]$ and $[\text{Hasp}-\text{K}]$ complexes. Distances are in Å.....	53
4.9	The reaction pathways for complexation and protonation of asp^{2-} species to form $[\text{Hasp}-\text{M}]$ complexes of (a) Lithium, (b) Sodium and (c) Potassium. Energies are in kcal/mol.....	63
4.10	The possible binding modes of H_2asp ligand toward cations.....	63
4.11	The most stable conformer of (a) SB and (b) CS structures of $[\text{H}_2\text{asp}-\text{M}]^+$ ($\text{M} = \text{Li}^+, \text{Na}^+, \text{K}^+$) complexes. Distances are in Å.....	65
4.12	The MIAs of H_2asp for the complexation of $[\text{H}_2\text{asp}-\text{M}]^+$, $\text{M} =$ lithium (▲-▲-▲), sodium (●-●-●) and potassium (■-■-■) against binding mode.....	67
4.13	The MIAs of various species of aspartic acid of lithium (▲-▲-▲), sodium (●-●-●) and potassium (■-■-■) against charge of their species.....	70

- 4.14 The reaction pathways for complexation and protonation of asp^{2-} and Hasp^- species to form $[\text{H}_2\text{asp-M}]^+$ complexes of (a) lithium (b) sodium and (c) potassium. Energies are in kcal/mol..... 72
- 4.15 Superimposition of the B3LYP/6-31+G(d,p)-optimized structures of various states of the most stable species of aspartic acid as forms: (a) H_3asp^+ (b) H_2asp (c) Hasp^- (d) asp^{2-} 73
- 4.16 The acid-dissociation equilibria of aspartic acid in gas phase presented as the bare structures and (b) hexahydrated species..... 74
- 4.17 Acid-dissociation equilibria of aspartic acid based on their (a) tri- (b) tetra- (c) penta- (d) hexahydrated structures..... 75



สถาบันวิทยบริการ
จุฬาลงกรณ์มหาวิทยาลัย

LIST OF SCHEMES

Scheme		Page
3.1	Acid–dissociation equilibria of aspartic acid.....	35
3.2	Thermodynamic cycle for calculation of theoretical pK_a of bare– structure of aspartic acid.....	35
3.3	Thermodynamic cycle for calculation of theoretical pK_a of n – hydrated structure of aspartic acid.....	35



สถาบันวิทยบริการ
จุฬาลงกรณ์มหาวิทยาลัย

LIST OF ABBRIVIVATIONS

Å	Angstrom
a	Anti
ΔG_{aq}	Aqueous Gibbs free energy
pK_a	Association constant
B3LYP	Beck 3 Lee–Yang–Parr
BSSE	Basis set super position error
CPCM	Conductor–like Polarized continuum model
CS	Charge–solvated
η	Chemical hardness
μ	Chemical potential
χ	Chi
DFT	Density functional theory
DPE	Deprotonation energy
E	Energy
H	Enthalpy
q	Geometric parameter
G	Gibbs free energy
g^+	Gauche ⁺
g^-	Gauche ⁻
\hat{H}	Hamiltonian operator
HF	Hartree–Fock
HOMO	Highest occupied molecular orbital
IEFPCM	Integral equation formalism Polarized continuum model
Kcal/mol	Kilocalorie per mole
LUMO	Lowest unoccupied molecular orbital
MIA	Metal ion affinity
χ	Mulliken electronegativity
ω	omega
Q	Partition function
PCM	Polarized continuum model
PES	Potential energy surface
ϕ	phi

ψ	psi
SB	Salt-bridge
TS	Transition state
ψ	Wave function
ZPE	Zero point energy



สถาบันวิทยบริการ
จุฬาลงกรณ์มหาวิทยาลัย

CHAPTER I

INTRODUCTION

1.1 Amino acids

1.1.1 General structure

Alpha-amino acids are the building blocks of proteins. A protein forms via the condensation of amino acids to form a chain of amino acid "residues" linked by peptide bonds. [1] Proteins are defined by their unique sequence of amino acid residues; this sequence is the primary structure of the protein. Amino acids can be linked in varying sequences to form a huge variety of proteins. Twenty standard amino acids are used by cells in protein biosynthesis, and these are specified by the general genetic code. These 20 amino acids are biosynthesized from other molecules, but organisms differ in which ones they can synthesize and which ones must be provided in their diet. The ones that cannot be synthesized by an organism are called essential amino acids.

As can be seen in Figure 1.1, R represents a side chain specific to each amino acid. The central carbon atom, called C_{α} , is a chiral central carbon atom (with the exception of glycine) to which the two termini and the R-group are attached. Amino acids are usually classified by the properties of the side chain into four groups. The side chain can make them behave like a weak acid, a weak base, a hydrophile if they are polar, and hydrophobe if they are nonpolar.

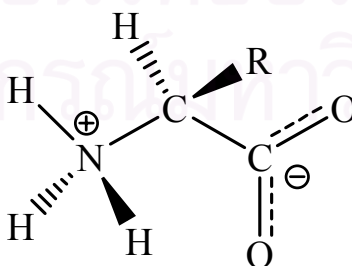


Figure 1.1 The general structure of amino acid.

As amino acids have both a primary amine group and a primary carboxyl group, these chemicals can undergo most of the reactions associated with these functional groups. These include nucleophilic addition, amide bond formation and imine formation for the amine group and esterification, amide bond formation and decarboxylation for the carboxylic acid group. The multiple side chains of amino acids can also undergo chemical reactions. The types of these reactions are determined by the groups on these side chains and are discussed in the articles dealing with each specific type of amino acid.

1.1.2 Conformation of amino acid and peptide

Protein folding has received intense study due to its fundamental importance in living organisms. The growing availability of protein sequences and increasing recognition are a result of misfolded proteins. Dipeptide models are increasingly used in peptide folding studies as they represent the smallest possible structural unit for the study of typical triamide conformations, such as β -turns, in protein folding. [2] The most popular models used in calculations are *N*-acetyl-*Xxx*-*N'*-methylamide or *N*-formyl-*Xxx*-*N'*-acetamide where *Xxx* is amino acid as shown in Figure 1.2. The conformations of peptide are defined by Ramachandran map [3,4], the details about the Ramachandran map are discussed in Chapter III.

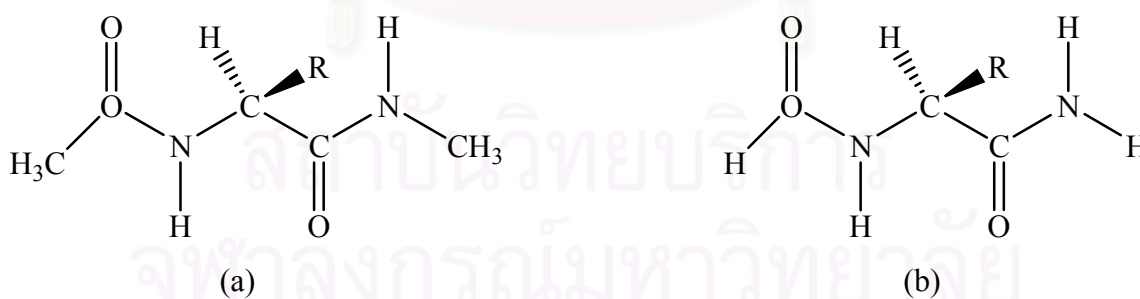


Figure 1.2 Dipeptide models used in calculations (a) *N*-acetyl-*Xxx*-*N'*-methylamide (b) *N*-formyl-*Xxx*-*N'*-acetamide, R represent side-chain of the amino acid.

1.1.3 Acid–base chemistry of amino acids

As amino acids have both the active groups of an amine and a carboxylic acid they can be considered both acid and base (though their natural pH is usually influenced by the R group). At a certain pH known as the isoelectric point, the amine group gains a positive charge (is protonated) and the acid group a negative charge (is deprotonated) as shown in Figure 1.3. The exact value is specific to each different amino acid. Like typical acidic compound, the acid strength of both amino and carboxylate groups are defined as association constants, K_a or the well-known form pK_a . This phenomenon can be observed by the titration method combined with potentiometry, NMR and UV spectroscopy. [5]

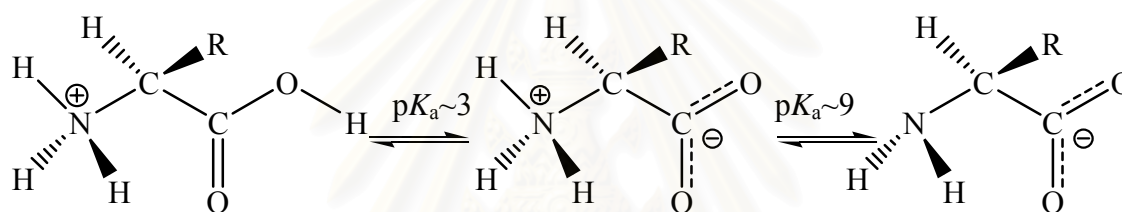


Figure 1.3 Acid–dissociation equilibria of amino acid.

Depending on the polarity of the side chain, amino acids vary in their hydrophilic or hydrophobic character. These properties are important in protein structure and protein–protein interactions. The importance of the physical properties of the side chains comes from the influence this has on the amino acid residues' interactions with other structures, both within a single protein and between proteins. The distribution of hydrophilic and hydrophobic amino acids determines the tertiary structure of the protein, and their physical location on the outside structure of the proteins influences their quaternary structure. For example, soluble proteins have surfaces rich with polar amino acids like serine and threonine, while integral membrane proteins tend to have outer ring of hydrophobic amino acids that anchors them into the lipid bilayer, and proteins anchored to the membrane have a hydrophobic end that locks into the membrane. Similarly, proteins that have to bind to positively-charged molecules have surfaces rich with negatively charged amino acids like glutamate and aspartate, while proteins binding to

negatively-charged molecules have surfaces rich with positively charged chains like lysine and arginine.

1.1.4 Metal complex of amino acids

The metalation of amino acids, peptides and nucleic acids plays a crucial role in several phenomena. In particular, alkali metal cations; lithium, sodium and potassium have been found in biological systems. The cations interact with proteins and peptide to control the structure and regulate the properties [6–8], transport process through trans-membrane channel. [9,10] The cations can bind to a variety of sites on peptides, including the amino nitrogen at the *N*-terminus and the carbonyl oxygen atom at the *C*-terminus as well as the binding atoms on the side chain of amino acids. The coordination modes of metal ions greatly influence their binding energies and to some extent their site of attachment to a ligand. Some cations have a strong preference for a particular coordination mode, while others can adopt different coordination geometries. These coordination preferences could play a significant role in the biological functions of metal-containing enzymes. The metal-specific binding sites of some proteins achieve their selectivity by providing a coordination environment preferred by only one metal ion naturally found in living system. The fact that a variety of metals can bind easily to peptides has been exploited in the field of mass spectrometry, where metal ions such as Li^+ , Na^+ , Cu^+ and Ag^+ have been used as ionizing agents for peptide sequencing. [11–13] Exploring the nature of these metal-ion peptide interactions will not only provide information on their binding energies to a class of biologically important molecules, but will also extremely useful in the interpretation of mass spectra of such complexes obtained either under metastable or via collision-induced dissociation conditions.

1.2 Aspartic acid

Aspartic acid (abbreviated as **Asp** or **D**) is an α -amino acid with the chemical formula $\text{NH}_2\text{CH}(\text{CH}_2\text{COOH})\text{COOH}$. Aspartic acid is non-essential in mammals, being produced from oxaloacetate by transamination. In plants and microorganisms, aspartic

acid is the precursor to several amino acids, including four that are essential: methionine, threonine, isoleucine, and lysine. The conversion of aspartic acid to these other amino acids begins with reduction of aspartic acid to its "semialdehyde," $\text{NH}_2\text{CH}(\text{CH}_2\text{COH})\text{COOH}$. Aspartic acid is also a metabolite in the urea cycle and participates in gluconeogenesis. Aspartic acid donates one nitrogen atom in the biosynthesis of inositol, the precursor to the purine bases. Aspartate (the conjugate base of aspartic acid) stimulates NMDA receptors, though not as strongly as the amino acid neurotransmitter glutamate does. It serves as an excitatory neurotransmitter in the brain and is an excitotoxin.

Aspartic acid is classified as polyprotic acid. The chemical formula is $\text{NH}_2\text{CH}(\text{CH}_2\text{COOH})\text{COOH}$. In equilibrium, cationic, zwitterionic, zwitter-anionic and dianionic species of aspartic acid were presented at the wide pH range of acidic to basic aqueous solution. [14,15] The structure of the four ionic species and corresponding acid-dissociation constants of aspartic acid are shown in Figure 1.4.

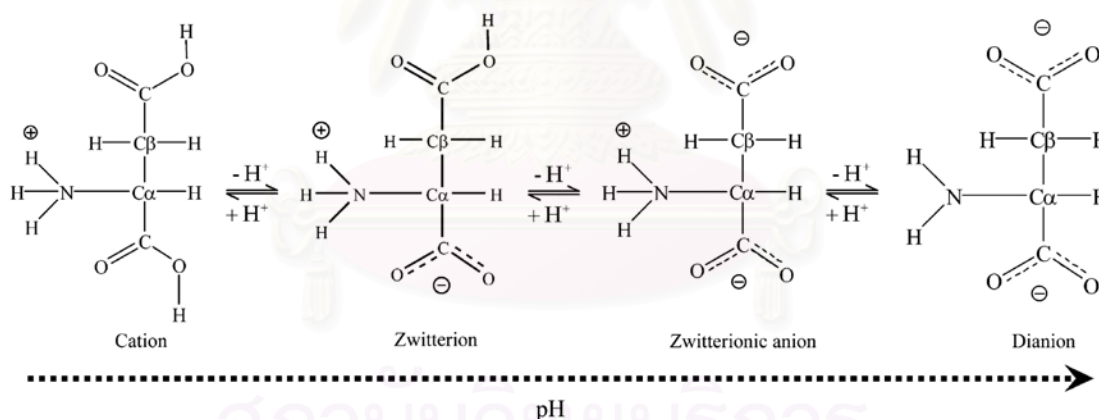


Figure 1.4 pH dependence of four typical species of aspartic acid in aqueous solution and protonation reversible mechanism.

1.3 Literature reviews

The experimental acid-dissociation constants $\text{p}K_{\text{a}1} = 2.10$, $\text{p}K_{\text{a}2} = 3.86$, $\text{p}K_{\text{a}3} = 9.82$ obtained by potentiometric titration method and $\text{p}K_{\text{a}1} = 2.00$, $\text{p}K_{\text{a}2} = 3.90$, $\text{p}K_{\text{a}3} = 9.80$ obtained by NMR titration method. [16,17]

The lithium and sodium affinities of aspartic acid have been experimentally determined using mass spectrometry with kinetic method. [18–20] The vanadium (III) complexes of various species of aspartic acid in a wide pH range have been determined using UV-Vis spectrometry. [21] The single crystal structures of zinc (II), nickel (II) and copper (II) complexes of aspartate (asp^{2-}) have also been solved. [22–24] The results show that aspartate ligand forms tri-coordinate structure with zinc or nickel ions using three binding atoms; amino-N, α - and β -carbonyl-O, respectively. Bi-coordinate structure is found for copper complex which aspartate ligand use only amino-N and α -carbonyl-O bind with the cation.

The conformations of dipeptide models of aspartic acid, *N*-acetyl-aspartic-*N'*-methylamide and *N*-formyl-aspartic-*N'*-acidamide have been studied using density functional theory and γ_L conformation is found to be the most stable form of aspartic acid in both peptide models. [25,26]

1.4 Objectives

This research is focused on three topics based on density functional calculation. Firstly, the gas phase conformations of various aspartic species including cationic (H_3asp^+), zwitterionic (H_2asp), zwitteranionic (Hasp^-) and dianionic (asp^{2-}) are explored using potential energy surface (PES) method. Secondly, the complexations between alkali cations; lithium, sodium and potassium and species asp^{2-} , Hasp^- , H_2asp of aspartic acid are investigated. Finally, acid-dissociation constants, $\text{p}K_a$ of aspartic species in aqueous solution are determined using Polarizable continuum model (PCM) as solvent-effect calculation.

CHAPTER II

THEORETICAL METHOD

2.1 Introduction to quantum mechanics

The word quantum comes from Latin and first used by Max Plank in 1900 to denote the constrained quantities or amounts in which energy can be emitted or adsorbed. “Mechanics” as used in Physics is traditionally the study of the behavior of bodies under the action of forces. The Term “quantum mechanics” is apparently first used by Born (the Born-Oppenheimer approximation) in 1924. Because of molecules are consisted of nuclei and electrons, quantum chemistry deals with the motion of electron under the influence of the electromagnetic force exerted by nuclear charges. An understanding of the behavior of electrons in molecules, structures and reactions of molecules, rest on quantum mechanics and in particular on the adornment of quantum chemistry, the Schrödinger equation. [27]

2.2 Solution of the Schrödinger equation of molecular systems

2.2.1 The Schrödinger equation

The ultimate goal of most quantum chemical approaches is the approximate solution of the time-independent, non-relativistic Schrödinger equation:

$$\hat{H}\Psi_i(\vec{x}_1, \vec{x}_2, \dots, \vec{x}_N, \vec{R}_1, \vec{R}_2, \dots, \vec{R}_M) = E\Psi_i(\vec{x}_1, \vec{x}_2, \dots, \vec{x}_N, \vec{R}_1, \vec{R}_2, \dots, \vec{R}_M) \quad 2.1$$

where \hat{H} is the Hamiltonian operator for a molecular system consisting of M nuclei and N electrons in the absence of magnetic or electric fields. \hat{H} is a differential operator representing the total energy:

$$\hat{H} = -\frac{1}{2} \sum_{i=1}^N \nabla_i^2 - \frac{1}{2} \sum_{A=1}^M \frac{1}{M_A} \nabla_A^2 - \sum_{i=1}^N \sum_{A=1}^M \frac{Z_A}{r_{iA}} + \sum_{i=1}^N \sum_{j>1}^N \frac{1}{r_{ij}} + \sum_{A=1}^M \sum_{B>A}^M \frac{Z_A Z_B}{R_{AB}} \quad 2.2$$

Here, A and B run over the M nuclei while i and j denote the N electrons in the systems. The first two terms describe the kinetic energy of the electrons and nuclei respectively, where the Laplacian operator ∇^2 is defined as a sum of differential operator (in Cartesian coordinates)

MA is the mass of nucleus A in multiples of mass of an electron. The remaining three terms define the potential parts of the Hamiltonian and represent the attractive electrostatic interaction between the nuclei and electrons and the repulsive potential due to the electron-electron and nucleus-nucleus interactions, respectively. R_{pq} (and similarly R_{qp}) is the distance between the particles p and q , i.e. $r_{pq} = |\vec{r}_p - \vec{r}_q|$. $\psi_i(\vec{x}_1, \vec{x}_2, \dots, \vec{x}_N, \vec{R}_1, \vec{R}_2, \dots, \vec{R}_M)$ stands for the wave function of the i^{th} state of the system, which depends on the $3N$ spatial coordinates $\{\vec{r}_i\}$, and the N spin coordinates $\{S_i\}$ of electrons, which are collectively termed $\{\vec{x}_i\}$, and the $3M$ spatial coordinates of the nuclei $\{\vec{R}_i\}$. The wavefunction Ψ_i contains all information that can be possibly known about the quantum system at hand. Finally, E_i is the numerical value of the energy of the state described by Ψ_i .

All equations given in this text appear in a very compact form, without any fundamental physical constants. We achieve this by employing the so-called system of atomic units, which is particularly adapted for working with the atoms and molecules. In this system, physical quantities are expressed as multiples of fundamental constants and if necessary, as combinations of such constants. The mass of an electron, m_e , the modulus of its charge, $|e|$, Planck's constants h divided by 2π , \hbar , and 4π , ϵ_0 , the permittivity of the vacuum, are all set to unity. Mass, charge, action etc. are then expressed as multiples of these constants, which can therefore be dropped from all equations. [27]

2.2.2 Born-Oppenheimer approximation

The Schrödinger equation can be further simplified if we take advantage of the significant difference between the masses of nuclei and electrons. Even the lightest nuclei, proton (^1H), weight roughly 1800 times more than an electron. Thus, the nuclei move much more slower than the electrons. The practical consequence is that we can at least

to a good approximation take the extreme point of view and consider the electrons as moving in the field of fixed nuclei. This is the famous *Born-Oppenheimer* or clamped nuclei approximation. If the nuclei fixed in space and do not move, their kinetic energies are zero and the potential energy due to nucleus-nucleus repulsion is merely a constant. Thus, the complete Hamiltonian give in equation 2.4 reduces to the so-called electronic Hamiltonian:

$$\hat{H}_{elec} = \frac{1}{2} \sum_{i=1}^n \nabla_i^2 - \sum_{i=1}^n \sum_{A=1}^K \frac{Z_A}{r_{iA}} + \sum_{i=1}^n \sum_{j>1}^n \frac{1}{r_{ij}} \quad 2.4$$

The solution of the Schrödinger equation with \hat{H}_{elec} is the electronic wavefunction Ψ_{elec} and the electronic energy E_{elec} . Ψ_{elec} depends on the electron coordinates, while the nuclear coordinates enter only parametrically and do not explicitly appear in Ψ_{elec} . The total energy E_{total} is then the sum of E_{elec} and the constant nuclear repulsion term:

$$E_{nuc} = \sum_{A=1}^K \sum_{B>A}^M \frac{Z_A Z_B}{r_{AB}} \quad 2.5$$

and

$$\hat{H}_{elec} \Psi_{elec} = E_{elec} \Psi_{elec} \quad 2.6$$

then

$$E_{total} = E_{lec} + E_{nuc} \quad 2.7$$

The attractive potential exerted on the electrons due to the nuclei-the expectation value of the second operator \hat{V}_{N_e} in the equation 2.4 is the often termed the external potential, V_{ext} , in the density functional theory, even though the external potential is not necessarily limited to the nuclear field but may include external magnetic or electric field etc. From now on we will only consider the electronic problem of equation 2.4-2.6 and the subscript “elec” will be dropped. [28]

2.2.3 The Hartree-Fock Method

The Hartree-Fock Method seeks to approximately solve the electronic Schrödinger equation, and it assumes that the wavefunction can be approximated by a single Slater determinant made up of one spin orbital per electron. Since the energy expression is

symmetric, the variation theorem holds, and so we know that the Slater determinant with the lowest energy is as close as we can get to the true wavefunction for the assumed functional form of the single determinant. The Hartree-Fock equation determines the set of spin orbitals which minimize the energy and gives us this best single determinant. So, we need to minimize the Hartree-Fock energy expression with respect to changes in the orbitals:

$$\chi_i \rightarrow \chi_i + \delta\chi_i \quad 2.8$$

We have also been assuming that the orbitals are orthonormal, and we want to ensure that our variation procedure leaves them orthonormal. The Hartree-Fock equation can be solved numerically (exact Hartree-Fock), or they can be solved in the space spanned by a set of basis set functions (Hartree-Fock-Roothaan equation). In either case, note that the solution depends on the orbitals. Hence, we need to guess some initial orbitals and then refine our guess iteratively. For this reason, Hartree-Fock is called *self-consistent-field* (SCF) approach.

The first term above in the square brackets:

$$\sum_{j \neq i} \left[\int dx_2 |\chi_j(x_2)|^2 r_{12}^{-1} \right] \chi_i(x_1) \quad 2.9$$

gives the Coulomb interaction of an electron in spin orbital χ_i with the average charge distribution of the other electrons. Here we see in what sense Hartree-Fock is a mean field theory. This is called *Coulomb* term and it is convenient to define a Coulomb operator as:

$$J_j(x_1) = \int dx_2 |\chi_j(x_2)|^2 r_{12}^{-1} \quad 2.10$$

this gives the average local potential point x_1 due to the charge distribution from the electron in orbital χ_j . We can define an exchange operator in terms of its action on an arbitrary spin orbital χ_i :

$$K_j(x_1)\chi_i(x_1) = \left[\int dx_2 \chi_j^*(x_2) r_{12}^{-1} \chi_i(x_2) \right] \chi_j(x_1) \quad 2.11$$

Introducing a basis set transforms the Hartree-Fock equation into the Roothaan equation. Denoting the atomic orbital basis functions as $\bar{\chi}$, we have the expression:

$$\chi_i = \sum_{\mu=1}^K c_{\mu i} \bar{\chi}_{\mu} \quad 2.12$$

for each spin orbital i . This leads to:

$$f(x_1) \sum_v c_{vi} \tilde{\chi}(x_1) = \epsilon_i \sum_v c_{vi} \tilde{\chi}(x_1) \quad 2.13$$

This can be simplified by introducing the matrix element notation:

$$S_{\mu\nu} = \int dx_1 \bar{\chi}_\mu^*(x_1) \bar{\chi}_\nu(x_1) \quad 2.14$$

$$F_{\mu\nu} = \int dx_1 \bar{\chi}_\nu^*(x_1) \bar{\chi}_\mu(x_1) \quad 2.15$$

Now the Hartree-Fock-Roothaan equation can be written in matrix form as:

$$\sum_v F_{\mu\nu} C_{vi} = \epsilon_i \sum_v S_{\mu\nu} C_{vi} \quad 2.16$$

or even more simply as matrices:

$$\mathbf{FC} = \mathbf{SC}\epsilon \quad 2.17$$

where ϵ is a diagonal matrix of orbital energies ϵ_i . This is like an eigenvalue equation except for the overlap matrix S . One performs a transformation of basis to go to an orthogonal basis to make S vanish. Then it's just a matter of solving an eigenvalue equation well, not quite. Since F depends on it's own solution (through the orbitals), the process must be done iteratively. This is why the solution of Hartree-Fock-Roothaan equation is often called the self-consistent-field procedure.

2.2.4 Basis sets

The approximate treatment of electron-electron distribution and motion assigns individual electron to one-electron function, termed *spin orbital*. These consist of product of spatial functions, termed *molecular orbitals (MO)*, $\psi_1(x,y,z)$, $\psi_2(x,y,z)$, $\psi_3(x,y,z)$,....and either α or β spin components. The spin orbitals are allowed complete freedom to spread throughout the molecule. Their exact forms are determined to minimize the total energy. In the simplest level of theory, a single assignment of electron to orbital is made by used ψ as atomic orbital wavefunction based on the Schrödinger equation for the hydrogen atom. This is not a suitable approach for molecular calculation. This problem can be solved by representing *MO* as linear combination of basis functions.

In practical calculation, the molecular orbitals $\psi_1, \psi_2, \dots, \psi_N$ are further restricted to be linear combinations of a set of N known one-electron function $\phi_1(x,y,z), \phi_2(x,y,z), \phi_3(x,y,z), \dots, \phi_N(x,y,z)$:

$$\psi_i = \sum_{\mu=1}^N c_{\mu i} \phi_{\mu} \quad 2.18$$

The functions $\phi_1, \phi_2, \dots, \phi_N$ which are defined in the specification of the model, are known as one-electron basis function called basis function. The set of basis function is called basis set. If the basis functions are the atomic orbitals for the atoms making up the molecule, function in equation 2.18 is often described as linear combination of atomic orbitals (LCAO). There are two types of basis function which commonly used in the electronic structure calculations, *Slater type orbitals* (STO) and *Gaussian type orbitals* (GTO).

The Slater orbitals are primarily used for atomic and diatomic systems where high accuracy is required and semi empirical calculations where all three- and four-center integrals are neglected. The Slater type orbitals have the function form:

$$b = A e^{-\zeta r} r^{n^*-1} Y_{lm}(\theta, \phi) \quad 2.19$$

Where parameter n^* and ζ are chosen to make the larger part of the orbitals look like atomic Hartree-Fock orbitals. There are a lot like hydrogen orbitals, but without the complicated nodal structure.

The Gaussian type orbitals can be written in terms of polar or cartesian coordinates:

$$g = x^a y^b z^c e^{-\alpha r^2} Y_{lm}(\theta, \phi) \quad 2.20$$

in which a, b, c are integers and α is a parameter that is usually fixed. Primitive Gaussian function is shown in equation 2.20. Normally, several of these Gaussian functions are summed to defined more realistic atomic orbital basis functions, as shown below:

$$b_{\mu} = \sum_p k_{\mu p} g_p \quad 2.21$$

The coefficient $k_{\mu p}$ in this expression are chosen to make the basis functions look as much like Slater orbitals as possible. Slater functions are good approximation to atomic wavefunctions but required excessive computer time more than Gaussian functions, while single-Gaussian functions are poor approximation to nearly ideal description of an atomic

wavefunction that Slater function provides. The solution to the problem of this poor functional behavior is to use several Gaussians to approximate a Slater function. In the simplest version of this basis, n Gaussian functions are superimposed with fixed coefficients to form Slater type orbital. Such a basis is denoted STO- n G, and $n = 3, 4$.

The limit of quantum mechanics involves an infinite set of basis function. This is clearly impractical since the computational expense of molecular orbital calculations is proportional to the power of the total number of basis functions. Therefore, ultimate choice of basis set size demands on a compromise between accuracy and efficiency. The classification of basis sets is given below.

2.2.4.1 Minimal basis sets

The minimum basis set is a selected basis function for every atomic orbital that is required to describe the free atom. For Hydrogen atom, the minimum basis set is just one 1s orbital. But for carbon atom, the minimum basis set consists of a 1s, 2s and the full set of three 2p orbitals. For example, the minimum basis set for the methane molecule consists of 4 1s orbitals, one per hydrogen atom, and the set of 1s, 2s and 2p orbitals described above for carbon. Thus, total set comprises of 9 basis functions.

Several minimum basis sets are used as common basis sets especially the STO- n G basis sets because they are available for almost all elements in the periodic table. The most common of basis sets is STO-3G, where a linear combination of three Gaussian type orbitals (GTOs) is fitted to Slater type orbital (STO). The individual GTOs are called primitive orbitals, while the combined functions are called contracted functions. For example, the STO-3G basis set for methane consists of total of 9 contracted functions built from 27 primitive functions.

2.2.4.2 Scaled orbital by splitting the minimum basis set

In the early calculation on the hydrogen molecule, it is discovered that STO 1s orbitals do not give the best result in the molecular environment when the Schrödinger equation is solved, because electron is attracted to both nuclei rather than just one nucleus.

In each molecular orbital, both large and small sets of orbital appear and they are mixed in the ratio that gives the lowest energy. The combination of a large orbital and a small orbital is essentially equivalent to an orbital of intermediate size. The result orbital is a size that best fit for the molecular environment since it is obtained from minimizing the energy. The advantage of this procedure is that the mixing coefficients in the molecular orbitals appear in a linear function. The simplest dodge is equivalent to scaling the single minimal basis set orbitals. The minimum basis set can scaled not only the valence orbitals of the minimal basis set (split valence basis set) but also all the orbitals of the minimal basis set (double zeta basis sets).

2.2.4.3 Split valence basis sets

A split valence basis sets uses a number of different sizes of basis functions per atomic orbital. They effectively account for change in size of atomic orbitals (but not the shape) to fit the molecular structures. The 6–31G basis set is an example of a double split valence basis set which uses 6 *primitive* Gaussians to form the basis function of the core orbitals. The 31 in 6–31G indicates the outer valence orbitals are split into two sets of basis functions, where 3 *primitive* Gaussians form basis function of more inner valence orbitals and 1 *primitive* Gaussian form basis function of the outermost orbitals. The alterations in the sizes of the outer orbitals in split valence basis sets allow for accurate descriptions of bonding interactions within the molecular structures.

2.2.4.4 Polarized basis sets

Polarization functions are used to describe a change in shape of atomic orbitals. They do this by adding orbitals with angular momentum to particular atoms depending on the set of polarization functions assigned. An example of this is 6–31G(d) (also denoted as 6–31G*), where the *d* orbital function are added to the 2nd row atoms such as carbon or oxygen, which contain only *p* orbitals. The 6–31G(d,p) basis sets (or 6–31G**) goes a step further by adding *p* orbital functions to the hydrogen atoms. This function tends to yield a greater accuracy of electron density and bonding interactions.

2.2.4.5 Diffuse basis sets

Species with significant electron density far from removed from the nuclear centers *e.g.* anions, lone pairs and excited states require diffuse functions to account for the outermost weaker bound electrons. Diffuse basis sets are recommended for calculations of electron affinities, proton affinities, inversion barriers and bond angle in anions. The addition of diffuse *s*- and *p*-type Gaussian functions to non-hydrogen atoms is denoted by plus sign-as 6-31+G. Further addition of diffuse functions to both hydrogen and larger atoms is indicated by a double plus. [28,29]

2.3 Density functional theory (DFT)

2.3.1. The Hohenberg–Khon theory

Within a Born–Oppenheimer approximation, the ground state of the system is a result of the position of the nuclei. In quantum mechanic Hamiltonian equation, the kinetic energy (\hat{T}_e) and the electron–electron interaction (\hat{V}_{ee}) adjust themselves to the external potential (\hat{V}_{ext}) to obtain the lowest total energy. Thus, the external potential can be uniquely determined from the knowledge of the electron density. The Hohenberg–Khon theory states that if *N* interacting electrons move in an external potential V_{ext} , the ground state electron density $\rho_0(r)$ minimizes the functional

$$E[\rho] = F[\rho] + \int \rho(r)V_{ext}(r)dr \quad 2.22$$

In equation 2.7, $F[\rho]$ is a universal functional of $\rho_0(r)$ and the minimum value of the functional E is E_0 , the exact ground state electronic energy.

$$\hat{F} = \hat{T}_e + \hat{V}_{ee} = \sum_i -\frac{1}{2}\nabla_i^2 + \sum_{i \neq j} \frac{1}{|r_i - r_j|} \quad 2.23$$

and the density can be obtained by using the variation principle.

2.3.2. The Khon–Sham (KS) equation

Khon and Sham introduced a method based on the Hohenberg–Khon theorem that allows one to minimize the functional $E[n(\mathbf{r})]$ by varying $\rho(\mathbf{r})$ over all densities containing N electrons. They derives the couple set of differential equations enabling the ground state density $\rho_0(\mathbf{r})$ to be found. Khon and Sham separated $F[\rho(\mathbf{r})]$ in the equation 2.7 into three distinct parts. The functional E becomes

$$E[\rho(\mathbf{r})] = T_s[\rho(\mathbf{r})] + \frac{1}{2} \iint \frac{\rho(\mathbf{r})\rho(\mathbf{r}')}{|\mathbf{r} - \mathbf{r}'|} d\mathbf{r}d\mathbf{r}' + E_{XC}[\rho(\mathbf{r})] + \int \mathbf{r}(\mathbf{r})V_{ext}(\mathbf{r})d\mathbf{r} \quad 2.24$$

Where $T_s[\rho(\mathbf{r})]$ is defined as the kinetic energy of a non–interacting electron gas with density $\rho(\mathbf{r})$,

$$T_s[\rho(\mathbf{r})] = -\frac{1}{2} \sum_i \int \psi_i^*(\mathbf{r}) \nabla^2 \psi_i(\mathbf{r}) d\mathbf{r} \quad 2.25$$

and $E_{XC}[\rho(\mathbf{r})]$ is the exchange–correlation energy functional. Introducing a normalization constraint on the electron density, $\int \rho(\mathbf{r})d\mathbf{r} = N$ by the Lagrange’s method of undetermined multiplier can obtain

$$\delta \{ E[\rho(\mathbf{r})] - \mu \left[\int \rho(\mathbf{r})d\mathbf{r} - N \right] \} = 0 \quad 2.26$$

where μ is an undetermined Lagrange multiplier. The number of electron in the system is constant so $\delta N = 0$. Then equation 2.11 is reduced to

$$\delta E[\rho(\mathbf{r})] - \mu \delta \left(\int \rho(\mathbf{r})d\mathbf{r} \right) = 0 \quad 2.27$$

Using the definition of the differential of the functional $\delta F = \int \frac{\delta F}{\delta f(x)} \delta f(x) dx$ is the fact

that the differential and the integral signs can be interchanged,

$$\int \frac{\delta E[\rho(\mathbf{r})]}{\delta \rho(\mathbf{r})} \delta \rho(\mathbf{r}) d\mathbf{r} - \mu \int \delta \rho(\mathbf{r}) d\mathbf{r} = 0 \quad 2.28$$

$$\int \left\{ \frac{\delta E[\rho(\mathbf{r})]}{\delta \rho(\mathbf{r})} - \mu \right\} \delta \rho(\mathbf{r}) d\mathbf{r} = 0 \quad 2.29$$

$$\frac{\delta E[\rho(\mathbf{r})]}{\delta \rho(\mathbf{r})} = \mu$$

Equation 2.14 can now be written in terms of an effective potential, $V_{eff}(\mathbf{r})$,

$$\frac{\delta T_s[\rho(r)]}{\delta \rho(r)} + V_{eff}(r) = \mu \quad 2.30$$

where

$$V_{eff}(r) = V_{ext}(r) + \int \frac{\rho(r')}{|r-r'|} dr' + V_{XC}(r) \quad 2.31$$

and

$$V_{XC}(r) = \frac{\delta E_{XC}[\rho(r)]}{\delta \rho(r)} \quad 2.32$$

To find the ground state energy, $E_0(r)$, and the ground state density, $\rho_0(r)$, the one electron Schrödinger equation

$$\left(-\frac{1}{2} \nabla_i^2 + V_{eff}(r) \right) \phi_i(r) = \varepsilon_i \phi_i(r) \quad 2.33$$

should be solved self-consistently with

$$r(r) = \sum_{i=1}^N |\phi_i(r)|^2 \quad 2.34$$

similar to the SCF procedure in the Hartree-Fock method. Then the density $\rho(r)$ can be solved iteratively. A self-consistent solution is required due to the dependence of $V_{eff}(r)$ on $\rho(r)$.

2.3.3 DFT exchange and correlations

The form of E_{XC} is generally unknown and its exact value has been calculated only for a few very simple systems. In the density functional theory, the exchange energy is defined as

$$E_x[\rho] = \left\langle \phi[\rho] \left| \hat{V}_{ee} \right| \phi[\rho] \right\rangle - U[\rho] \quad 2.35$$

when $U[\rho]$ is the Hartree piece of the columbic potential. The correlation term is defined as the remaining unknown piece of the energy:

$$E_c[\rho] = F[\rho] - T_s[\rho] - U[\rho] - E_x[\rho] \quad 2.36$$

Due to the definition of $F[\rho]$, the correlation energy consists of two separate contributions:

$$E_c[\rho] = T_c[\rho] + U[\rho] \quad 2.37$$

When $T_c[\rho]$ and $U_c[\rho]$ are respectively the kinetic contribution and the potential contribution of the correlation energy.

In electronic structure calculations, E_{XC} is the most commonly approximation within the local density approximation or generalized–gradient approximation. In the local density approximation (LDA), the value of $E_{XC}[\rho(r)]$ is approximated by exchange–correlation energy of an electron in homogeneous electron gas of the same density $\rho(r)$, *i.e.*

$$E_{XC}^{LDA}[\rho(r)] = \int \epsilon_{XC}(\rho(r))\rho(r)dr \quad 2.38$$

The most accurate data for $\epsilon_{XC}(\rho(r))$ is calculated from Quantum Monte Carlo calculation. For the systems with slowly varying charge densities, this approximation generally gives very good results. An obvious approach to improve the LDA, so called generalized gradient approximation (GGA), is to include gradient corrections by making E_{XC} a function of the density and its gradient as shown below

$$E_{XC}^{GGA}[\rho(r)] = \int \epsilon_{XC}(\rho(r))\rho(r)dr + \int F_{XC}[\rho(r), |\nabla\rho(r)|]dr \quad 2.39$$

where F_{XC} is a correction chosen to satisfy one or several known limits for E_{XC} . Clearly, there is no unique equation for the F_{XC} , and several functions have been proposed. The development of the improved functions is currently a very active area of research although incremental improvements are likely. It is ambiguous whether the research will be successful in providing the substantial increase in accuracy that is desired.

2.3.4 Hybrid functions

From the Hamiltonian equation and the definition of the exchange–correlation energy, an exact connection can be made between the E_{XC} and the corresponding potential connecting with the non–interacting reference and the actual system. The resulting equation is called the Adiabatic Connection Formula (ACF) and involves an integration over the parameter λ which turns on the electron–electron interaction

$$E_{XC} = \int_0^1 \langle \psi_\lambda | V_{XC}(\lambda) | \psi_\lambda \rangle d\lambda \quad 2.40$$

In the $\lambda=0$ limit, the electrons are non-interacting and there is consequently no correlation. Since the KS wave function is simply the single Slater determinant of orbitals and the KS orbitals are identical to the HF orbitals, the exact exchange energy is precisely the HF exchange energy:

$$E_X[\phi_i; \lambda = 0] = -\frac{1}{2} \sum_{\sigma} \sum_{i,j} \int d^3r \int d^3r' \frac{\phi_{i\sigma}^*(r) \phi_{j\sigma}(r') \phi_{i\sigma}^*(r') \phi_{j\sigma}(r)}{|r - r'|} = E_X^{exact} \quad 2.41$$

The approximation of the exchange–correlation can be made by summing E_{XC} terms of different values of λ within the limitation $\lambda = 0$ to 1. The choice of terms is arbitrary. The approximation of the exchange–correlation can be made by summing E_{XC} terms of different values of λ within the limitation $\lambda = 0$ to 1. The choice of terms is arbitrary. Hybrid functions include the mixture of Hartree–Fock exchange with DFT exchange–correlation.

B3LYP function uses Becke’s exchange functional with a part of the mixed Hartree–Fock exchange and a scaling factor on the correlation part but using the LYP correlation function. The exchange–correlation energy has the form of

$$AE_X^{Slater} + (1 - A)E_X^{HF} + B\Delta E_X^{Beck} + (1 - C)E_C^{VWN} + CE_C^{LYP} \quad 2.42$$

where the exchange includes the Slater exchange E_X^{Slater} , or local spin density exchange, along with correlations involving the gradient of the density and the correlation is provided by the LYP and VWN correlations. The constants A, B and C are determined by fitting to the G1 molecule set. The values of the three parameters are determined by fitting to the 56 atomization energies, 42 ionization potentials, 8 proton affinities, and 10 first–row atomic energies in the G1 molecule set, computing values of $A=0.80$, $B=0.72$ and $C=0.81$. [27-29]

2.4 Potential energy surface (PES); minima and transition state

The Potential energy surface (PES) is a central concept in computational chemistry. A PES is the relationship–mathematical or graphical–between the energy of a molecule and its geometry. Stationary points on a PES are points where $\frac{\partial E}{\partial q} = 0$ for all q , where q is a

geometric parameter. The stationary points of chemical interest are minima $\frac{\partial^2 E}{\partial q_i \partial q_j} > 0$ for

all q and transition states or first order–saddle point; $\frac{\partial^2 E}{\partial q_i \partial q_j} > 0$ for one q along the reaction

coordinate (IRC), and > 0 for all other q . chemistry is the study of PES stationary points and the pathways connecting them as shown in Figure 2.1.

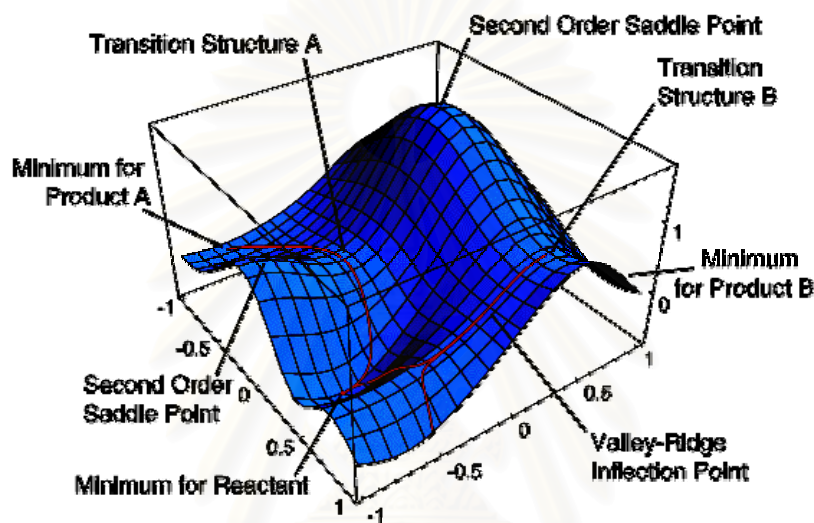


Figure 2.1 Potential energy surface describes energy of a molecule in terms of its structure. The minimum corresponds to an equilibrium structure first order saddle point corresponds to a transition state for a reaction a reaction path is the steepest descent path connecting a transition state to minima.

Geometry optimizations is the process of starting with an input structure “guess” and finding a stationary point on the PES. The stationary point found will normally be the one closet to the input structure, not necessarily the global minimum. A transition state optimization usually requires a special algorithm, since it is more demanding than that required to find a minimum. Modern optimization algorithms use analytic first derivatives and second derivatives. It is usually wise to check that a stationary points ids the desired species (a minimum or a transition state) by calculating its vibrational spectrum (its normal mode vibrations). The algorithm for this work by calculating Hessian (force constant matrix) and diagonalizing it to give a matrix with the “direction vectors” of the

normal modes, and a diagonal matrix with the force constants of these modes. A procedure of “mass weighting” the force constants gives the normal-mode vibrational frequencies. For a real minimum all the vibrational are real, while a transition state has one imaginary vibration, corresponding to the motion along the reaction coordinate. The criteria for transition state are appearance, the present of one imaginary frequency corresponding to the reaction coordinate, and energy above that of the reactant and the product. Besides serving to characterize the stationary point, calculation of vibrational frequencies enables one to predict IR spectrum and provides the zero point energy (ZPE). [30]

2.5 Rate constant

An activated complex AB^\ddagger or transition state is formed at the potential energy maximum as shown in Figure 2.2. The high-energy complex represents an unstable molecular arrangement, in which bonds break and form to generate the product AB or to degenerate back to the reactants A and B as shown in equation 2.28. In the simple form of transition state theory, it is supposed that the transition state (TS) is in equilibrium with the reactants, and that its abundance in the reaction mixture can be expressed in terms of an equilibrium constants, which is normally denoted K :

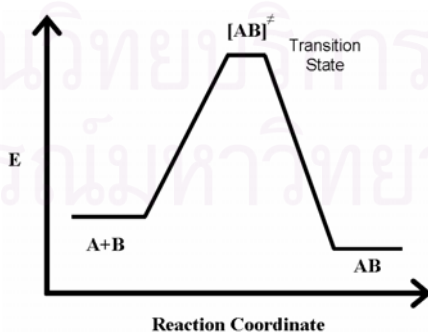


Figure 2.2 Energy profile E: Potential energy reaction coordinate for A and B via TS $[AB]^\ddagger$.

Then, if we supposed that the rate at which products are formed is proportional to the concentration of the TS, we can write

$$\text{Rate of formation of products} = k[\text{TS}]$$

we see that the rate constant k is proportional to the equilibrium constants K^\ddagger for the formation of the TS. We have already seen that an equilibrium constant may be expressed in terms of the standard reaction Gibbs energy, which in this case is the activation Gibbs energy, $\Delta^\ddagger G$, for the formation of the TS from the reactants. It follows from the equation 2.28 that

$$K = e^{-\Delta^\ddagger G / RT} \quad 2.44$$

Furthermore $\Delta^\ddagger G$ is given by

$$\Delta^\ddagger G = \Delta^\ddagger H - T\Delta^\ddagger S \quad 2.45$$

Combining equation 2.29 and the equation 2.30 and solving for $\ln k$ yields

$$\ln K = \frac{-\Delta^\ddagger H}{RT} + \frac{-\Delta^\ddagger S}{R} \quad 2.46$$

The *Eyring equation*: is found by substituting equation 2.31 into equation 2.29

$$k = \frac{k_B T}{h} e^{-\frac{\Delta^\ddagger H}{RT}} e^{\frac{\Delta^\ddagger S}{R}} \quad \text{or} \quad k = \frac{k_B T}{h} e^{-\frac{\Delta^\ddagger G}{RT}} \quad 2.47$$

2.6 Thermochemistry

The term energy in chemistry can mean potential energy, enthalpy, or Gibbs energy. The potential energy on a computed Born-Oppenheimer surface represents 0K enthalpy difference without ZPE. Enthalpy difference ΔH and free energy difference ΔG are related through the entropy difference:

$$\Delta G = \Delta H - T \Delta S \quad 2.48$$

To get an intuitive feel for ΔH , ΔG and ΔS we can regard it as essentially measure of the reaction enthalpy between product and reactant:

$$\Delta H = H_{\text{product}} - H_{\text{reactant}} \quad 2.49$$

$$\Delta G = G_{\text{product}} - G_{\text{reactant}} \quad 2.50$$

$$\Delta S = S_{\text{product}} - S_{\text{reactant}} \quad 2.51$$

2.6.1 Partition functions

The first step in determining the thermal contributions to the enthalpies and entropies of a molecule is to determine its partition function, Q which is a measure of the number of accessible states to the molecule (translational, rotational, vibrational and electronic states) at a particular temperature.

When given the energies E_i of the available quantum states of a molecule, Q is defined as:

$$Q = \sum_{i=1}^{\infty} g_i e^{-\beta E_i} \quad 2.52$$

Where g_i is the degeneracy of the i^{th} state and $\beta = \frac{1}{k_B T}$

Where k_B is Boltzmann's constant and T is the temperature of interest. The summation in Equation 2.37 is over all possible quantum states of the system.

It is assumed that the translational (T), rotational (R), vibrational (V) and electronic (E) modes of the system can be separated, thus allowing the energy of each level, E_i , to be separated into T , R , V and E contributions as

$$E = E_i^T + E_i^R + E_i^V + E_i^E \quad 2.53$$

While the translational modes are truly independent from the rest, the separations of other modes are based on an approximation, in particular the Born-Oppenheimer approximation for electronic and vibrational motion and the rigid rotor approximation which assumes (that the geometry of the molecule does not change as it rotates) for vibrational and rotational modes. Within these approximations, the total molecular partition function can therefore be factorized into translational, rotational, vibrational and electronic contributions:

$$Q = Q^T Q^R Q^V Q^E \quad 2.54$$

The translational partition function is given by:

$$Q^T = \frac{V}{\Lambda^3} \quad 2.55$$

$$\Lambda = h \left(\frac{\beta}{2\pi m} \right)^{1/2} \quad 2.56$$

Where h is Planck's constants, m is the mass of the molecule and V is the available volume to it. For a gas phase system this is the molar volume (usually determined by the ideal gas equation) at the specific temperature and pressure.

The formulation for rotational partition functions depends on whether or not the molecule is linear. For linear molecules

$$Q^R = \frac{k_B T}{\sigma h c B} \quad 2.57$$

and for non linear

$$Q^R = \frac{1}{\sigma} \left(\frac{k_B T}{hc} \right)^{3/2} \left(\frac{\pi}{ABC} \right)^{1/2} \quad 2.58$$

Where σ is the rotational symmetry number of the molecule, c is the speed of light and A , B , C are the rotational constants. The vibrational partition function in the harmonic approximation is

$$Q^V = \prod_i \frac{1}{1 - e^{-\beta h c \tilde{\nu}_i}} \quad 2.59$$

Where $\tilde{\nu}$ is the harmonic vibrational frequencies (expressed as wave numbers) and the product is taken over all ($3N-6$ or $3N-5$) vibrational modes (excluding the reaction coordinate for transition states). For the electronic partition function it is usually assumed that there is no thermal excitation into the higher electronic states. Then the partition function, Q^E , is simply given by the degeneracy of the appropriate electronic state.

2.6.2 Thermodynamic properties

The thermal contributions to thermodynamic properties such as enthalpy, entropy, free energy, heat capacity, etc. are all derived from the molecular partition functions. For a system of N molecules the internal energy (relative to energy at 0 K) is given by

$$U_T^0 - U_0^0 = -N \left(\frac{\partial \ln Q}{\partial \beta} \right) \quad 2.60$$

where the derivative is taken at constant volume. The enthalpy is therefore

$$H_T^0 - H_0^0 = (U_T^0 - U_0^0) + p\Delta V \quad 2.61$$

$$= (U_T^0 - U_0^0) + Nk_B T \quad 2.62$$

The entropy of system is given by

$$S^0 = \frac{(U_T^0 - U_0^0)}{T} + Nk_B \ln Q \quad 2.63$$

Then the change in Gibbs free energy is

$$G_T^0 - G_0^0 = (H_T^0 - H_0^0) - TS^0 \quad 2.64$$

$$= Nk_B T - Nk_B T \ln Q \quad 2.65$$

The Gibbs free energy change for a reaction is, of course, related to the equilibrium constant for the reaction:

$$\Delta_r G^0 = -Nk_B T \ln K_{eq} \quad 2.66$$

2.7 Chemical indices and Frontier orbital

The Mulliken electronegativity (χ), chemical hardness (η) and electronic chemical potential (μ) for compound were computed using orbital energies of the highest occupied molecular orbital (HOMO) and the lowest unoccupied molecular orbital (LUMO). The chemical hardness, electronic chemical potential and Mulliken electronegativity were derived from the first ionization potential (I) and electron affinity (A) of the N -electron molecular system with a total energy (E) and external potential $v(\vec{r})$ using the relations

$$\chi = (\partial E / \partial N)v(\vec{r}) = -\mu \cong 1/2(I + A) \quad 2.67$$

$$\eta = (\partial E / \partial N^2)v(\vec{r}) \cong 1/2(I - A) \quad 2.68$$

and the first ionization potential and electron affinity are $I=E(N-1)-E(N)$ and $A=E(N)-E(N+1)$. [31] According to the Koopmans theorem, I and A were computed from the HOMO and LUMO energies using the relations: $I=-E_{\text{HOMO}}$ and $A=-E_{\text{LUMO}}$.

2.8 Polarized continuum solvation model

The Polarizable Continuum Model (PCM) by Tomasi and coworkers is one of the most frequently used continuum solvation methods and has seen numerous variations

over the years. The PCM model (Figure 2.3) calculates the molecular free energy in solution as the sum over three terms

$$G_{\text{sol}} = G_{\text{es}} + G_{\text{dr}} + G_{\text{cav}} \quad 2.69$$

These components represent the electrostatic (es) and the dispersion–repulsion (dr) contributions to the free energy, and the cavitation energy (cav). All three terms are calculated using a cavity defined through interlocking *van der Waals*–spheres centered at atomic positions. The reaction field is represented through point charges located on the surface of the molecular cavity (Apparent Surface Charge (ASC) model). The particular version of PCM that will be discussed here is the one using the United Atom for Hartree–Fock (UAHF) model to build the cavity. In this model the vdW–surface is constructed from spheres located on heavy (that is, non–hydrogen) elements only (United Atom approach). The vdW–radius of each atoms is a function of atom type, connectivity, overall charge of the molecule, and the number of attached hydrogen atoms. In evaluating the three terms in equation 2.69 this cavity is used in slightly different ways. While calculation of the cavitation energy G_{cav} uses the surface defined by the van der Waals–spheres, the solvent accessible surface is used to calculate the dispersion–repulsion contribution G_{dr} to the solution free energy. The latter differs from the former through additional consideration of the (idealized) solvent radius. The electrostatic contribution to the free energy in solution G_{es} uses an approximate version of the solvent excluding surface constructed through scaling all radii by a constant factor e.g. 1.2 for water and then adding some more spheres not centered on atoms in order to arrive at a somewhat smoother surface. Localization and calculation of the surface charges is approached through systematic division of the spherical surface in small regions (tesserae) of known area and calculation of one point charge per surface element. [32]

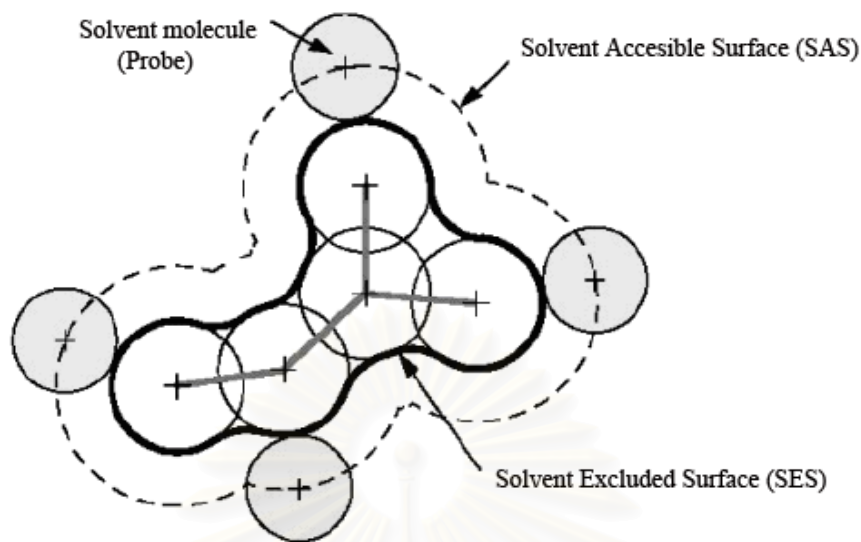


Figure 2.3 Solvent accessible surface (SAS) traced out by the center of the probe representing a solvent molecule. The solvent excluded surface (SES) is the topological boundary of the union of all possible probes that do not overlap with the molecule.

2.9 Basis set super position error (BSSE)

A consequence of using finite atom-centered basis sets in calculations of interaction energies including covalent bonding, hydrogen bonding and van der Waals interactions is the presence of basis set super position error. This is the phenomenon whereby, given an interacting system AB , the moiety A can be stabilized by the nearby presence of the basis functions belonging to the moiety B (in addition to any true interaction between A and B) and vice versa. This is because these additional basis functions compensate for the incompleteness of A 's own basis, thus improving the description of A and lowering its energy. Thus the system is not only stabilized by any true interactions between A and B but also by this superposition effect.

An estimate of the magnitude of this effect (and hence a possible correction involves for it) can be obtained by the counterpoise method of Boys and Bernadi. This involves calculating the energy of each moiety (atom or fragment) of both with its own basis functions, E_A , E_B and in the presence of the basis functions of the entire system $E_{A[B]}$, $E_{[A]B}$ the counterpoise corrections for A and B are given by

$$\Delta E_A^{CP} = A_{A[B]} - E_A \quad 2.70$$

$$\Delta E_B^{CP} = A_{[A]B} - E_B \quad 2.71$$

The sum of these counterpoise corrections, $\Delta E_A^{CP} + \Delta E_B^{CP}$, therefore represents the total correction to the interaction energy and then the counterpoise corrected interaction energy is give by

$$\Delta E_{AB}^{corrected} = E_A + E_B - E_{AB} + \Delta E_A^{CP} + \Delta E_B^{CP} \quad 2.72$$

It should be noted that $E_{A[B]}$ and $E_{[A]B}$ and are evaluated at the geometry optimization for AB that the geometry is used to calculate E_{AB} . If A and/ B are molecular fragments, these geometries can be different from their equilibrium geometries (those used to calculate E_A and E_B), this can be a potential source of inaccuracy in $\Delta E_A^{CP} + \Delta E_B^{CP}$. This is a further highlight of the approximate nature of the counterpoise correction. [30]

CHAPTER III

DETAILS OF THE CALCULATIONS

All computations were performed with the GAUSSIAN 03 program. [33] The molecular graphics of all molecular structures were generated with the MOLEKEL 4.3 program. [34] There are three area studied in this work. Details of each area are presented below:

3.1 Conformation of cationic, zwitterionic and anionic species of aspartic acid and their protonation

3.1.1 Definitions and Ramachandran map

Definition of atomic numbering for H_3asp^+ as representation of aspartic acid and definition of dihedral angles ω (H1–O1–C1–C2), ψ (O1–C1–C2–N1), ϕ (H4–N1–C2–C1), χ_1 (N1–C2–C3–C4), χ_2 (C2–C3–C4–O3) and χ_3 (C3–C4–O3–H2) are shown in Figure 3.1. The dihedral angles χ_3 and ω were obtained from full optimizations and χ_3 is used to indicate the *endo* and *exo* conformational types of carboxylic group; the *endo* and *exo* forms are defined as $\chi_3=0$ and 180° , respectively. *E* and *Z* isomerism of the dihedral angle ω was applied for conformational nomenclature. Due to the *endo/exo* and *E/Z* definitions, all aspartic acid structures of various forms can be categorized into species $\text{H}_3\text{asp}^+ \text{-endo-E}$, (b) $\text{H}_3\text{asp}^+ \text{-endo-Z}$, (c) $\text{H}_3\text{asp}^+ \text{-exo-E}$, (d) $\text{H}_3\text{asp}^+ \text{-exo-Z}$, (e) $\text{H}_2\text{asp-endo}$, (f) $\text{H}_2\text{asp-exo}$, (g) Hasp^- and (h) asp^{2-} as shown in Figure 3.2.

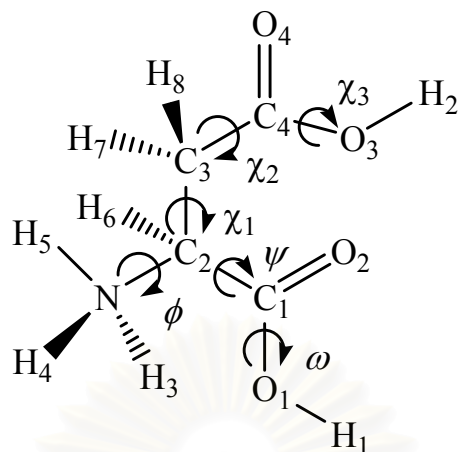


Figure 3.1 Definition of atomic numbering for H_3asp^+ as representative of aspartic acid and definition of dihedral angles ω (H1-O1-C1-C2), ψ (O1-C1-C2-N1), ϕ (H4-N1-C2-C1), χ_1 (N1-C2-C3-C4), χ_2 (C2-C3-C4-O3) and χ_3 (C3-C4-O3-H2).

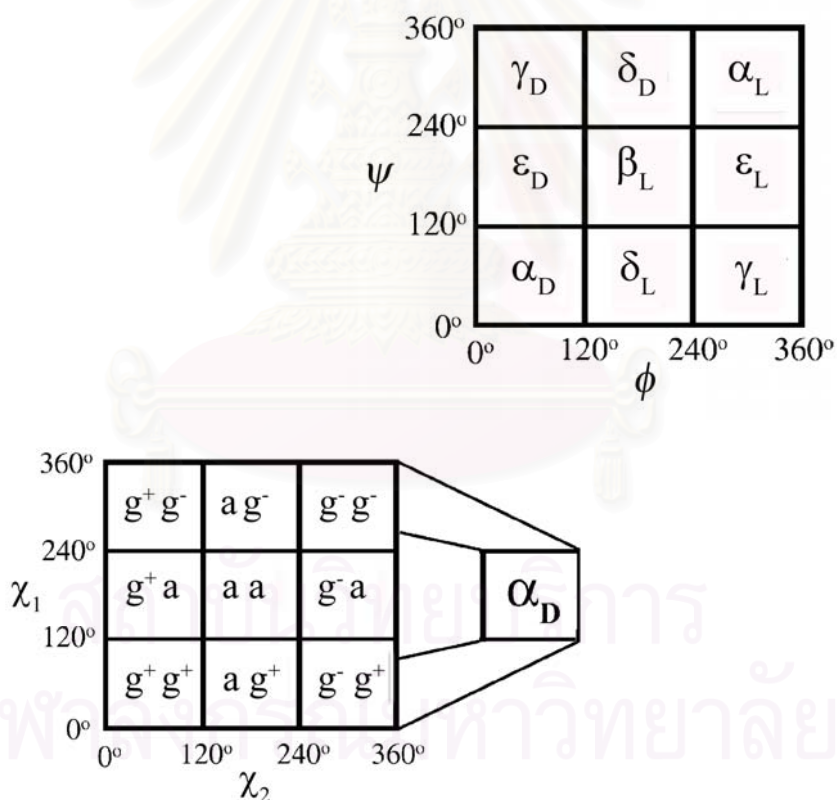


Figure 3.2 Aspartic acid species (a) H_3asp^+ -endo-E, (b) H_3asp^+ -endo-Z, (c) H_3asp^+ -exo-E, (d) H_3asp^+ -exo-Z, (e) H_2asp -endo, (f) H_2asp -exo, (g) Hasp^- and (h) asp^{2-} species.

All geometric minima for each species of aspartic acid on the conformational PES are represented by Ramachandran and IUPAC maps as shown in Figure 3.3. To combine the conformational convention and each species of aspartic acid, its full name has been therefore specified as ‘species type–endo/exo–Z/E’ of ‘BB [SC]’ such as conformer of H_3asp^+ –endo–Z of γ_{D} [$g^+ g^-$]. Energies for each structural conformers of H_3asp^+ and H_2asp species are therefore the functions of $E(\psi, \phi, \chi_1, \chi_2, \omega)$ and $E(\psi, \phi, \chi_1, \chi_2, \chi_3)$, respectively. For the anionic species of Hasp^- and asp^{2-} , their energies are a function of $E(\psi, \phi, \chi_1, \chi_2)$.

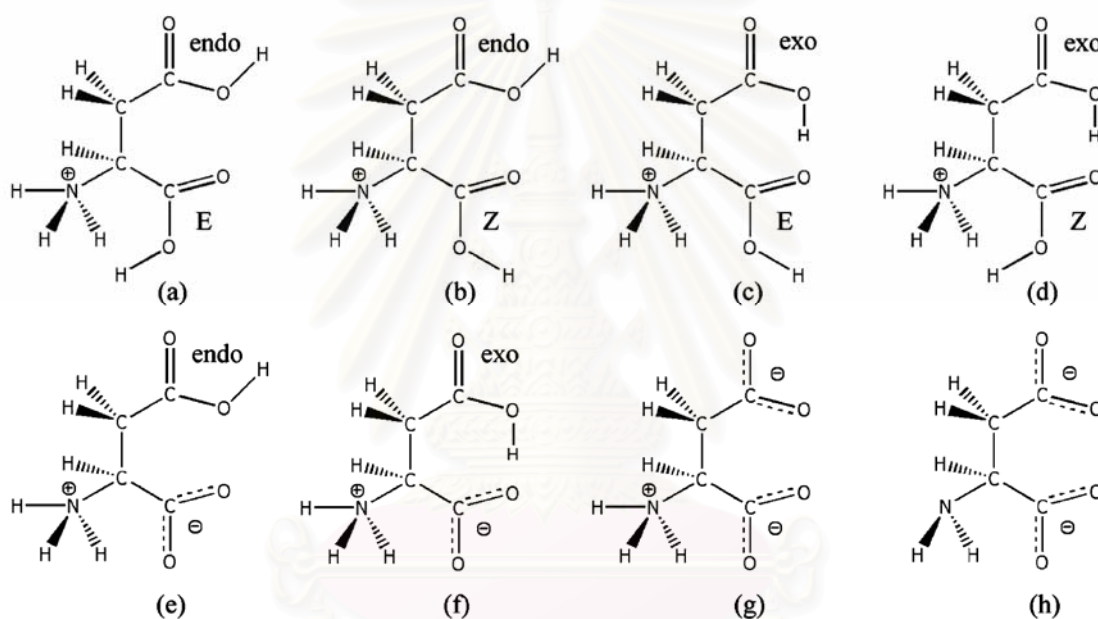


Figure 3.3 A schematic representation of relation between a backbone (BB) conformation Ramachandran map (top) and a side-chain (SC) conformation map designated by IUPAC convention (bottom). The Ramachandran and IUPAC–SC conformation maps, defined as ‘BB[SC]’ conformational notation of aspartic acid.

3.1.2 Potential energy surface

The PESs of all species (H_3asp^+ –endo–E, H_3asp^+ –endo–Z, H_3asp^+ –exo–E, H_3asp^+ –exo–Z, H_2asp –endo, H_2asp –exo, Hasp^- and asp^{2-}) of aspartic acid were computed with 30° increments along four dihedral angles ($\psi, \phi, \chi_1, \chi_2$) using the hybrid density functional theory (DFT) at B3LYP/6–31G(d) level of theory. [35,36]

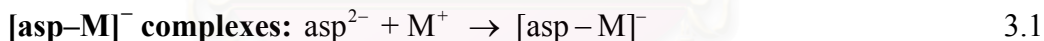
3.2 Complexation between alkali cations and aspartic acid species

3.2.1 Geometry optimization

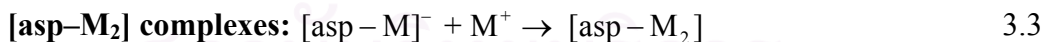
The geometry optimizations of $[\text{asp}-\text{M}]^-$, $[\text{asp}-\text{M}_2]$, $[\text{Hasp}-\text{M}]$ and $[\text{H}_2\text{asp}-\text{M}]^+$ complexes ($\text{M} = \text{Li}^+$, Na^+ and K^+) were carried out using density function theory (DFT). The DFT computations have been performed with Becke's three parameters hybrid density functional using the Lee, Yang and Parr correlation functional (B3LYP). [35,36] The B3LYP/6-311++G(d,p) level of theory has been employed for all geometry optimizations and their thermodynamic properties were derived from the vibrational frequency computations at the same level. Counterpoise corrections were applied for energy improvement by eliminating the basis set superposition error (BSSE) [37,38] for the most stable complex conformers.

3.2.2 Metal ion affinities (MIAs) and Deprotonation energies (DPEs)

As metal ion affinity (MIA) is defined as the negative of the reaction enthalpy (ΔH°), the MIA for the complexations of $[\text{asp}-\text{M}]^-$, $[\text{asp}-\text{M}_2]$, $[\text{Hasp}-\text{M}]$ and $[\text{H}_2\text{asp}-\text{M}]^+$ described by following equations:



$$\text{MIA}(1) = -[H^\circ_{[\text{asp}-\text{M}]^-} - (H^\circ_{\text{asp}^{2-}} + H^\circ_{\text{M}^+})] \quad 3.2$$

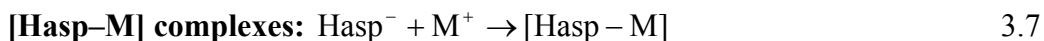


$$\text{MIA}(2) = -[H^\circ_{[\text{asp}-\text{M}_2]} - (H^\circ_{[\text{asp}-\text{M}]^-} + H^\circ_{\text{M}^+})] \quad 3.4$$

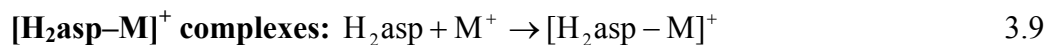
As different complexes, $[\text{asp}-\text{M}_{(p)}]^-$ and $[\text{asp}-\text{M}_{(q)}]^-$ defined as the components based on the binding mode types p and q, the two possible MAI(2)s can therefore be evaluated from the following formulas:

$$\text{MIA}(2)_p = -[H^\circ_{[\text{asp}-\text{M}_2]} - (H^\circ_{[\text{asp}-\text{M}_{(p)}]^-} + H^\circ_{\text{M}^+_{(q)}})] \quad 3.5$$

$$\text{MIA}(2)_q = -[H^\circ_{[\text{asp}-\text{M}_2]} - (H^\circ_{[\text{asp}-\text{M}_{(q)}]^-} + H^\circ_{\text{M}^+_{(p)}})] \quad 3.6$$



$$\text{MIA} = -[H^\circ_{[\text{Hasp-M}]} - (H^\circ_{\text{Hasp}^-} + H^\circ_{\text{M}^+})] \quad 3.8$$



$$\text{MIA} = -[H^\circ_{[\text{H}_2\text{asp-M}]^+} - (H^\circ_{\text{H}_2\text{asp}} + H^\circ_{\text{M}^+})] \quad 3.10$$

where the $[\text{asp-M}]^-$, $[\text{asp-M}_2]$, $[\text{Hasp-M}]$ and $[\text{H}_2\text{asp-M}]^+$ complexes are formed from the asp^{2-} , Hasp^- and H_2asp species and M^+ alkali metal cations. The standard enthalpy ΔH°_{298} and Gibbs free energy changes ΔG°_{298} of complexation reactions were obtained by the thermodynamical analysis at 298 K, 1 atmosphere using the vibrational frequency calculations at the B3LYP/6-311++G(d,p) level of theory.

Because of Hasp^- and H_2asp species can be deprotonated, thus deprotonation energy (DPE) of their alkali complexes is determined. DPEs of $[\text{Hasp-M}]$ and $[\text{H}_2\text{asp-M}]^+$ complexes are defined as the reaction energy described by equations 3.11 and 3.12

$$\text{DPE} = [(E^\circ_{[\text{asp-M}]^-} + E^\circ_{\text{H}^+}) - E^\circ_{[\text{Hasp-M}]}] \quad 3.11$$

$$\text{DPE} = [(E^\circ_{[\text{Hasp-M}]} + E^\circ_{\text{H}^+}) - E^\circ_{[\text{H}_2\text{asp-M}]^+}] \quad 3.12$$

where the $E^\circ_{[\text{H}_2\text{asp-M}]^+}$, $E^\circ_{[\text{Hasp-M}]}$, $E^\circ_{[\text{asp-M}]^-}$ and $E^\circ_{[\text{H}^+]}$ are energies of $[\text{H}_2\text{asp-M}]^+$, $[\text{Hasp-M}]$, $[\text{asp-M}]^-$ complex species and free proton, respectively.

3.3 Aqueous acid-dissociation constants (pK_a) of aspartic acid

3.3.1 Quantum chemical and PCM solvation model

Structure optimizations of all species of aspartic acid were carried out using density functional theory (DFT) method. The calculations have been performed with hybrid density functional B3LYP, the Becke's three-parameter exchange functional [35] with the Lee-Yang-Parr correlation functional. [36] The structure optimization of species H_3asp^+ , H_2asp , Hasp^- and asp^{2-} and their n -hydrated $((\text{H}_2\text{O})_n, n=3-6)$ have been carried out at the B3LYP/6-31+G(d,p) level of theory. The single-point calculations at the same level of theory have been employed for solvent-effect computation using the polarizable continuum model (PCM) of Tomasi and co-workers. [39-44] The conductor-like polarizable continuum model (CPCM) [45-48] and Integral-Equation-Formalism Polarizable Continuum Model (IEFPCM) have been used in single-point calculations for

the PCM solvent effect. [45,48] The molecular cavity models used in the PCM models are the united atom for Hartree–Fock (UAHF) and the united–atom Kohn–Sham topological model (UAKS). [43]

Gibbs free energies (G_{gas}) of various species of aspartic acid in gas phase were obtained from the frequency calculations of the B3LYP/6–31+G(d,p). The solvation free energies (ΔG_{solv}) of the various species of aspartic acid in aqueous solution were obtained from the single–point B3LYP/6–31+G(d,p) calculations combined with the PCM models CPCM and IEFPCM with dielectric constant $\epsilon = 78.37$ and using with the cavity models UAKS and UAHF.

3.3.2 Thermodynamic cycles and acid–dissociation models

Thermodynamic cycles for calculations of the theoretical $\text{p}K_{\text{a}1}$, $\text{p}K_{\text{a}2}$ and $\text{p}K_{\text{a}3}$ for acid dissociations of aspartic acid species Hasp , H_2asp^+ and asp^- are shown in the Scheme 3.1 as representative for the bare structure system and in the Scheme 3.2 as representative for the n –hydrated structures, respectively. These thermodynamic cycles are modified from the cycles which are taken from ref. 51. The first ($\text{p}K_{\text{a}1}$), second ($\text{p}K_{\text{a}2}$) and third ($\text{p}K_{\text{a}3}$) dissociation constants are defined using the well known thermodynamic equation 3.14

$$\text{p}K_{\text{a}1} = \Delta G_{\text{aq}} / 2.303RT \quad 3.13$$

The Gibbs free energies of aqueous acid dissociation reactions are computed by adding a solvation contribution to the gas phase value using the following equations

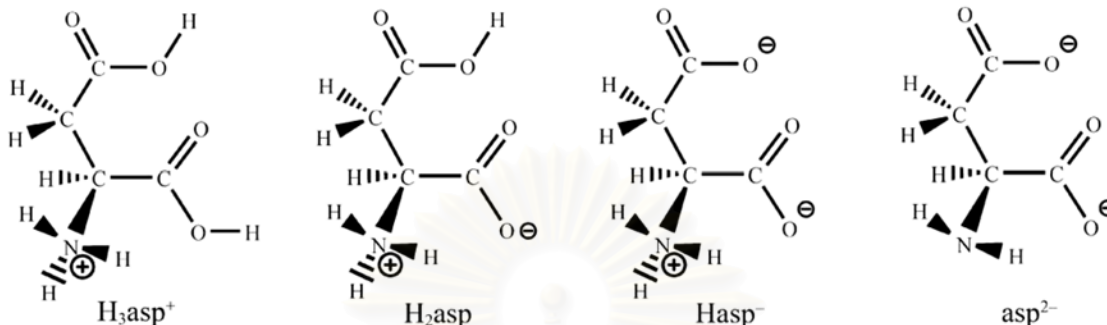
$$\Delta G_{\text{aq}} = \Delta G_{\text{gas}} + \Delta \Delta G_{\text{solv}} \quad 3.14$$

$$\Delta G_{\text{gas}} = G_{\text{gas}}(A) + G_{\text{gas}}(H^+) - G_{\text{gas}}(HA^+) \quad 3.15$$

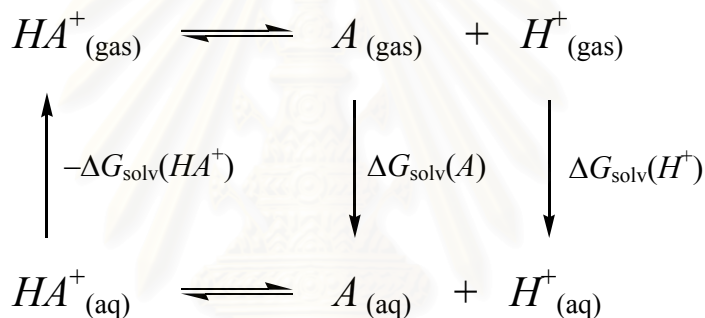
$$\Delta \Delta G_{\text{solv}} = \Delta G_{\text{solv}}(A) + \Delta G_{\text{solv}}(H^+) - \Delta G_{\text{solv}}(HA^+) \quad 3.16$$

where HA^+ and A are species for HA^+ to A dissociation as representative for dissociations of H_3asp^+ to H_2asp , H_2asp to Hasp^- , and Hasp^- to asp^{2-} . Thermodynamic cycles for calculations of the theoretical $\text{p}K_{\text{a}1}$, $\text{p}K_{\text{a}2}$ and $\text{p}K_{\text{a}3}$ for acid–dissociation of aspartic acid species H_2asp , Hasp^- and asp^{2-} are shown in Scheme A1, A2 and A3 for their bare structures and Scheme A4, A5 and A6 for their n –hydrated, $n=3$ –6, structures, respectively. As experimental derivation, $\Delta G_{\text{gas}}(H^+) = -6.28$ kcal/mol (at the reference

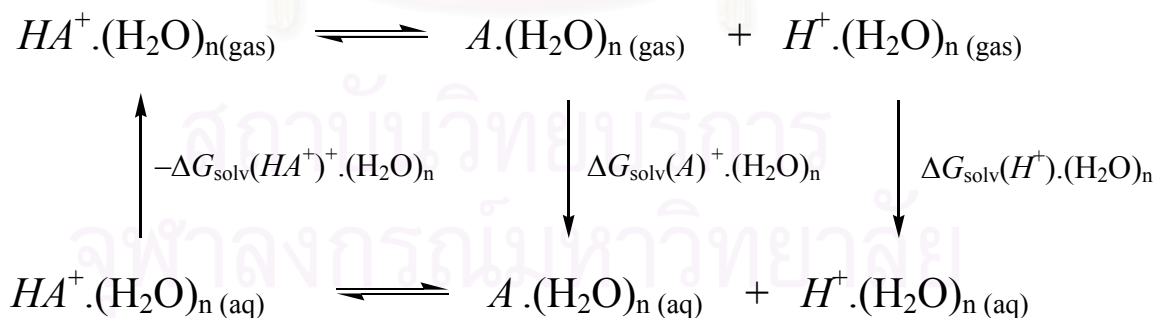
state of 1 atm) [51] and $\Delta\Delta G_{\text{solv}}(H^+) = -264.61$ kcal/mol (at the reference state of 1 M) [52] were used in the calculations.



Scheme 3.1 Acid–dissociation equilibria of aspartic acid.



Scheme 3.2 Thermodynamic cycle for calculation of theoretical pK_a of bare–structure of aspartic acid.



Scheme 3.3 Thermodynamic cycle for calculation of theoretical pK_a of n -hydrated structure of aspartic acid.

CHAPTER IV

RESULTS AND DISCUSSION

4.1 Conformation of cationic, zwitterionic and anionic species of aspartic acid and their water-added forms

4.1.1 PES of various forms of aspartic acid and their geometrical conformations

As the stabilities of bare structure of all species were examined, the proper zwitterionic structures of the species H_2asp and $Hasp^-$ are not stable because their amino proton can easily transfer to their carboxylate oxygen. Due to the stability test of hydrated structures of the species H_2asp and $Hasp^-$, it was found that these two species are stabilized by at least three water molecules. The PESs for the species H_2asp and $Hasp^-$ were therefore computed as their trihydrated forms but for the species H_3asp^+ and asp^{2-} , their bare structures were employed.

Conformational structures of $H_3asp^+-endo-E$, $H_3asp^+-endo-Z$, $H_3asp^+-exo-E$, $H_3asp^+-exo-Z$, $H_2asp-endo$, $H_2asp-exo$, $Hasp^-$ and asp^{2-} species optimized at B3LYP/6-31G(d) level of theory are shown in Tables B1, B2, B3, B4, B5, B6, B7 and B8, Appendix B. Classifications of the types of internal hydrogen bonding for aspartic acid are shown in Figure 4.1. Two types of backbone/backbone (BB/BB) and five types of side-chain/backbone (SC/BB) hydrogen bonding were defined. The types and distances of existing hydrogen bonding for various H_3asp^+ forms of aspartic acid is shown in Table 4.1 and for various H_2asp , $Hasp^-$ and asp^{2-} forms are shown in Table 4.2. Bond distances of the internal hydrogen bonding of types 1a, 1b, 2a, 2b, 2c, 2d and 2e found in all conformations are within 1.768–1.949, 1.724–2.158, 1.875–1.910, 1.690–1.916 Å, at 2.010 Å and 1.706–1.760 Å, respectively. The numbers of stable conformers for $H_3asp^+-endo-E$, $H_3asp^+-endo-Z$, $H_3asp^+-exo-E$, $H_3asp^+-exo-Z$, $H_2asp-endo$, $H_2asp-exo$, $Hasp^-$ and asp^{2-} are 8, 13, 5, 8, 4, 7, 9 and 3 conformers and their conformational structures are shown in Figures A1, A3, A5, A7, A9, A11, A13 and A15 as contained in Appendix A, respectively. The landscape representations of the side-chain conformational PESs,

$E=E(\chi_1, \chi_2)$ associated with the backbone conformations of $H_3asp^+-endo-E$, $H_3asp^+-endo-Z$, $H_3asp^+-exo-E$, $H_3asp^+-exo-Z$, $H_2asp-endo$, $H_2asp-exo$, $Hasp^-$ and asp^{2-} are shown in Figures A2, A4, A6, A8, A10, A12, A14 and A16, respectively. The bottoms of the Figures A2, A4, A6, A8, A10, A12, A14 and A16 show integrated scatter-plot diagrams of the existing conformations which correspond to the PESs located at the top of the figures.

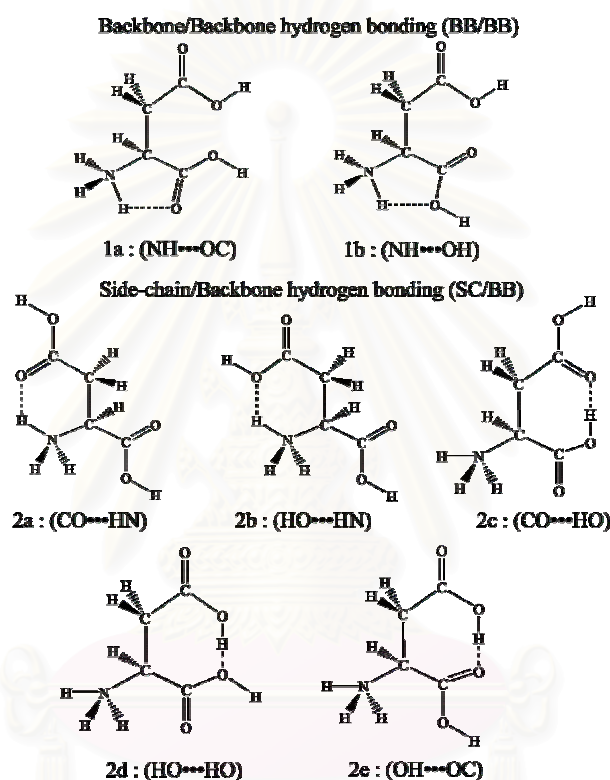


Figure 4.1 Classification of the types of internal hydrogen bonding for various species of aspartic acid.

Based on the geometrical parameters of the conformations of species H_3asp^+ , H_2asp or $Hasp^-$, their conformations are identical when their dihedral angles χ_1 and χ_2 are the same value and if their dihedral angles differ by 120° or ψ differ by 180° . In case of the species asp^{2-} , their conformations are identical when their dihedral angles χ_2 or ψ differ by 180° .

Table 4.1 The present hydrogen bonding, its type and distance for conformations of the aspartic acid H_3asp^+ species

Conformer	Hydrogen bond			
	BB/BB types	BB/BB Distances (Å)	SC/BB types	SC/BB Distances (Å)
H_3asp^+ -endo-E form				
$\gamma_D [a a]^{a1}$	1a	1.768	2d	1.780
$\gamma_D [g^- a]^{b1}$	1a	1.620	2b	1.910
$\gamma_D [g^- g^-]$	1a	1.901	2c	1.820
$\gamma_D [g^- g^+]^{c1}$	1a	1.949	2a	1.750
$\alpha_D [a g^+]$	1a	1.734	2c	1.694
$\alpha_D [g^+ a]^{d1}$	–	–	2b	1.879
$\alpha_D [g^+ g^-]^{e1}$	–	–	2a	1.750
$\beta_L [g^- g^+]$	–	–	2a	1.759
H_3asp^+ -endo-Z form				
$\gamma_D [a g^-]^{a2}$	–	–	–	–
$\gamma_D [g^- a]^{b2}$	–	–	2b	1.875
$\gamma_D [g^- g^+]^{c2}$	–	–	2a	1.662
$\delta_D [g^+ a]^{d2}$	–	–	–	–
$\epsilon_D [g^+ g^-]^{e2}$	–	–	2b	1.888
$\epsilon_D [a g^-]^{f2}$	–	–	2a	1.760
$\epsilon_D [a g^-]^{g2}$	1b	2.153	–	–
$\epsilon_D [g^- g^+]^{h2}$	–	–	2a	1.750
$\epsilon_D [g^- a]$	1b	1.882	2b	1.882
$\epsilon_L [a a]$	1b	2.158	–	–
$\alpha_D [a g^+]^{i2}$	–	–	–	–
$\alpha_D [g^+ a]^{j2}$	1b	1.883	2a	1.868
$\alpha_D [g^+ g^-]^{k2}$	–	–	2a	1.750
H_3asp^+ -exo-E form				
$\gamma_D [g^- g^+]^{a3}$	–	–	2a	1.688
$\epsilon_D [g^- g^+]$	–	–	2a,2c	1.864,1.867
$\alpha_D [g^- a]^{b3}$	–	–	2d	2.010
$\alpha_D [g^+ g^-]^{c3}$	–	–	2a	2.133
$\delta_L [a g^+]^{d3}$	1a	1.724	2c	1.690
H_3asp^+ -exo-Z form				
$\gamma_D [a g^-]^{a4}$	–	–	–	–
$\gamma_D [g^- g^+]^{b4}$	–	–	2a	2.236
$\delta_D [g^+ g^-]$	–	–	2a	1.722
$\epsilon_D [a g^-]^{c4}$	1b	1.724	–	–
$\epsilon_D [g^- g^+]^{d4}$	1b	2.156	2a	2.156
$\beta_L [g^+ g^-]^{e4}$	–	–	2a	1.722
$\alpha_D [g^- a]^{f4}$	–	–	2c	1.916
$\alpha_D [g^+ g^-]^{g4}$	–	–	2a	1.712

^{a1} Identical to $\delta_D [a a]$ and $\alpha_L [a a]$. ^{b1} Identical to $\delta_D [g^- a]$ and $\alpha_L [g^- a]$. ^{c1} Identical to $\delta_D [g^- g^+]$ and $\alpha_L [g^- g^+]$. ^{d1} Identical to $\delta_L [g^+ a]$ and $\gamma_L [g^+ a]$. ^{e1} Identical to $\gamma_L [g^+ g^-]$. ^{a2} Identical to $\delta_D [a g^-]$ and $\alpha_L [a g^-]$. ^{b2} Identical to $\delta_D [g^- a]$ and $\alpha_L [g^- a]$. ^{c2} Identical to $\delta_D [g^- g^+]$. ^{d2} Identical to $\alpha_L [a a]$. ^{e2} Identical to $\epsilon_L [g^- a]$. ^{f2} Identical to $\beta_L [g^+ g^-]$ and $\epsilon_L [g^- g^-]$. ^{g2} Identical to $\epsilon_L [a g^-]$. ^{h2} Identical to $\beta_L [g^- g^+]$ and $\epsilon_L [g^- g^+]$. ⁱ² Identical to $\delta_L [a g^+]$. ^{j2} Identical to $\delta_L [g^+ a]$ and $\gamma_L [g^+ a]$. ^{k2} Identical to $\delta_L [g^+ g^-]$ and $\gamma_L [g^+ g^-]$. ^{a3} Identical to $\delta_D [g^- g^+]$ and $\alpha_L [g^- g^+]$. ^{b3} Identical to $\delta_L [g^- a]$ and $\gamma_L [g^- a]$. ^{c3} Identical to $\delta_L [g^+ g^-]$ and $\gamma_L [g^+ g^-]$. ^{d3} Identical to $\gamma_L [a g^+]$. ^{a4} Identical to $\delta_D [a g^-]$ and $\alpha_L [a g^-]$. ^{b4} Identical to $\delta_D [g^- g^+]$ and $\alpha_L [g^- g^+]$. ^{c4} Identical to $\beta_L [a g^-]$ and $\epsilon_L [a g^-]$. ^{d4} Identical to $\beta_L [g^- g^+]$ and $\epsilon_L [g^- g^+]$. ^{e4} Identical to $\epsilon_L [g^+ g^-]$. ^{f4} Identical to $\delta_L [g^- a]$ and $\gamma_L [g^- a]$. ^{g4} Identical to $\gamma_L [g^+ g^-]$.

As the bare structures of the species H_3asp^+ and asp^{2-} and the trihydrated forms of the species H_2asp and Hasp^- were employed in the PESs computations using the B3LYP/6–31G(d) theoretical level. The most stable conformers of H_3asp^+ , $\text{H}_2\text{asp}(3\text{H}_2\text{O})$, $\text{Hasp}^-(3\text{H}_2\text{O})$ and asp^{2-} of aspartic acid in gas phase are $\gamma_{\text{D}} [\text{g}^- \text{g}^+]$ which is identical to $\delta_{\text{D}} [\text{g}^- \text{g}^+]$ (see Table B2 and Figure A2), $\alpha_{\text{L}} [\text{a} \text{g}^-]$ (see Table B6 and Figure A6), $\varepsilon_{\text{L}} [\text{g}^+ \text{a}]$ which is identical to $\beta_{\text{L}} [\text{g}^+ \text{a}]$ (see Table B7 and Figure A7) and $\beta_{\text{L}} [\text{g}^+ \text{a}]$ which is identical to $\beta_{\text{L}} [\text{g}^+ \text{g}^-]$, $\delta_{\text{L}} [\text{g}^+ \text{a}]$ and $\delta_{\text{L}} [\text{g}^+ \text{g}^-]$ (see Table B8 and Figure A8), respectively.

Table 4.2 The present hydrogen bonding, its type and distance for conformations of the aspartic acid H_2asp , Hasp^- and asp^{2-} species

Conformer	Hydrogen bond			
	BB/BB types	BB/BB Distances (Å)	SC/BB types	SC/BB Distances (Å)
<i>H₂asp-endo form</i>				
$\alpha_{\text{D}} [\text{g}^+ \text{g}^-]$	1a	1.570	–	–
$\varepsilon_{\text{D}} [\text{g}^+ \text{g}^-]$	1a	1.839	–	–
$\delta_{\text{D}} [\text{g}^+ \text{g}^-]$	1a	1.635	–	–
$\varepsilon_{\text{L}} [\text{g}^- \text{g}^+]$	–	–	–	–
<i>H₂asp-exo form</i>				
$\gamma_{\text{D}} [\text{a} \text{g}^-]$	–	–	–	–
$\gamma_{\text{D}} [\text{g}^- \text{a}]$	1a	1.855	–	–
$\gamma_{\text{D}} [\text{g}^- \text{g}^+]$	–	–	2e	1.760
$\delta_{\text{D}} [\text{g}^+ \text{a}]$	1a	1.733	–	–
$\varepsilon_{\text{D}} [\text{g}^+ \text{g}^-]$	1a	1.655	–	–
$\varepsilon_{\text{D}} [\text{a} \text{g}^-]$	1a	1.602	–	–
$\varepsilon_{\text{D}} [\text{a} \text{g}^-]$	–	–	2e	1.706
<i>Hasp⁻ form</i>				
$\alpha_{\text{D}} [\text{g}^+ \text{a}]^{\text{a1}}$	–	–	2a	1.470
$\delta_{\text{D}} [\text{a} \text{g}^-]$	–	–	–	–
$\varepsilon_{\text{D}} [\text{g}^+ \text{g}^-]^{\text{b1}}$	–	–	2a	1.737
$\varepsilon_{\text{D}} [\text{g}^+ \text{a}]$	–	–	2a	1.532
$\varepsilon_{\text{D}} [\text{g}^+ \text{g}^-]$	1a	1.850	2a	1.438
$\gamma_{\text{L}} [\text{g}^+ \text{g}^-]^{\text{c1}}$	–	–	2a	1.658
$\gamma_{\text{L}} [\text{g}^+ \text{g}^-]$	1a	1.801	2a	1.446
$\varepsilon_{\text{L}} [\text{g}^+ \text{a}]^{\text{d1}}$	–	–	2a	1.552
$\varepsilon_{\text{L}} [\text{g}^+ \text{g}^-]$	–	–	2a	1.632
<i>asp²⁻ form</i>				
$\gamma_{\text{D}} [\text{g}^+ \text{a}]^{\text{a2}}$	–	–	2a	2.250
$\alpha_{\text{L}} [\text{g}^- \text{g}^+]^{\text{b2}}$	–	–	2a	1.947
$\beta_{\text{L}} [\text{g}^+ \text{a}]^{\text{c2}}$	–	–	2a	2.027

^{a1} Identical to $\gamma_{\text{L}} [\text{g}^+ \text{a}]$. ^{b1} Identical to $\beta_{\text{L}} [\text{g}^+ \text{g}^-]$. ^{c1} Identical to $\delta_{\text{L}} [\text{g}^+ \text{g}^-]$. ^{d1} Identical to $\beta_{\text{L}} [\text{g}^+ \text{a}]$. ^{a2} Identical to $\gamma_{\text{D}} [\text{g}^+ \text{g}^-]$, $\varepsilon_{\text{D}} [\text{g}^+ \text{a}]$, $\varepsilon_{\text{D}} [\text{g}^+ \text{g}^-]$. ^{b2} Identical to $\alpha_{\text{L}} [\text{g}^- \text{a}]$, $\varepsilon_{\text{L}} [\text{g}^- \text{g}^+]$, $\varepsilon_{\text{L}} [\text{g}^- \text{a}]$. ^{c2} Identical to $\beta_{\text{L}} [\text{g}^+ \text{g}^-]$, $\delta_{\text{L}} [\text{g}^+ \text{a}]$, $\delta_{\text{L}} [\text{g}^+ \text{g}^-]$.

Table 4.3 B3LYP/6–31+G(d,p)–optimized conformations of various species of trihydrated and tetrahydrated forms of aspartic acid, their selected geometrical data and total energies

Species	Conformation	Optimized parameters					
		ϕ	ψ	χ^1	χ^2	χ^3	ω
Trihydrated form							
H ₃ asp ⁺	γ_D [g ⁻ g ⁺]	25.36	-18.98	-50.18	27.13	0.68	0.76
H ₂ asp	α_L [a g ⁻]	-72.92	-18.69	145.70	-106.50	166.30	-
Hasp ⁻	ε_L [g ⁺ a]	-36.74	-149.30	43.77	143.40	-	-
asp ²⁻	β_L [g ⁺ a]	-169.70	-163.70	58.26	167.41	-	-
Tetrahydrated form							
H ₃ asp ⁺	γ_D [g ⁻ g ⁺]	30.30	-34.67	-54.37	26.65	0.23	0.62
H ₂ asp	α_L [a g ⁻]	-79.39	-19.14	148.89	-108.89	166.20	-
Hasp ⁻	ε_L [g ⁺ a]	-39.11	-150.30	47.47	134.33	-	-
asp ²⁻	β_L [g ⁺ a]	-165.20	-153.60	58.87	157.00	-	-

Table 4.4 B3LYP/6–31+G(d,p)–optimized conformations of various species of aspartic acid in gas phase

Species	Conformation		
	Bare	Trihydrated	Tetrahydrated
H ₃ asp ⁺	γ_D [g ⁻ g ⁺] ^a	γ_D [g ⁻ g ⁺] ^a	γ_D [g ⁻ g ⁺] ^a
H ₂ asp	-	α_L [a g ⁻]	α_L [a g ⁻]
Hasp ⁻	-	ε_L [g ⁺ a]	ε_L [g ⁺ a] ^c
asp ²⁻	β_L [g ⁺ a] ^d	β_L [g ⁺ a]	β_L [g ⁺ a]

^a Identical to δ_D [g⁻ g⁺]. ^b Unstable species. ^c Identical to β_L [g⁺ a]. ^d Identical to β_L [g⁺ g⁻], δ_L [g⁺ a] and δ_L [g⁺ g⁻].

Table 4.5 Stabilization energies of protonation reaction of tri- and tetrahydrated forms of species asp²⁻, Hasp⁻ and H₂asp of aspartic acid

Protonation/reaction steps	$\Delta E^{a,b}$	ΔH^a	ΔG^a
Trihydrated			
$\Delta E1: asp^{2-}(3H_2O) + H^+ \rightarrow Hasp^-(3H_2O)$	-235.56	-234.12	-236.87
$\Delta E2: Hasp^-(3H_2O) + H^+ \rightarrow H_2asp(3H_2O)$	-300.45	-299.32	-301.95
$\Delta E3: H_2asp(3H_2O) + H^+ \rightarrow H_3asp^+(3H_2O)$	-368.48	-367.75	-369.12
Tetrahydrated			
$\Delta E1: asp^{2-}(4H_2O) + H^+ \rightarrow Hasp^-(4H_2O)$	-244.68	-243.54	-246.85
$\Delta E2: Hasp^-(4H_2O) + H^+ \rightarrow H_2asp(4H_2O)$	-308.57	-307.88	-309.13
$\Delta E3: H_2asp(4H_2O) + H^+ \rightarrow H_3asp^+(4H_2O)$	-379.97	-378.10	-381.03

^a In kcal/mol. ^b With ZPVE corrections.

4.1.2 Water-added structures and their protonation

The B3LYP/6-31+G(d,p)-optimized structures of various trihydrated and tetrahydrated species of aspartic acid and their selected geometrical data are tabulated in Table 4.3. The B3LYP/6-31G(d)-optimized structures of the bare molecule of species H_3asp^+ and asp^{2-} , trihydrated ($\text{H}_3\text{asp}^+(3\text{H}_2\text{O})$, $\text{H}_2\text{asp}(3\text{H}_2\text{O})$, $\text{Hasp}^-(3\text{H}_2\text{O})$ and $\text{asp}^{2-}(3\text{H}_2\text{O})$) and tetrahydrated ($\text{H}_3\text{asp}^+(4\text{H}_2\text{O})$, $\text{H}_2\text{asp}(4\text{H}_2\text{O})$, $\text{Hasp}^-(4\text{H}_2\text{O})$ and $\text{asp}^{2-}(4\text{H}_2\text{O})$) species were fully reoptimized at B3LYP/6-31+G(d,p) level as shown in Figure 4.2. Conformations of the B3LYP/6-31+G(d,p)-optimized geometries of all aspartic acid species are shown Table 4.4. The most stable conformation for each aspartic acid species existing as trihydrated and tetrahydrated forms and their protonation and deprotonation schemes are shown in Figure 4.5. The stabilization energies of protonation of tri- and tetrahydrated form of aspartic acid derived from their total energies computed at B3LYP/6-31+G(d, p) level of theory with zero-point vibrational energy (ZPVE) are listed in Table 4.5. Three protonation steps are exothermic reactions and their stabilization energies of the stepwise protonation are -244.68 , -308.57 and -379.97 kcal/mol, respectively.

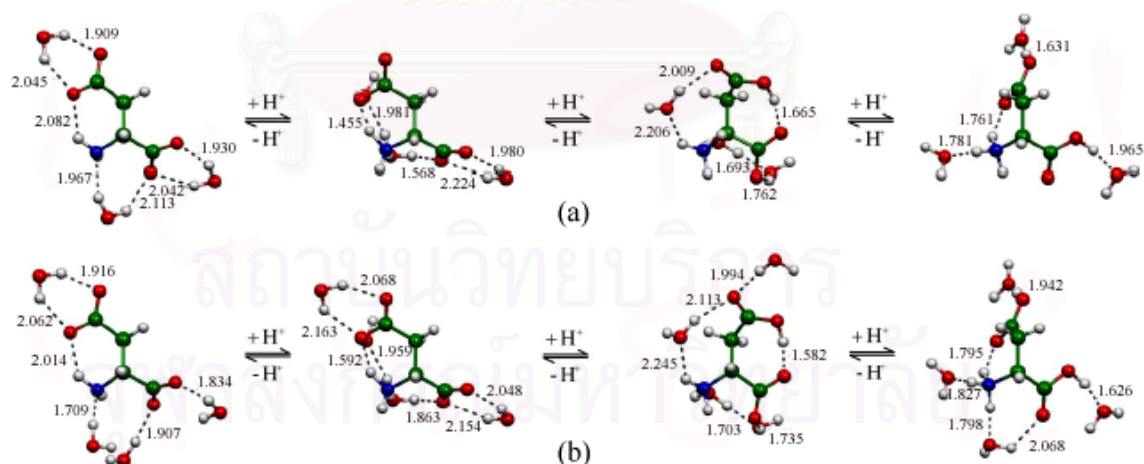


Figure 4.2 The B3LYP/6-31+G(d,p) optimized structures of the most stable conformers of four species of aspartic acid as (a) trihydrated and (b) tetrahydrated forms and their protonation schemes. The hydrogen bond distances are in Å.

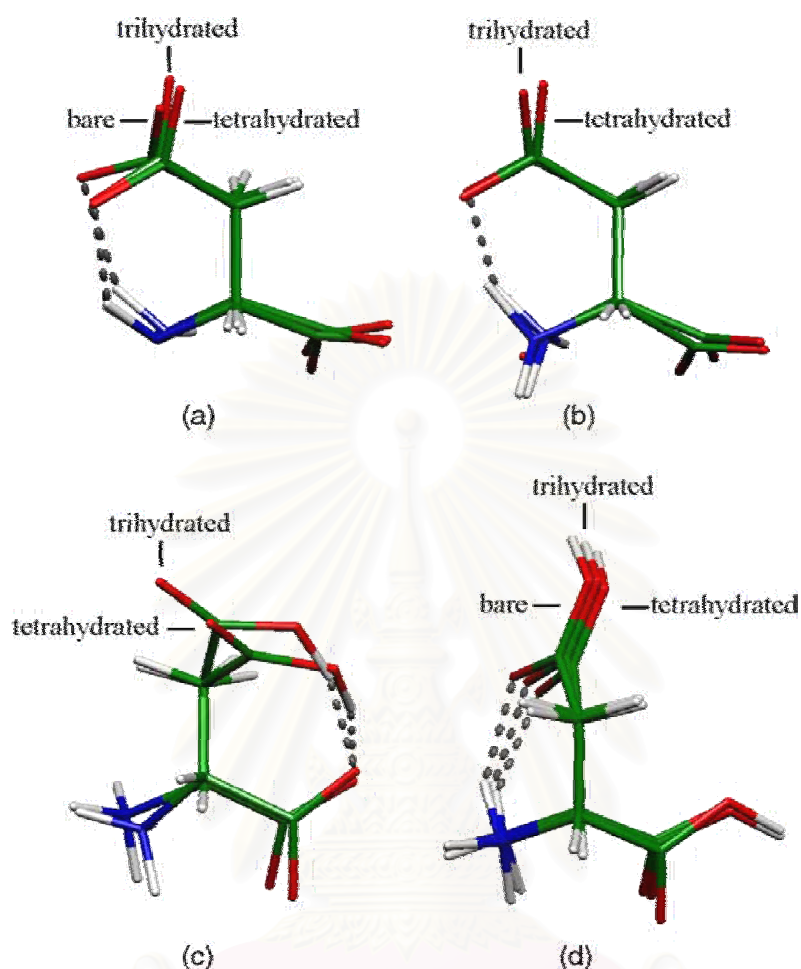


Figure 4.3 Superimpose pictures of the geometrical changes of the most stable conformers of species (a) asp^{2-} , (b) Hasp^- , (c) H_2asp and (d) H_3asp^+ . For clarity, water molecules are not displayed.

Based on the B3LYP/6-31+G(d, p) computations of different structural models (the bare, trihydrated and tetrahydrated structures), the conformation for the species H_3asp^+ ($\gamma_D [g^- g^+]$), H_2asp ($\alpha_L [a g^-]$), Hasp^- ($\epsilon_L [g^+ a]$) and asp^{2-} ($\beta_L [g^+ a]$) are not changed as shown in Table 4.4. As compared to other species, the geometrical change of the species Hasp^- has obviously occurred as shown in Figure 4.3. Due to the change of trihydrated to tetrahydrated system, Figure 4.3 (c) illustrates that the side-chain carboxylic group of the species Hasp^- is the main cause of its geometrical change; the change of its dihedral angles χ_1 and χ_2 are 4 and 9°, respectively. [37]

4.2 Complexation between alkali cations and aspartic species

4.2.1 Conformational analysis of alkali metal complexes of dianionic species of aspartic acid

The possible binding modes shown in Figure 4.4 are defined as six binding types. As the binding mode is defined as the ratio of the number of metal ions (N_M) to the number of binding sites of the ligand (N_L), the $N_M:N_L$ ratios are 1:1 for binding mode types I and II, 1:2 for types III, VI and V and 1:3 for type VI. For a dinuclear complex, the type of the binding mode is defined as a combination of the types of the mononuclear complexes (types I, II, III, IV, V and VI).

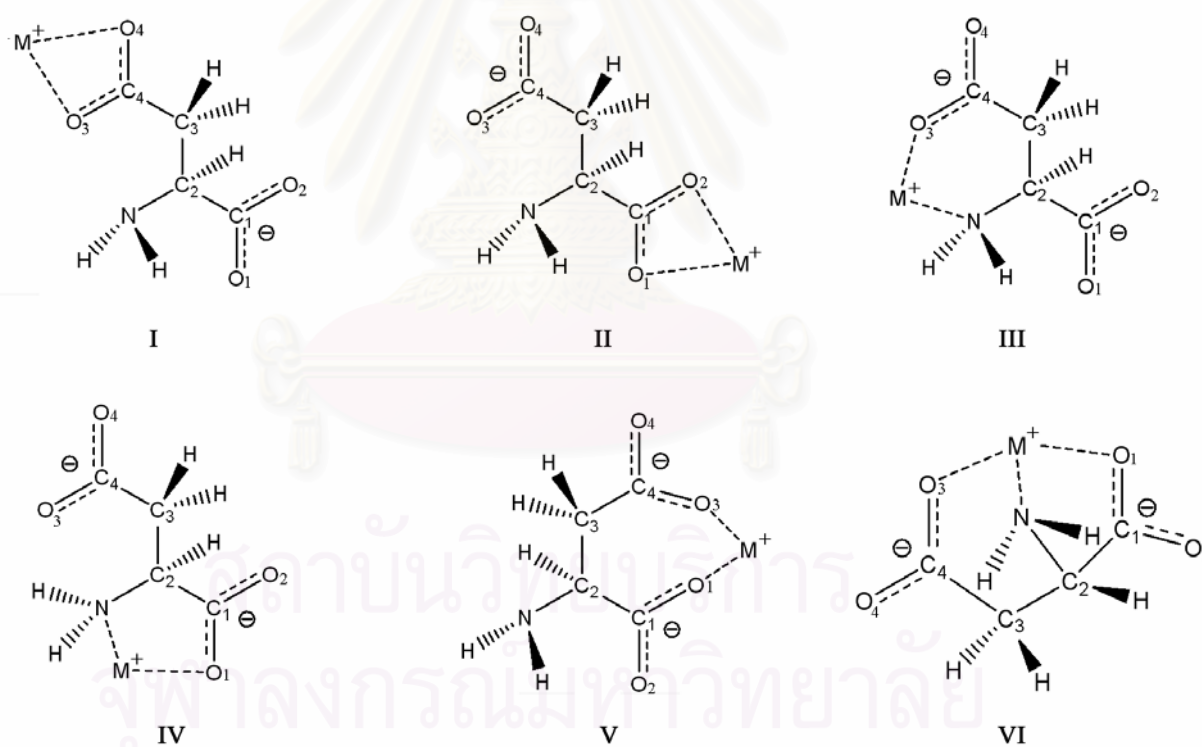


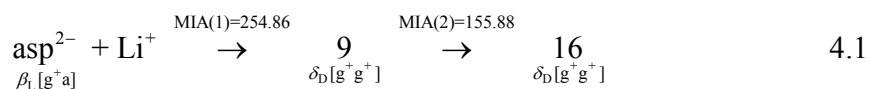
Figure 4.4 The proposed possible sites for binding mode of interaction between cation and aspartate (asp^{2-}) moiety.

4.2.1.1 Lithium complexes

The B3LYP/6-311++G(d,p)-optimized structures of $[\text{asp-Li}]^-$ and $[\text{asp-Li}_2]$ complexes are shown in Figure A17. Nine and seven conformers of the mono and di-lithium complexes with aspartate anion, respectively, were found. The most stable conformer for $[\text{asp-Li}]^-$ and $[\text{asp-Li}_2]$ were shown in Figure 4.5. The most stable structure for the $[\text{asp-Li}]^-$ and $[\text{asp-Li}_2]$ complexes are the conformers **9** and **16**. The relative B3LYP/6-311++G(d,p)-computed energies of $[\text{asp-Li}]^-$ and $[\text{asp-Li}_2]$ complexes, respectively, compared to the complexes **9** and **16** and the Ramachandran/IUPAC [3,4] nomenclatures for conformations of aspartic acid species are given at the bottom of each molecule are tabulated in Table 4.6. The monolithium complexes **1**, **2**, **4**, **5**, **7** and **9** are single mode of types I, II, III, IV, V and VI, respectively, but **3**, **6** and **8** are combination modes of types I + II, I + V and II + V, respectively. The di-lithium complexes **10**, **11**, **12**, **13**, **14**, **15** and **16** are all combination modes. The MIA(1)s of the lithium complexes with aspartate anion are shown in Table 4.6. Due to the most stable conformer **9**, the aspartate ligand prefers to bind with the lithium using its amino nitrogen and carboxylate oxygen atoms. For dinuclear complex **16**, a doubly tri-coordinated structure is formed by interaction between the asp^{2-} ligand and the two lithium cations. The lithium cation firstly forms a tri-coordinated structure which is similar to **9**, then the second lithium cation forms a tri-coordinated structure using two α -carboxylate and one β -carboxylate oxygen atoms as shown in Figure 4.5. Comparing the asp^{2-} complex with two lithium cations to the $[\text{asp-Zn}\cdot 3\text{H}_2\text{O}]$ [43] and $[\text{asp-Ni}(\text{im})_3]$ [44] complexes, the N-M⁺, O₁-M⁺ and O₃-M⁺ bond lengths of both transition metal complexes are slightly longer than those of the lithium complexes.

The relative stabilities of the $[\text{asp-Li}]^-$ and $[\text{asp-Li}_2]$ complexes are in decreasing orders: **9** > **7** > **6** > **8** > **4** > **3** > **5** > **1** \approx **2** and **16** > **13** > **10** > **14** \approx **12** \approx **15** > **11**, respectively. The MIA(1)s of the $[\text{asp-Li}]^-$ complexes are within 226.30–254.86 kcal/mol. The relative lithium ion affinities of the aspartate dianion are in decreasing order: **9** > **7** > **6** \approx **8** \approx **4** > **3** > **5** > **1** \approx **2**. Based on the lower values of the MIA(2)s of the $[\text{asp-Li}]^-$ complexes, their relative lithium ion affinities are in decreasing

order: $10 > 15 \approx 16 \approx 12 \approx 14 > 13 > 11$. The most preferable feature of the conformational reaction of the lithium/asp²⁻ complex can therefore be proposed as:



Due to Equation 4.1, the aspartic acid conformations based on the Ramachandran nomenclature [3,4] of the free-form (asp²⁻), mono (**9**) and dinuclear (**16**) complexes are $\beta_L[\text{g}^+ \text{a}]$, $\delta_D[\text{g}^+ \text{g}^+]$ and $\delta_D[\text{g}^+ \text{g}^+]$, respectively. The aspartic acid features either in the complex **9** or **16** are the same conformation.

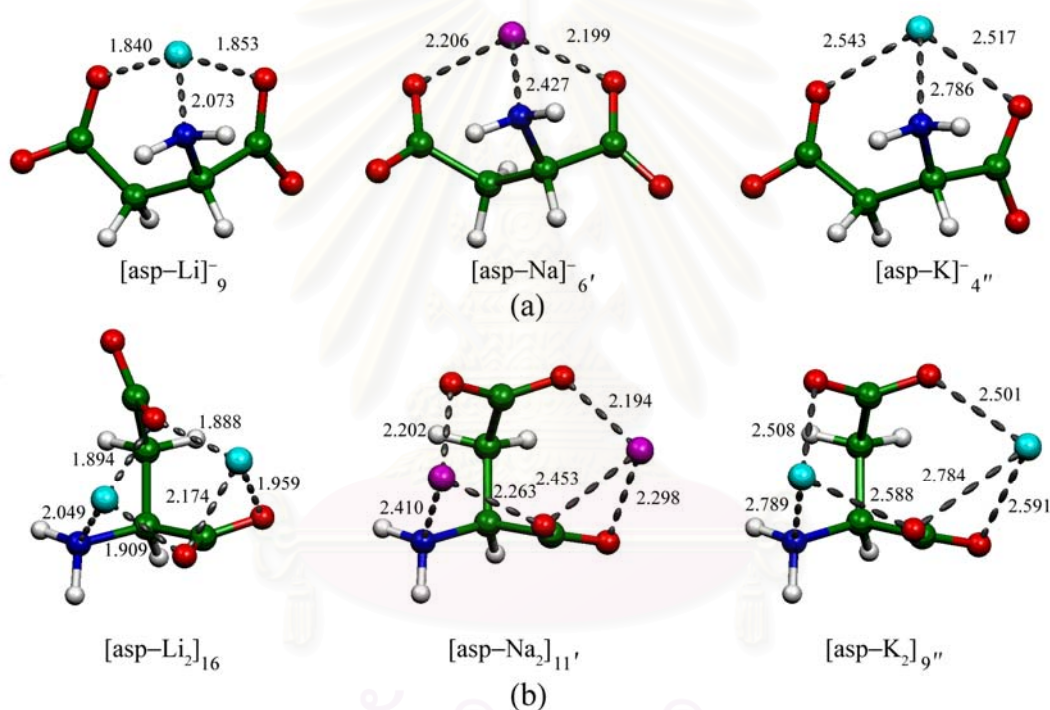


Figure 4.5 The most stable conformer of (a) $[\text{asp-M}]^-$ and (b) $[\text{asp-M}_2]$ ($M = \text{Li}^+, \text{Na}^+, \text{K}^+$) complexes. Distances are in Å.

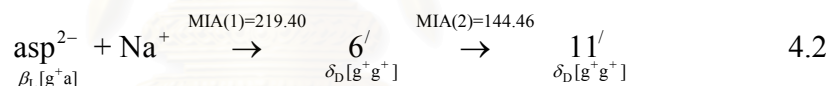
Table 4.6 Relative B3LYP/6–311++G(d,p) energies and MIAs of minima for [asp–M][–] and [asp–M₂] complexes, M=Li⁺, Na⁺, K⁺

Complexes/ systems	Aspartate conformers	Binding mode	ΔE^a	MIAs ^a
[asp–Li] [–]				
1	$\gamma_L[g^-g^-]^b$	I	28.09	226.30
2	$\gamma_D[g^-g^+]^c$	II	28.41	226.07
3	$\gamma_D[g^-g^+]^c$	I+III	17.31	237.46
4	$\gamma_D[g^-a]^d$	III	15.23	239.46
5	$\delta_D[g^-g^+]^e$	IV	19.11	235.69
6	$\gamma_D[g^-g^+]^f$	I+V	5.05	249.60
7	$\gamma_D[g^-a]^g$	V	2.71	251.93
8	$\gamma_D[a g^+]^h$	II+V	6.27	248.40
9	$\delta_D[g^+g^+]^i$	VI	0.00	254.86
[asp–Li ₂] ^{–m}				
10	$\gamma_L[g^-g^-]^b$	I+II	16.48	167.20 (167.43)
11	$\gamma_D[g^-a]^d$	I+III	30.57	153.41 (140.25)
12	$\delta_D[g^-g^+]^e$	I+IV	17.24	166.69 (155.53)
13	$\delta_D[g^+g^+]^i$	I+VI	6.65	177.50 (148.94)
14	$\gamma_D[g^-a]^d$	II+III	17.10	153.55 (166.95)
15	$\gamma_D[g^-g^+]^c$	I+II+III	17.40	157.14 (166.75)
16	$\delta_D[g^+g^+]^i$	II+V+VI	0.00	162.23 (155.88)
[asp–Na] [–]				
1'	$\gamma_L[g^-g^-]^b$	I	21.73	197.10
2'	$\gamma_D[g^-g^+]^c$	II	21.97	197.43
3'	$\gamma_D[g^-g^+]^c$	I+III	12.51	206.80
4'	$\gamma_D[a g^+]^j$	I+V	3.34	219.00
5'	$\gamma_D[a g^+]^j$	V	0.26	215.84
6'	$\delta_D[g^+g^+]^i$	VI	0.00	219.40
[asp–Na ₂] ^{–n}				
7'	$\gamma_L[g^-g^-]^b$	I+II	20.51	145.76 (167.43)
8'	$\delta_D[g^-g^+]^e$	I+IV	24.85	141.50 (^p)
9'	$\delta_D[g^+g^+]^i$	I+VI	20.36	146.03 (123.73)
10'	$\gamma_D[g^-g^+]^c$	I+II+III	20.13	145.96 (136.59)
11'	$\delta_D[g^+g^+]^i$	II+V+VI	0.00	148.02 (144.46)
[asp–K] [–]				
1''	$\gamma_D[g^-g^+]^c$	II	19.80	177.21
2''	$\gamma_D[g^-g^+]^c$	I+II	10.11	187.15
3''	$\gamma_D[g^-g^+]^k$	I+IV	3.08	193.94
4''	$\gamma_D[a g^+]^l$	VI	0.00	197.09
[asp–K ₂] ^{–o}				
5''	$\gamma_L[g^-g^-]^b$	I+II	16.90	^p (128.66)
6''	$\delta_D[g^-g^+]^e$	I+IV	22.31	^p
7''	$\delta_D[g^+g^+]^i$	I+VI	19.65	^p (106.10)
8''	$\gamma_D[g^-g^+]^c$	I+II+III	15.17	116.04 (^p)
9''	$\delta_D[g^+g^+]^i$	II+V+VI	0.00	130.54 (126.04)

^a In kcal/mol with ZPE corrections. ^b Identical to $\delta_L[g^-g^-]$. ^c Identical to $\delta_D[g^-g^+]$. ^d Identical to $\alpha_L[g^-a]$. ^e Identical to $\alpha_L[g^-g^+]$. ^f Identical to $\alpha_L[a g^-]$. ^g Identical to $\alpha_L[g^-g^-]$. ^h Identical to $\alpha_L[a g^+]$. ⁱ Identical to $\alpha_L[g^+g^+]$. ^j Identical to $\alpha_L[a g^-]$. ^k Identical to $\alpha_L[g^-g^-]$. ^l Identical to $\alpha_L[a g^-]$. ^m based on the [asp–Li][–] complex components, types p and q in parenthesis, as presented in Figure A17. ⁿ based on the [asp–Na][–] complex components, types p and q in parenthesis, as presented in Figure A18. ^o based on the [asp–K][–] complex components, types p and q in parenthesis, as presented in Figure A19. ^r No corresponding [asp–M][–] complex components is found.

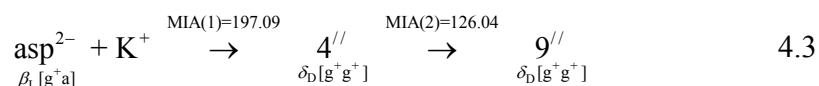
4.2.1.2 Sodium complexes

The B3LYP/6-311++G(d,p)-optimized structures of [asp-Na]⁻ and [asp-Na₂] complex conformers are shown in Figure A18. Six and five conformers for mono and dinuclear complexes of the Na⁺/asp²⁻ system were found. The most stable conformer for [asp-Na]⁻ and [asp-Na₂] were shown in Figure 4.5. The relative energies of [asp-Na]⁻ and [asp-Na₂] complex conformers, respectively, related to the complex conformers **6'** and **11'** are listed in Table 4.6. The monosodium complexes **1'**, **2'**, **5'** and **6'** are single mode of types I, II, V and VI, respectively, but **3'** and **4'** are combination modes of types I + II and I + V, respectively. The disodium complexes, **7'**, **8'**, **9'**, **10'** and **11'** are all the combination modes. The relative stabilities of the [asp-Na]⁻ and [asp-Na₂] complex conformers are in decreasing order: **6'** > **5'** > **4'** > **3'** > **1'** ≈ **2'** and **11'** > **10'** ≈ **9'** ≈ **7'** > **8'**, respectively. The MIAs of the [asp-Na]⁻ and [asp-Na₂] complex conformers are within the narrow ranges of 195.62–17.92 and 124.91–55.58 kcal/mol, respectively. The most preferable feature of the conformational reaction of the Na⁺/asp²⁻ complex system can therefore be proposed as:



4.2.1.3 Potassium complexes

The B3LYP/6-311++G(d,p) optimized structures of [asp-K]⁻ and [asp-K₂] complex conformers are shown in Figure A19. The most stable conformer for [asp-K]⁻ and [asp-K₂] were shown in Figure 4.5. All mono and di-potassium complexes except **1''** and **4''** are combination modes. The relative stabilities of [asp-K]⁻ and [asp-K₂] complex conformers are in decreasing order: **4''** > **3''** > **2''** > **1''** and **9''** > **8''** > **5''** > **7''** > **6''**, respectively. The relative energies of [asp-K]⁻ and [asp-K₂] complex conformers, respectively, related to the complex conformers **4''** and **9''** are listed in Table 4.6. The MIAs of the [asp-K]⁻ and [asp-K₂] complex conformers are within the narrow ranges of 177.21–197.09 and 106.10–130.54 kcal/mol, respectively. The most preferable feature of the conformational reaction of the K⁺/asp²⁻ complex system can therefore be proposed as:



4.2.1.4 Binding energies of aspartate complexes

Relative binding energies of the complexation reactions of $[\text{asp-M}]^-$ and $[\text{asp-M}_2]$ are in decreasing order: $[\text{asp-Li}]^- > [\text{asp-Na}]^- > [\text{asp-K}]^-$ and $[\text{asp-Li}_2] > [\text{asp-Na}_2] > [\text{asp-K}_2]$, respectively. The pre-organization energies of aspartate anion based on the structure changes from the isolated to the $[\text{asp-M}]^-$ complex forms and $[\text{asp-M}]^-$ to $[\text{asp-M}_2]$ complexes forms computed at the B3LYP/6-311++G(d,p) level are reported in Table 4.7. Thermodynamic quantities of the formation reaction of the most stable complex conformers of $[\text{asp-M}]^-$ and $[\text{asp-M}_2]$ complexes computed at the B3LYP/6-311++G(d,p) level are shown in Table 4.8. The BSSE-corrected energies of the most stable complex formers were obtained and shown that they are not very different from their non-corrected energies. The E_{HOMO} , E_{LUMO} and Frontier molecular orbital energy gap, $\Delta E_{\text{HOMO-LUMO}}$ of the alkali cations, free ligand, and all the most stable complex conformers for $[\text{asp-M}]^-$ and $[\text{asp-M}_2]$ complexes computed at the B3LYP/6-311++G(d,p) level are shown in Table 4.9. Relative reactivities of $[\text{asp-M}]^-$ and $[\text{asp-M}_2]$ complexes are in order: $[\text{asp-K}]^- > [\text{asp-Na}]^- > [\text{asp-Li}]^-$ and $[\text{asp-K}_2] > [\text{asp-Na}_2] > [\text{asp-Li}_2]$, respectively, but their absolute values are not very different. As the energy gap for K^+ and Na^+ cations are, respectively, lower than Na^+ and Li^+ cations by 0.38 and 0.88 eV, their relative reactivities are correspondingly in decreasing order: $\text{K}^+ > \text{Na}^+ > \text{Li}^+$.

สถาบันวิทยบริการ
จุฬาลงกรณ์มหาวิทยาลัย

Table 4.7 Pre-organization energies of aspartate dianion (asp^{2-}) in the formation reaction of the most stable $[\text{asp-M}]^-$ and $[\text{asp-M}_2]$ complexes

Reaction	$\Delta E_{\text{preog}}^a$	$\Delta E_{\text{ZPE,preog}}^{a,b}$	$\Delta H_{\text{preog}}^a$	$\Delta G_{\text{preog}}^a$
$\text{asp}^{2-} \rightarrow [\text{asp}^{2-}]_9$	28.44	30.08	28.98	32.17
$\text{asp}^{2-} \rightarrow [\text{asp}^{2-}]_{6'}$	21.42	22.36	21.69	22.29
$\text{asp}^{2-} \rightarrow [\text{asp}^{2-}]_{4''}$	20.64	21.70	21.02	23.00
$[\text{asp}^{2-}]_9 \rightarrow [\text{asp}^{2-}]_{16}$	14.21	13.99	14.30	13.83
$[\text{asp}^{2-}]_{6'} \rightarrow [\text{asp}^{2-}]_{11'}$	16.39	16.68	17.18	17.49
$[\text{asp}^{2-}]_{4''} \rightarrow [\text{asp}^{2-}]_{9''}$	13.50	13.58	14.12	12.82

^a In kcal/mol. ^b The ZPVE corrected energies.

Table 4.8 Thermodynamic quantities of the formation reaction of the most stable complex conformers for $[\text{asp-M}]^-$ and $[\text{asp-M}_2]$ complexes

Reaction	ΔE^a	BSSE ^a	ΔE_{BSSE}^a	MIA ^a	$\Delta G_{298}^{\circ a}$
$\text{asp}^{2-} + \text{Li}^+ \rightarrow [\text{asp-Li}]^-$	-253.76	1.79	-251.97	254.86	-245.46
$\text{asp}^{2-} + \text{Na}^+ \rightarrow [\text{asp-Na}]^-$	-218.76	2.35	-216.41	219.40	-210.25
$\text{asp}^{2-} + \text{K}^+ \rightarrow [\text{asp-K}]^-$	-193.55	1.50	-192.05	197.09	-185.45
$[\text{asp-Li}]^- \rightarrow [\text{asp-Li}_2]$	-154.77	2.65	-152.12	155.88	-146.57
$[\text{asp-Na}]^- \rightarrow [\text{asp-Na}_2]$	-143.79	0.70	-143.09	144.46	-135.12
$[\text{asp-K}]^- \rightarrow [\text{asp-K}_2]$	-125.52	2.61	-122.91	126.04	-117.32

^a In kcal/mol. ^b $\text{MIA}(1) = -[H_{[\text{asp-M}]^-}^{\circ} - (H_{\text{asp}^{2-}}^{\circ} + H_{\text{M}^+}^{\circ})]$ for $[\text{asp-M}]^-$ complexation and $\text{MIA}(2) = -[H_{[\text{asp-M}_2]}^{\circ} - (H_{[\text{asp-M}]^-}^{\circ} + H_{\text{M}^+}^{\circ})]$ for $[\text{asp-M}_2]$ complexation.

Bond distances between the alkali metal cation and the amino-nitrogen atom of the aspartate ion of the most stable complex conformers of $[\text{asp-M}]^-$ and $[\text{asp-M}_2]$ are 2.073 and 2.049 Å for the lithium, 2.427 and 2.410 Å for sodium and 2.786 and 2.789 Å for potassium complex systems, respectively (see Table 4.10). Bond distances between the alkali metal cations and the oxygen atoms of the aspartate ions are within 1.804–1.909 Å for the lithium, 2.199–2.453 Å for sodium and 2.501–2.784 Å for potassium complex systems. Relative bond distances between the alkali metal cation M^+ and the binding atoms of the aspartate ion in $[\text{asp-M}]^-$ and $[\text{asp-M}_2]$ complexes are in decreasing order: $\text{K}^+ > \text{Na}^+ > \text{Li}^+$. [40]

Table 4.9 The E_{HOMO} , E_{LUMO} and frontier molecular orbital energy gap, $\Delta E_{\text{HOMO-LUMO}}$ of free ligand, and various most stable complex conformers for $[\text{asp-M}]^-$ and $[\text{asp-M}_2]$ complexes

Species	$\Delta E_{\text{HOMO-LUMO}}^{\text{a}}$	$\eta^{\text{a,b}}$	$\mu^{\text{a,c}}$	$\chi^{\text{a,d}}$
Li^+	2.026	1.013	-1.018	1.018
Na^+	1.142	0.571	-0.590	0.590
K^+	0.754	0.377	-0.439	0.439
asp^{2-}	0.161	0.080	0.146	-0.146
$[\text{asp-Li}]^-$	0.237	0.118	-0.134	0.134
$[\text{asp-Na}]^-$	0.227	0.114	-0.128	0.128
$[\text{asp-K}]^-$	0.220	0.110	-0.128	0.128
$[\text{asp-Li}_2]$	0.250	0.125	-0.140	0.140
$[\text{asp-Na}_2]$	0.236	0.118	-0.135	0.135
$[\text{asp-K}_2]$	0.218	0.109	-0.133	0.133

^a In eV. ^b Chemical hardness, $\eta = \Delta E_{\text{HOMO-LUMO}}/2$. ^c Electronic chemical potential, $\mu = (E_{\text{HOMO}} + E_{\text{LUMO}})/2$. ^d The Mulliken electronegativity, $\chi = -(E_{\text{HOMO}} + E_{\text{LUMO}})/2$.

Table 4.10 Bond distances of alkali metal cations and binding atoms of aspartate ions in the most stable complex conformers $[\text{asp-M}]^-$ and $[\text{asp-M}_2]$

Bonds	Complex/Distances ^a					
	$[\text{asp-Li}]^-$	$[\text{asp-Na}]^-$	$[\text{asp-K}]^-$	$[\text{asp-Li}_2]$	$[\text{asp-Na}_2]$	$[\text{asp-K}_2]$
$\text{M}^+-\text{N}^{\text{b}}$	2.073	2.427	2.786	2.049	2.410	2.789
$\text{M}^+-\text{O}_1^{\text{b}}$	1.853	2.199	2.517	1.909	2.263	2.588
$\text{M}^+-\text{O}_3^{\text{b}}$	1.804	2.206	2.543	1.894	2.202	2.508
$\text{M}^+-\text{O}_1^{\text{c}}$	–	–	–	1.959	2.453	2.784
$\text{M}^+-\text{O}_2^{\text{c}}$	–	–	–	2.174	2.298	2.591
$\text{M}^+-\text{O}_3^{\text{c}}$	–	–	–	1.888	2.194	2.501

^a In Angstrom. ^b Refers to the M^+_{q} of complex $[\text{asp-M}_2]$ ^c Refers to the M^+_{p} of complex $[\text{asp-M}_2]$.

สถาบันวิทยบริการ
จุฬาลงกรณ์มหาวิทยาลัย

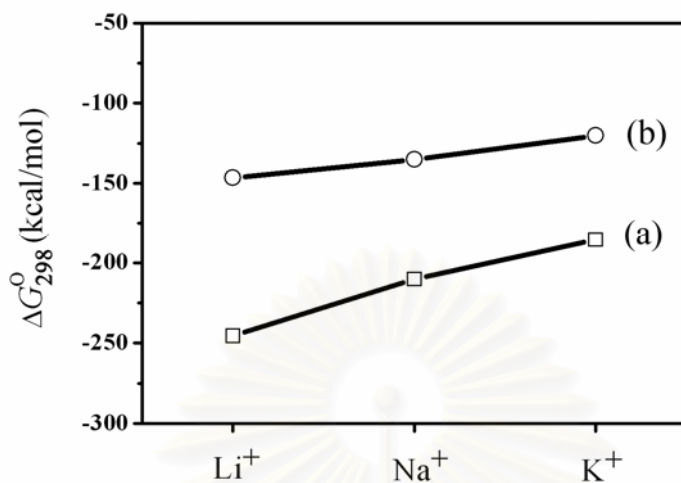


Figure 4.6 Plot of complexation free energies of the (a) $[\text{asp-M}]^-$ ($-\square-\square-\square-$) and (b) $[\text{asp-M}_2]$ ($-\circ-\circ-\circ-$) against sizes of the alkali metal ions M ($M = \text{Li}^+, \text{Na}^+$ and K^+).

4.2.2 Conformational analysis of alkali metal complexes of anionic species of aspartic acid

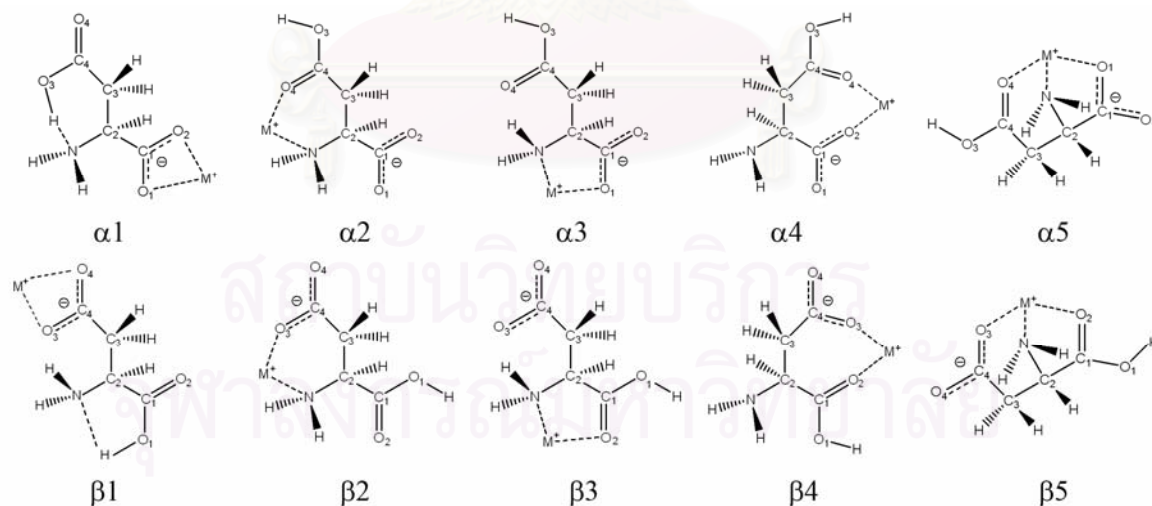


Figure 4.7 The possible binding modes of Hasp^- ligand toward cations.

The B3LYP/6-311++G(d,p)-optimized structures of free-form zwitter-anionic conformers (Hasp⁻) based on two conformational types of α -[NH₂·CH(CH₂·COOH)COO⁻] and β -[NH₂·CH(CH₂·COO⁻)COOH] are shown in Figure A24. It shows that there are at least seven types of free-form conformers of [Hasp-M], M = Li⁺, Na⁺, K⁺ complexes as four α -[Hasp-M] and three β -[Hasp-M] complexes species. Possible binding modes of Hasp⁻ aspartate binding atoms toward the alkali metal cations, M = Li⁺, Na⁺, K⁺ are defined as displayed in Figure 4.7. As 10 possible binding modes, five for α -[Hasp-Li] and another five for β -[Hasp-Li] are defined as single binding mode, others combined modes can be possibly defined as combination of these single modes such as a combined mode of $\alpha 1 + \alpha 2$. As the binding mode is defined as the ratio of the number of metal ion (N_M) to the number of binding site of the ligand (N_L), the $N_M:N_L$ ratios are 1:1 for binding mode types $\alpha 1$ and $\beta 1$, 1:2 for types $\alpha 2$ - $\alpha 4$ and $\beta 2$ - $\beta 4$, and 1:3 for types $\alpha 5$ and $\beta 5$.

4.2.2.1 Lithium complexes

The B3LYP/6-311++G(d,p)-optimized structures of α - and β -[Hasp-Li] complex conformers and their conversion reactions are shown in Figures A25 and A26, Appendix, respectively. At least a transition state for interconversion between two [Hasp-Li] complex conformers has been found. Eleven and seventeen interconversion equilibria for α - and β -[Hasp-Li] complexes conformers were found respectively and categorized as five single-step and three double-steps reactions for α -[Hasp-Li] complex system, and two single-step, two double-steps, one tetra-steps and one hepta-steps reactions for β -[Hasp-Li] complex system as shown in Figures A25 and A26. The most stable conformer of [Hasp-Li] complex system is the conformer **19** as shown in Figure 4.8. The relative B3LYP/6-311++G(d,p) energies, MIAs and DPEs for [Hasp-Li] complex species are tabulated in Table 4.13. It shows that [Hasp-Li] complex conformers are mostly in the single binding mode, except conformers **7-11** for α -[Hasp-Li] complex type, conformers **28, 29, 37-39** for β -[Hasp-Li] complex type.

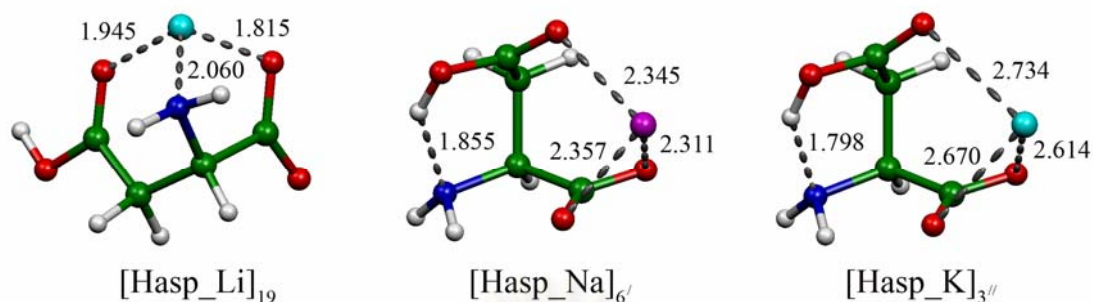


Figure 4.8 The most stable conformer of [Hasp–Li], [Hasp–Na] and [Hasp–K] complexes. Distances are in Å.

The relative stabilities of [Hasp–Li] complexes are in decreasing order: **19 > 39 ≈ 8 > 33 ≈ 11 > 6 > 22 ≈ 36 ≈ 25 ≈ 3 > 17 > 18 > 15 ≈ 2 > 4 ≈ 32 ≈ 20 > 38 ≈ 14 ≈ 21 ≈ 5 ≈ 9 ≈ 24 > 28 > 10 ≈ 29 ≈ 7 ≈ 27 > 1 > 26 > 35 > 37 > 16 > 34 > 13 > 31 > 12 > 30**. Maximum values of MIA and DPE are found in the conformers **19** and **11**, respectively. The MIAs and DPEs of all [Hasp–Li] complexes are within 129.15–169.76 kcal/mol and 302.56–344.05 kcal/mol, respectively. Interconversion reactions between 2 of 39 [Hasp–Li] complexes with their transition states and their energies, thermodynamic properties, rate and equilibrium constants are shown in Table 4.12. Based on our previous work on dianionic–cation [asp–M][–] complexes [40], the most stable complex conformer of [Hasp–Li] is similar to [asp–Li][–]. The Hasp[–] in the complex form adopted to be tri–dentate ligand binding with lithium cation by using N–amino, α– and β–oxygen atoms, respectively. The aspartic acid ligand in either [Hasp–Li] or [asp–Li][–] complexes are similar in backbone conformation (δ_D) but slightly different in side–chain conformation (g^+a for [Hasp[–]Li] and g^+g^+ for [asp–Li][–]). MIA of [Hasp–Li] (169.76 kcal/mol) is very lower than that of [asp–Li] (254.86 kcal/mol).

Table 4.11 Relative B3LYP/6–311++G(d,p) energies, MIAs and DPEs for α -[Hasp–Li] and β -[Hasp–Li] complexes

Complexes/ systems	Aspartate conformations	Binding Mode	ΔE^a	MIA ^a	DPE ^a
α -[Hasp–Li]					
1	$\gamma_L [g^+ g^-]^b$	$\alpha 1$	10.80	148.11	336.70
2	$\gamma_L [g^- g^-]^c$	$\alpha 1$	7.30	161.92	340.20
3	$\gamma_L [g^- a]^d$	$\alpha 1$	5.65	163.90	341.84
4	$\gamma_D [a a]^e$	$\alpha 1$	7.33	161.85	340.16
5	$\alpha_D [a g^+]^f$	$\alpha 1$	8.27	161.17	339.23
6	$\alpha_D [a g^-]^g$	$\alpha 1$	4.20	147.31	343.29
7	$\alpha_L [g^+ g^-]^h$	$\alpha 1 + \alpha 4$	9.18	150.49	316.17
8	$\gamma_D [g^+ a]^i$	$\alpha 1 + \alpha 4$	2.70	166.86	322.66
9	$\gamma_D [g^+ g^-]^j$	$\alpha 1 + \alpha 4$	8.47	160.55	316.89
10	$\gamma_D [a g^-]^k$	$\alpha 1 + \alpha 4$	9.14	160.86	338.35
11	$\gamma_D [a g^+]^l$	$\alpha 1 + \alpha 4$	3.44	166.65	344.05
12	$\gamma_L [g^- g^+]^m$	$\alpha 2$	31.72	138.08	302.59
13	$\gamma_D [g^- g^-]^n$	$\alpha 2$	24.07	145.55	310.24
14	$\delta_D [g^- g^-]^o$	$\alpha 3$	8.16	142.75	330.03
15	$\delta_D [g^- a]^p$	$\alpha 3$	7.24	162.41	330.95
16	$\gamma_L [a g^-]^q$	$\alpha 4$	13.52	156.36	308.16
17	$\gamma_L [a g^+]^r$	$\alpha 4$	6.44	163.24	315.24
18	$\delta_D [g^+ g^-]^s$	$\alpha 5$	6.72	163.22	312.36
19	$\delta_D [g^+ a]^t$	$\alpha 5$	0.00	169.76	319.09
β -[Hasp–Li]					
20	$\epsilon_D [g^- g^+]^{a1}$	$\beta 1$	7.46	154.65	339.71
21	$\gamma_D [g^- g^-]^{b1}$	$\beta 1$	8.24	155.06	338.94
22	$\delta_D [g^- g^-]^{c1}$	$\beta 1$	5.00	140.34	342.17
23	$\gamma_D [a g^-]^{d1}$	$\beta 1$	9.22	153.96	337.95
24	$\epsilon_D [a a]^{e1}$	$\beta 1$	8.55	153.44	338.63
25	$\epsilon_D [a g^-]^{f1}$	$\beta 1$	5.30	149.03	341.88
26	$\gamma_D [g^- g^+]^{g1}$	$\beta 2$	11.42	152.02	322.90
27	$\gamma_D [g^- g^-]^{h1}$	$\beta 2$	9.24	153.03	327.16
28	$\epsilon_D [g^- g^+]^{i1}$	$\beta 1 + \beta 2$	9.02	153.41	327.37
29	$\gamma_D [g^- g^+]^{j1}$	$\beta 1 + \beta 2$	10.83	152.79	336.35
30	$\delta_D [g^- g^-]^{k1}$	$\beta 3$	34.48	129.15	303.72
31	$\beta_L [g^- g^+]^{l1}$	$\beta 3$	27.74	134.83	310.45
32	$\delta_D [g^+ g^+]^{m1}$	$\beta 5$	7.43	156.31	311.66
33	$\beta_L [g^+ g^+]^{n1}$	$\beta 5$	3.09	159.46	315.99
34	$\beta_L [a g^+]^{o1}$	$\beta 4$	19.12	142.92	302.56
35	$\delta_D [a g^+]^{p1}$	$\beta 4$	11.98	151.37	309.70
36	$\delta_D [a g^-]^{q1}$	$\beta 4$	5.04	149.44	316.64
37	$\beta_L [a g^-]^{r1}$	$\beta 1 + \beta 4$	12.53	149.60	311.61
38	$\delta_L [a g^-]^{s1}$	$\beta 1 + \beta 4$	7.94	155.72	316.20
39	$\alpha_D [a g^-]^{t1}$	$\beta 1 + \beta 4$	2.20	152.50	321.94

^a In kcal/mol with ZPE correction, ^b Identical to $\delta_L [g^- g^+]$, ^c Identical to $\delta_L [g^- g^+]$, ^d Identical to $\delta_L [g^- a]$, ^e Identical to $\alpha_L [a a]$, ^f Identical to $\gamma_L [a g^+]$, ^g Identical to $\gamma_L [a g^-]$, ^h Identical to $\delta_D [g^+ g^-]$, ⁱ Identical to $\gamma_D [g^+ a]$, ^j Identical to $\gamma_D [g^+ g^+]$, ^k Identical to $\alpha_L [a g^-]$, ^l Identical to $\delta_L [a g^+]$, ^m Identical to $\gamma_L [g^- g^+]$, ⁿ Identical to $\gamma_L [g^- g^-]$, ^o Identical to $\alpha_L [g^- g^+]$, ^p Identical to $\delta_D [g^- a]$, ^q Identical to $\epsilon_L [a g^-]$, ^r Identical to $\epsilon_L [a g^+]$, ^s Identical to $\beta_L [g^+ g^+]$, ^t Identical to $\beta_L [g^+ a]$, ^{a1} Identical to $\gamma_D [g^- g^+]$, ^{b1} Identical to $\epsilon_D [g^- g^-]$, ^{c1} Identical to $\beta_L [g^- g^-]$, ^{d1} Identical to $\epsilon_D [a g^-]$, ^{e1} Identical to $\gamma_D [a a]$, ^{f1} Identical to $\gamma_D [a g^-]$, ^{g1} Identical to $\delta_D [g^- g^+]$, ^{h1} Identical to $\beta_L [g^+ g^+]$, ⁱ¹ Identical to $\delta_D [g^+ g^+]$, ^{j1} Identical to $\delta_D [a g^+]$, ^{k1} Identical to $\beta_L [a g^+]$, ^{l1} Identical to $\beta_L [a g^-]$, ^{m1} Identical to $\delta_D [a g^-]$.

Table 4.12 Thermodynamic quantities, equilibrium and rate constants of conversion reactions of the [Hasp–Li] complex systems, computed at B3LYP/6–311++G(d,p) level of theory

Reactions ^a /systems	$\Delta^{\ddagger}E^b$	$\Delta^{\ddagger}G^b$	ΔE_{298}^b	ΔH_{298}^b	ΔG_{298}^b	K_{298}	k_{298}^c
1 → TSr1_2 → 2	31.15	31.30	-3.50	-3.26	-3.74	5.51 x 10 ⁻²	7.05 x 10 ⁻¹¹
2 → TSt2_3 → 3	10.06	11.00	-1.65	-1.70	-1.42	1.09 x 10 ¹	5.35 x 10 ⁴
4 → TSt4_5 → 5	32.61	32.92	0.94	0.97	0.73	2.90 x 10 ⁻¹	4.56 x 10 ⁻¹²
5 → TSr5_6 → 6	6.30	7.58	-4.07	-4.73	-1.52	1.30 x 10 ¹	1.72 x 10 ⁷
7 → TSr7_8 → 8	27.69	28.51	-5.77	-5.83	-4.76	3.09 x 10 ⁰	7.19 x 10 ⁻⁹
8 → TSt8_9 → 9	10.47	10.88	6.49	6.60	6.38	2.09 x 10 ⁰	6.62 x 10 ⁴
10 → TSt10_11 → 11	27.92	28.31	-6.72	-6.82	-6.19	3.43 x 10 ⁴	1.09 x 10 ⁻⁸
12 → TSt12_13 → 13	27.72	27.83	-5.70	-5.81	-5.64	1.34 x 10 ⁴	2.47 x 10 ⁻⁸
14 → TSt14v15 → 15	33.73	34.34	-0.92	-1.70	-0.18	1.34 x 10 ⁰	4.14 x 10 ⁻¹³
16 → TSt16_17 → 17	27.38	27.45	-7.65	-7.76	-7.56	3.50 x 10 ⁵	4.66 x 10 ⁻⁸
18 → TSt18_19 → 19	10.60	11.00	-1.65	-1.70	-1.42	1.09 x 10 ¹	5.35 x 10 ⁴
20 → TSt20_21 → 21	32.98	32.98	0.77	0.80	0.71	3.06 x 10 ⁻¹	4.16 x 10 ⁻¹²
21 → TSr21_22 → 22	10.62	10.80	-3.23	-3.60	-2.50	6.82 x 10 ¹	7.46 x 10 ⁴
23 → TSt23_24 → 24	31.16	31.67	-0.68	-0.66	-0.62	2.86 x 10 ⁰	3.76 x 10 ⁻¹¹
24 → TSr24_25 → 25	7.16	7.98	-3.25	-3.54	-2.24	4.39 x 10 ¹	8.77 x 10 ⁶
26 → TSt26_27 → 27	32.27	32.39	-2.18	-2.20	-2.15	3.76 x 10 ¹	1.12 x 10 ⁻¹¹
27 → TSr27_29 → 29	2.61	3.70	-0.21	-0.38	0.65	3.30 x 10 ⁻¹	1.20 x 10 ¹⁰
28 → TSt28_29 → 29	34.03	33.94	1.80	1.81	1.68	5.83 x 10 ⁻²	8.21 x 10 ⁻¹³
26 → TSr26_28 → 28	2.47	3.49	-0.59	-0.77	0.19	7.31 x 10 ⁻¹	1.72 x 10 ¹⁰
30 → TSt30_31 → 31	28.97	29.25	-6.74	-6.87	-6.44	5.25 x 10 ⁴	2.24 x 10 ⁻⁹
32 → TSt32_33 → 33	30.73	30.87	-4.33	-4.35	-4.31	1.45 x 10 ³	1.45 x 10 ⁻¹⁰
34 → TSt34_35 → 35	26.74	26.72	-7.41	-7.26	-6.80	9.74 x 10 ⁴	1.60 x 10 ⁻⁷
35 → TSr35_36 → 36	8.82	9.31	-6.94	-7.19	-6.53	6.12 x 10 ⁴	9.29 x 10 ⁵
35 → TSr35_38 → 38	0.54	1.87	-4.04	-4.34	-2.71	9.64 x 10 ¹	2.63 x 10 ¹¹
34 → TSr34_37 → 37	0.0013	1.61	-6.59	-6.68	-5.64	1.35 x 10 ⁴	4.09 x 10 ¹¹
37 → TSt37_38 → 38	32.86	32.88	4.59	4.93	3.88	1.44 x 10 ⁻³	4.91 x 10 ⁻¹²
38 → TSr38_39 → 39	12.85	12.02	-5.74	-5.91	-5.51	1.10 x 10 ⁴	9.64 x 10 ³
36 → TSr36_39 → 39	13.31	14.24	-2.83	-3.06	-1.69	1.73 x 10 ¹	2.26 x 10 ²

^a The letters 'r' and 't' specify for the rotational (about C_β-CO₂ bond) transition-state and proton-transfer transition-state, respectively. ^b In kcal/mol. ^c In s⁻¹.

4.2.2.2 Sodium complexes

The B3LYP/6–311++G(d,p)-optimized structures of [Hasp–Na] complex conformers and their conversion reactions are shown in Figures A27 and A28, respectively. At least a transition state for interconversion between two [Hasp–Na] complex conformers has been found. Seven and six interconversion equilibria for α - and β -[Hasp–Na] complexes conformers were found respectively and categorized as three single-step and two double-steps reactions for α -[Hasp–Na] complex system, and four single-step and one double-steps for β -[Hasp–Na] complex system as shown in Figures

A27 and A28. The most stable conformer of [Hasp–Na] complex system is the conformer **6'** as shown in Figure 4.8. The gas and aqueous phase relative B3LYP/6–311++G(d,p) energies, MIAs and DPEs for [Hasp–Na] complex species are tabulated in Table 4.13. It shows that [Hasp–Na] complex conformers are mostly in the single binding mode, except conformers **4'–6'**, **9'** and **10'** for α -[Hasp–Na] complex type, conformers **18'**, **19'**, **22'** and **23'** for β -[Hasp–Na] complex type.

The relative stabilities of [Hasp–Na] complexes are in decreasing order: **6' > 23' > 5' > 10' > 3' = 17' > 12' > 8' > 15' > 1' > 22' > 2' = 21' \approx 13' > 7' > 14' > 16' = 19' > 9' > 4' > 18' > 11' > 20'**. Maximum values of MIA and DPE are both found in the conformer **5'**. The MIAs and DPEs of all [Hasp–Na] complexes are within 121.58–142.21 kcal/mol and 317.95–348.91 kcal/mol, respectively. Interconversion reactions between 2 of 23 [Hasp–Na] complexes with their transition states and their energies, thermodynamic properties, rate and equilibrium constants are shown in Table 4.14. Interestingly, the most stable complex conformer of [Hasp–Na] is different to its corresponding dianionic complex [asp–Na][–]. The aspartic ligand adopted as γ_D conformer either in [Hasp–Na] or [asp–Na][–] but different in binding mode of interaction. For the anionic complex, the asp^{2–} ligand binds preferentially with sodium cation as tridentate binding mode using N–amino, α – and β –oxygen atoms, respectively. But for anionic complex [Hasp–Na], the Hasp[–] ligand preferred to bind with the cation using two α –oxygen and one β –oxygen atoms, respectively.

Table 4.13 Relative B3LYP/6–311++G(d,p) energies, MIAs and DPEs of minima for α -[Hasp–Na] and β -[Hasp–Na] complexes

Complexes/ systems	Aspartate conformations	Binding Mode	ΔE^a	MIAs ^a	DPE ^a
α -[Hasp–Na]					
1'	$\gamma_L [g^- a]^b$	$\alpha 1$	4.40	139.49	346.48
2'	$\gamma_L [g^- g^-]^c$	$\alpha 1$	6.09	137.92	344.69
3'	$\gamma_L [g^+ g^-]^d$	$\alpha 1$	2.53	131.17	348.26
4'	$\alpha_D [a g^+]^e$	$\alpha 1$	8.41	135.78	342.37
5'	$\alpha_D [a g^+]^f$	$\alpha 1$	1.88	142.21	348.91
6'	$\gamma_D [a a]^g$	$\alpha 1$	0.00	133.88	329.05
7'	$\alpha_L [g^+ g^-]^h$	$\alpha 1 + \alpha 4$	6.24	137.59	344.54
8'	$\gamma_D [g^+ g^+]^i$	$\alpha 1 + \alpha 4$	4.12	121.58	346.66
9'	$\gamma_D [a g^-]^j$	$\alpha 1 + \alpha 4$	8.12	135.86	321.19
10'	$\gamma_D [a g^+]^k$	$\alpha 1 + \alpha 4$	2.36	142.02	326.95
11'	$\delta_D [g^+ g^-]^l$	$\alpha 5$	10.72	133.41	318.33
12'	$\delta_D [g^+ a]^m$	$\alpha 5$	3.76	140.69	325.29
β -[Hasp–Na]					
13'	$\varepsilon_D [g^- g^+]^{b1}$	$\beta 1$	6.14	136.88	344.88
14'	$\gamma_D [g^- g^+]^{c1}$	$\beta 1$	6.72	137.47	344.31
15'	$\delta_D [g^- g^+]^{d1}$	$\beta 1$	4.33	130.68	346.69
16'	$\varepsilon_D [a a]^{e1}$	$\beta 1$	7.87	134.98	343.16
17'	$\varepsilon_D [a g^-]^{f1}$	$\beta 1$	2.53	123.17	348.50
18'	$\gamma_D [g^- g^+]^{c1}$	$\beta 1 + \beta 2$	9.72	134.58	331.85
19'	$\varepsilon_D [g^- g^+]^{b1}$	$\beta 1 + \beta 2$	7.87	135.26	333.70
20'	$\beta_L [g^+ g^-]^{g1}$	$\beta 5$	11.11	133.87	317.95
21'	$\delta_D [g^+ g^-]^{h1}$	$\beta 5$	6.09	137.17	322.96
22'	$\delta_L [a g^-]^{i1}$	$\beta 1 + \beta 4$	5.73	138.59	326.67
23'	$\beta_L [a g^-]^{j1}$	$\beta 1 + \beta 4$	1.41	133.66	330.99

^a In kcal/mol with ZPE correction, ^b Identical to $\delta_L [g^- g^+]$, ^c Identical to $\delta_L [g^- g^-]$, ^d Identical to $\delta_L [g^- a]$, ^e Identical to $\gamma_L [a g^+]$, ^f Identical to $\alpha_L [a a]$, ^g Identical to $\gamma_L [a g^-]$, ^h Identical to $\delta_D [g^+ g^-]$, ⁱ Identical to $\gamma_D [g^+ g^+]$, ^j Identical to $\alpha_L [a g^-]$, ^k Identical to $\delta_L [a g^+]$, ^l Identical to $\beta_L [g^+ g^-]$, ^m Identical to $\beta_L [g^+ a]$, ^{b1} Identical to $\gamma_D [g^- g^+]$, ^{c1} Identical to $\varepsilon_D [g^- g^+]$, ^{d1} Identical to $\beta_L [g^- g^+]$, ^{e1} Identical to $\gamma_D [a a]$, ^{f1} Identical to $\gamma_D [a g^-]$, ^{g1} Identical to $\beta_L [g^+ g^+]$, ^{h1} Identical to $\delta_D [g^+ g^+]$, ⁱ¹ Identical to $\beta_L [a g^-]$, ^{j1} Identical to $\delta_D [a g^-]$.

Table 4.14 Thermodynamic quantities, equilibrium and rate constants of conversion reactions of the [Hasp–Na] complex systems

Reactions ^a /systems	$\Delta^\ddagger E^b$	$\Delta^\ddagger G^b$	ΔE_{298}^b	ΔH_{298}^b	ΔG_{298}^b	K_{298}	k_{298}^c
1' → TS1' 2' → 2'	32.42	32.40	1.69	1.86	1.33	1.06 x 10 ⁻¹	1.11 x 10 ⁻¹¹
2' → TSr2' 3' → 3'	8.33	8.57	-3.56	-4.08	-2.72	9.82 x 10 ¹	3.22 x 10 ⁶
4' → TSr4' 5' → 5'	26.50	27.05	-6.54	-6.71	-6.06	2.78 x 10 ⁴	9.25 x 10 ⁻⁸
5' → TSr5' 6' → 6'	9.09	9.64	-1.88	-2.22	-1.04	5.82 x 10 ⁰	5.34 x 10 ⁵
7' → TSr7' 8' → 8'	8.02	8.84	-2.12	-2.29	-1.46	1.18 x 10 ¹	2.06 x 10 ⁶
9' → TSr9' 10' → 10'	27.53	27.81	-5.76	-5.87	-5.45	9.96 x 10 ³	2.53 x 10 ⁻⁸
11' → TSr11' 12' → 12'	26.97	27.01	-6.96	-6.99	-6.85	1.05 x 10 ⁵	9.90 x 10 ⁻⁸
13' → TSr13' 14' → 14'	32.30	32.25	0.57	0.58	0.36	5.42 x 10 ⁻¹	1.42 x 10 ⁻¹¹
14' → TSr14' 15' → 15'	10.83	10.90	-2.38	-2.60	-2.08	3.35 x 10 ¹	6.35 x 10 ⁴
16' → TSr16' 17' → 17'	6.27	7.23	-5.34	-5.59	-4.38	1.62 x 10 ³	3.11 x 10 ⁷
18' → TSr18' 19' → 19'	31.85	31.91	-1.85	-1.85	-1.73	1.84 x 10 ¹	2.51 x 10 ⁻¹¹
20' → TSr20' 21' → 21'	33.93	34.40	5.01	4.47	6.15	3.10 x 10 ⁻⁵	3.74 x 10 ⁻¹³
22' → TSr22' 23' → 23'	11.93	11.60	-4.32	-4.47	-4.38	1.63 x 10 ³	1.96 x 10 ⁴

^a The letters 'r' and 't' specify for the rotational (about C_β-CO₂ bond) transition-state and proton-transfer transition-state, respectively. ^b In kcal/mol. ^c In s⁻¹.

4.2.2.3 Potassium complexes

The B3LYP/6-311++G(d,p)-optimized structures of [Hasp–K] complex conformers and their conversion reactions are shown in Figure A29 and A30. At least a transition state for interconversion between two [Hasp–K] complex conformers has been found. Six interconversion equilibria for α -[Hasp–K] and six equilibria for β -[Hasp–K] complexes conformers were found and categorized as four single-step and one double-steps reactions for α -[Hasp–K] complex system, and four single-step and one double-steps for β -[Hasp–K] complex system as shown in Figure A29 and A30. The most stable conformer of [Hasp–K] complex system is the conformer **3''** as shown in Figure 4.8. The relative B3LYP/6-311++G(d,p) energies, MIAs and DPEs for [Hasp–K] complex species are tabulated in Table 4.15. It shows that [Hasp–K] complex conformers are mostly in the single binding mode, except conformers **1''–3''**, **8''**, **9''** for α -[Hasp–K] complex type, conformers **17''**, **18''**, **21''** and **22''** for β -[Hasp–K] complex type.

Table 4.15 Relative B3LYP/6–311++G(d,p) energies, MIAs and DPEs of minima for α -[Hasp–K] and β -[Hasp–K] complexes

Complexes/ systems	Aspartate conformations	Binding Mode	ΔE^a	MIA ^a	DPE ^{a,b}
α -[Hasp–K]					
1''	$\alpha_D [a g^-]^b$	$\alpha 1 + \alpha 4$	8.69	119.77	346.49
2''	$\alpha_D [a g^+]^c$	$\alpha 1 + \alpha 4$	3.37	124.91	351.81
3''	$\gamma_D [a a]^d$	$\alpha 1 + \alpha 4$	0.00	118.05	338.60
4''	$\gamma_L [g^- a]^e$	$\alpha 1$	7.91	120.00	347.27
5''	$\gamma_L [g^- g^-]^f$	$\alpha 1$	7.57	120.77	347.61
6''	$\alpha_L [g^+ g^-]^g$	$\alpha 1$	8.03	119.98	347.14
7''	$\gamma_D [g^+ g^+]^h$	$\alpha 1$	4.57	105.14	350.43
8''	$\gamma_D [a g^-]^i$	$\alpha 1 + \alpha 4$	9.05	119.34	346.13
9''	$\gamma_D [a g^+]^j$	$\alpha 1 + \alpha 4$	3.94	124.28	351.24
10''	$\delta_D [g^+ g^-]^k$	$\alpha 5$	14.97	113.26	320.41
11''	$\delta_D [g^+ a]^l$	$\alpha 5$	8.38	120.14	326.99
β -[Hasp–K]					
12''	$\epsilon_D [g^- g^+]^{b1}$	$\beta 1$	8.08	119.11	347.09
13''	$\gamma_D [g^- g^+]^{c1}$	$\beta 1$	8.68	119.69	346.50
14''	$\delta_D [g^- g^+]^{d1}$	$\beta 1$	5.85	113.34	349.33
15''	$\epsilon_D [a a]^{e1}$	$\beta 1$	9.90	117.11	345.28
16''	$\epsilon_D [a g^-]^{f1}$	$\beta 1$	3.39	106.52	351.79
17''	$\epsilon_D [g^- g^+]^{b1}$	$\beta 1 + \beta 2$	10.43	117.99	335.05
18''	$\gamma_D [g^- g^+]^{c1}$	$\beta 1 + \beta 2$	8.63	118.62	336.85
19''	$\delta_D [g^+ g^+]^{g1}$	$\beta 5$	10.67	116.73	324.70
20''	$\beta_L [g^+ g^+]^{h1}$	$\beta 5$	6.85	121.70	328.52
21''	$\delta_L [a g^-]^{i1}$	$\beta 1 + \beta 4$	7.29	121.17	331.31
22''	$\beta_L [a g^-]^{j1}$	$\beta 1 + \beta 4$	3.01	116.18	335.59

^a In kcal/mol with ZPE correction, ^b Identical to $\gamma_L [a g^-]$, ^c Identical to $\gamma_L [a g^+]$, ^d Identical to $\alpha_L [a a]$, ^e Identical to $\delta_L [g^- g^+]$, ^f Identical to $\delta_L [g^- a]$, ^g Identical to $\delta_D [g^+ g^-]$, ^h Identical to $\gamma_D [g^+ g^+]$, ⁱ Identical to $\alpha_L [a g^-]$, ^j Identical to $\delta_L [a g^+]$, ^k Identical to $\beta_L [g^+ g^-]$, ^l Identical to $\beta_L [g^+ a]$, ^{b1} Identical to $\gamma_D [g^- g^+]$, ^{c1} Identical to $\epsilon_D [g^- g^+]$, ^{d1} Identical to $\beta_L [g^- g^+]$, ^{e1} Identical to $\gamma_D [a a]$, ^{f1} Identical to $\gamma_D [a g^-]$, ^{g1} Identical to $\beta_L [g^+ g^+]$, ^{h1} Identical to $\delta_D [g^+ g^+]$, ⁱ¹ Identical to $\beta_L [a g^-]$, ^{j1} Identical to $\delta_D [a g^-]$.

The relative stabilities of [Hasp–K] complexes are in decreasing order: **3'' > 22'' > 2'' \approx 16'' > 9'' > 7'' > 14'' > 20'' > 21'' > 5'' > 4'' \approx 6'' \approx 12'' > 11'' > 18'' \approx 13'' \approx 1'' > 8'' > 15'' > 17'' > 19'' > 10''**. Maximum values of both MIA and DPE are found in the conformer **2''**. The MIAs and DPEs of all [Hasp–K] complexes are within 105.14–124.91 kcal/mol and 320.41–351.81 kcal/mol, respectively. Interconversion reactions between 2 of 22 [Hasp–K] complexes with their transition states and their energies, thermodynamic properties, rate and equilibrium constants are shown in Table 4.15. As well as sodium complex, the aspartic ligand binds preferentially with potassium cation as

tri-dentate mode. MIA difference between [Hasp-K] (118.05 kcal/mol) and [asp-K]⁻ (197.09 kcal/mol) is not very much when compare to sodium and lithium complexes. [40]

Table 4.16 Thermodynamic quantities, equilibrium and rate constants of conversion reactions of the [Hasp-K] complex systems

Reactions ^a /systems	$\Delta^{\ddagger}E$ ^b	$\Delta^{\ddagger}G$ ^b	ΔE_{298} ^b	ΔH_{298} ^b	ΔG_{298} ^b	K_{298}	k_{298} ^c
1'' → TS1''_2'' → 2''	27.39	27.96	-5.32	-5.43	-4.80	3.28 x 10 ³	1.98 x 10 ⁻⁸
2'' → TSr2''_3'' → 3''	8.44	8.87	-3.37	-3.69	-2.74	1.01 x 10 ²	1.95 x 10 ⁶
4'' → TS4''_5'' → 5''	30.75	30.61	0.34	0.48	0.01	9.82 x 10 ⁻¹	2.25 x 10 ⁻¹⁰
6'' → TSr6''_7'' → 7''	8.01	8.36	-3.28	-3.46	-2.65	8.82 x 10 ¹	4.61 x 10 ⁶
8'' → TSr8''_9'' → 9''	29.19	30.66	-5.11	-5.23	-4.50	1.99 x 10 ³	2.07 x 10 ⁻¹⁰
10'' → TS10''_11'' → 11''	26.85	26.87	-6.59	-6.60	-6.53	6.17 x 10 ⁴	1.25 x 10 ⁻⁷
12'' → TS12''_13'' → 13''	31.80	31.02	0.59	0.60	0.33	5.76 x 10 ⁻¹	1.13 x 10 ⁻¹⁰
13'' → TSr13''_14'' → 14''	10.42	10.34	-2.82	-3.05	-2.50	6.80 x 10 ¹	1.63 x 10 ⁵
15'' → TSr15''_16'' → 16''	4.28	6.30	-6.51	-6.80	-5.37	8.58 x 10 ³	1.50 x 10 ⁸
17'' → TS17''_18'' → 18''	31.35	31.58	-1.80	-1.81	-1.62	1.55 x 10 ¹	4.43 x 10 ⁻¹¹
19'' → TS19''_20'' → 20''	29.92	30.05	-3.82	-3.80	-3.74	5.49 x 10 ²	5.81 x 10 ⁻¹⁰
21'' → TS21''_22'' → 22''	10.09	10.26	-4.28	-4.41	-4.81	3.34 x 10 ³	1.87 x 10 ⁵

^a The letters 'r' and 't' specify for the rotational (about C_β-CO₂ bond) transition-state and proton-transfer transition-state, respectively. ^b In kcal/mol. ^c In s⁻¹.

4.2.2.4 Comparative reactions of aspartate complexes

Formation energies, Gibbs free energies of reaction, MIAs and pre-organization of aspartate conformers to form each complex are shown in Table 4.17. Relative stabilities of [Hasp-M] complexes are in order: [Hasp-Li] > [Hasp-Na] > [Hasp-K]. The BSSE energies for [Hasp-M] complexations are very small. Magnitudes of MIAs of [Hasp-M]-aspartate ligands are in order: [Hasp-Li]-aspartate > [Hasp-Na]-aspartate > [Hasp-K]-aspartate. The complexation reactions in gas phase are more preferable than in aqueous system by 155.47, 125.84 and 111.20 kcal/mol for lithium, sodium and potassium complexes, respectively. The pre-organization energies of [Hasp-M]-aspartate ligands are within a range of 10.20–17.01 kcal/mol (2.82–7.59 kcal/mol in aqueous system) and in order: [Hasp-Li] > [Hasp-Na] > [Hasp-K]. The energy gaps of free form aspartate conformers and their most stable complexes conformers are shown in Table 4.18. Based on the energy gaps, relative reactivities of seven conformers of [Hasp⁻]-ligands are in decreasing order:

$\text{Hasp}_{\text{IV}}^- > \text{Hasp}_{\text{V}}^- > \text{Hasp}_{\text{I}}^- > \text{Hasp}_{\text{II}}^- > \text{Hasp}_{\text{VII}}^- > \text{Hasp}_{\text{VI}}^- > \text{Hasp}_{\text{III}}^-$. Reactivities of $[\text{Hasp-M}]$ complexes are in order: $[\text{Hasp-Li}] > [\text{Hasp-K}] > [\text{Hasp-Na}]$.

Table 4.17 Quantities for the formation reactions of the most stable conformers for $[\text{Hasp-M}]$ complexes and pre-Organization for their aspartate structures

Reaction	$\Delta E^{a,b}$	$BSSE^a$	ΔE_{BSSE}^a	MIA ^a	$\Delta G_{298}^{\circ a}$
<i>Complexation:</i>					
$[\text{Hasp}^-]_{\alpha_{\text{D}}[\text{g}^+\text{a}]} + \text{Li}^+ \rightarrow [\text{Hasp}_{\delta_{\text{D}}[\text{g}^+\text{a}]} \text{Li}]_{19}$	-168.53	1.49	-167.03	169.76	-160.24
$[\text{Hasp}^-]_{\gamma_{\text{L}}[\text{g}^+\text{g}^-]} + \text{Na}^+ \rightarrow [\text{Hasp}_{\gamma_{\text{D}}[\text{a a}]} \text{Na}]_{6'}$	-133.34	0.81	-132.53	133.88	-124.77
$[\text{Hasp}^-]_{\gamma_{\text{L}}[\text{g}^+\text{g}^-]} + \text{K}^+ \rightarrow [\text{Hasp}_{\gamma_{\text{D}}[\text{a a}]} \text{K}]_{3''}$	-117.68	0.36	-117.32	118.05	-109.39
<i>Pre-organization:</i>					
$[\text{Hasp}^-]_{\alpha_{\text{D}}[\text{g}^+\text{a}]} \rightarrow [\text{Hasp}^-]_{\delta_{\text{D}}[\text{g}^+\text{a}]19}$	17.01	–	–	15.74 ^c	19.07
$[\text{Hasp}^-]_{\gamma_{\text{L}}[\text{g}^+\text{g}^-]} \rightarrow [\text{Hasp}^-]_{\gamma_{\text{D}}[\text{a a}]6'}$	13.67	–	–	13.71 ^c	14.12
$[\text{Hasp}^-]_{\gamma_{\text{L}}[\text{g}^+\text{g}^-]} \rightarrow [\text{Hasp}^-]_{\gamma_{\text{D}}[\text{a a}]3''}$	10.20	–	–	10.22 ^c	10.58

^a In kcal/mol. ^b The ZPVE corrected energies. ^c Enthalpy in kcal/mol.

Table 4.18 The frontier molecular orbital energy gap, $\Delta E_{\text{HOMO-LUMO}}$ and various chemical indices of cations, free ligand, and various most stable complex conformers for $[\text{Hasp-M}]$

species	$\Delta E_{\text{HOMO-LUMO}}^a$	$\eta^{a,b}$	$\mu^{a,c}$	$\chi^{a,d}$
Hasp_{I}^- ^e	4.408	2.204	-3.745	3.745
$\text{Hasp}_{\text{II}}^-$ ^f	4.299	2.150	-3.624	3.624
$\text{Hasp}_{\text{III}}^-$ ^g	3.864	1.932	-3.362	3.362
$\text{Hasp}_{\text{IV}}^-$ ^h	5.442	2.721	-3.938	3.938
Hasp_{V}^- ⁱ	4.572	2.286	-3.821	3.821
$\text{Hasp}_{\text{VI}}^-$ ^j	4.027	2.014	-3.487	3.487
$\text{Hasp}_{\text{VII}}^-$ ^k	4.136	2.068	-3.554	3.554
$[\text{Hasp-Li}]_{19}$	4.789	2.395	-3.954	3.954
$[\text{Hasp-Na}]_{6'}$	5.742	2.871	-4.532	4.532
$[\text{Hasp-K}]_{3''}$	5.606	2.803	-4.465	4.465

^a In eV. ^b Chemical hardness, $\eta = \Delta E_{\text{HOMO-LUMO}}/2$. ^c Electronic chemical potential, $\mu = (E_{\text{HOMO}} + E_{\text{LUMO}})/2$. ^d The Mulliken electronegativity, $\chi = -(E_{\text{HOMO}} + E_{\text{LUMO}})/2$. ^e Belongs to $\gamma_{\text{L}}[\text{g}^+\text{g}^-]$ conformation, ^f Belongs to $\gamma_{\text{L}}[\text{g}^+\text{g}^+]$ conformation, ^g Belongs to $\alpha_{\text{D}}[\text{g}^+\text{a}]$ conformation, ^h Belongs to $\gamma_{\text{L}}[\text{a g}^-]$ conformation, ⁱ Belongs to $\delta_{\text{D}}[\text{g}^+\text{g}^+]$ conformation, ^j Belongs to $\alpha_{\text{D}}[\text{g}^+\text{g}^+]$ conformation, ^k Belongs to $\gamma_{\text{D}}[\text{g}^+\text{g}^+]$ conformation.

4.2.2.5 Binding mode and ion size effects

The most stable [Hasp–M] complexes were found as tri-coordinated form ($\alpha 5$ mode) for the lithium complex and as bi-coordinated form ($\alpha 1 + \alpha 4$ combine mode) for the complexes of sodium and potassium as shown Figure 4.8. Table 4.19 shows that the average bond-distances of $M^+ - O$ bond for the [Hasp–M] complexes are in order: [Hasp–K]–bond > [Hasp–Na]–bond > [Hasp–Li]–bond which corresponds to the order of ionic size: potassium ($r_K = 1.548 \text{ \AA}$) > sodium ($r_{Na} = 1.1 \text{ \AA}$) and lithium ($r_{Li} = 0.76 \text{ \AA}$). The ion sizes of potassium and sodium ions obviously affect the coordination of the complexes with Hasp[–] (see Figure 4.8). This ionic size effect has never occurred in their complexes with aspartate dianion (asp^{2–} species). [40]

Table 4.19 Bond distances of alkali metal cations and binding atoms of aspartate ions in the most stable conformers of [Hasp–M] complexes

Bonds/distances ^a	Complexes		
	[Hasp–Li] ^b	[Hasp–Na] ^c	[Hasp–K] ^c
M ⁺ –N	2.060	–	–
M ⁺ –O ₁	1.815	2.357	2.670
M ⁺ –O ₂	–	2.275	2.614
M ⁺ –O ₄	1.945	2.354	2.734

^a In \AA . ^b Defined as $\alpha 5$ binding mode. ^c Defined as $\alpha 1 + \alpha 4$ binding mode.

4.2.2.6 Reaction paths to form [Hasp–M] complexes

As complexation based on the asp^{2–} species is considered, the [Hasp–M] complexes, M = Li⁺, Na⁺ and K⁺ can be formed via protonation and complexation processes using two reaction pathways as shown in Figure 4.9. It shows that top and bottom paths belong to reaction sequences of complexation → protonation and protonation → complexation, respectively. The protonation of asp^{2–} species to form Hasp[–] species being more likely to occur than the complexation of [asp–M][–] to form [Hasp–M] complex. Therefore, protonation → complexation sequence is predicted to be

the most preferable pathway of the [Hasp–M] complex formation. The energies of overall reactions to form complexes with lithium, sodium and potassium are -572.82 , -547.81 and -532.55 kcal/mol, respectively. The conformers of asp^{2-} , Hasp^- , $[\text{asp}-\text{M}]^-$ and $[\text{Hasp}-\text{M}]$ shown in Figure 4.9 are significant because they correspond to their structural reaction coordinates. [41]

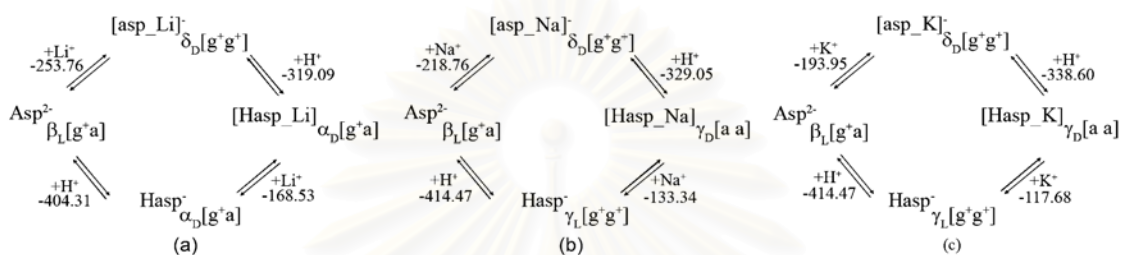


Figure 4.9 The reaction pathways for complexation and protonation of asp^{2-} species to form $[\text{Hasp}-\text{M}]$ complexes of (a) Lithium, (b) Sodium and (c) Potassium. Energies are in kcal/mol.

4.2.3 Conformational analysis of alkali metal complexes of zwitterionic species of aspartic acid

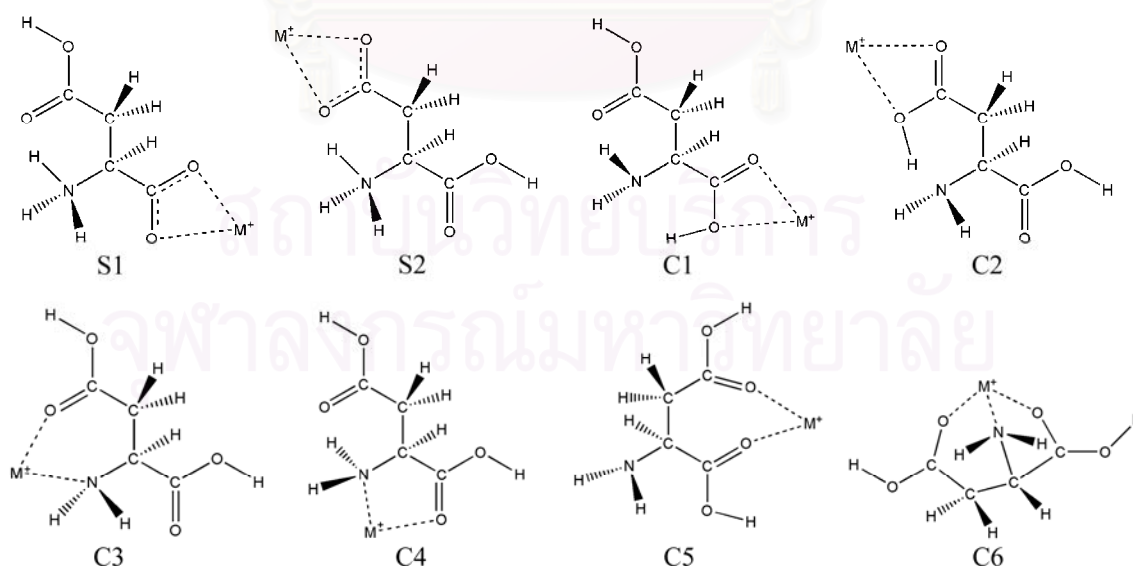


Figure 4.10 The possible binding modes of H_2asp ligand toward cations.

Eight possible binding modes are found for $[\text{H}_2\text{asp-Li}]^+$, two for SB and six for CS structures as shown Figure 4.10. As the binding mode is defined as the ratio of the number of metal ion (N_M) to the number of binding site of the ligand (N_L), the $N_M:N_L$ ratios are 1:1 for binding mode types S1, S2, C1, C2, 1:2 for types C3, C4, C5 and 1:3 for types C6.

4.2.3.1 Lithium Complexes

Fifteen $[\text{H}_2\text{asp-Li}]^+$ complex conformers obtained from structure optimization using the B3LYP/6-311++G(d,p) calculations and their relative energies are shown in Figure A27. The most stable conformer for SB and CS structures of $[\text{H}_2\text{asp-Li}]^+$ complexes are shown in Figure 4.11. The most stable $[\text{H}_2\text{asp-Li}]^+$ complex conformer is the charge-solvated, **CS11** conformer which is the only one of the tri-coordination structure. The MIAs of H_2asp , DPEs of $[\text{H}_2\text{asp-Li}]^+$ complex and their conformations are shown in Table 4.20. It shows that the relative stabilities of these complexes are in order: **CS11** > **CS8** > **CS9** \approx **CS10** > **SB1** > **SB3** > **CS7** > **CS6** \approx **CS5** > **CS2** > **SB4** \approx **CS1** \approx **CS4** > **SB2** > **CS3**. The complex conformer **CS11** is also found to possess the maximum values of MIA and DPE. The MIAs of H_2asp conformer and DPEs for all conformers of their lithium complexes are within the range of 43.41–73.26 and of 208.78–252.08 kcal/mol, respectively. The most stable complex conformer of $[\text{H}_2\text{asp-Li}]^+_{\text{CS11}}$ possess the charge-solvated tri-coordination structure as same as the most stable conformers $[\text{asp-Li}]^-_9$ [40] for di-anionic system and $[\text{Hasp-Li}]_{19}$ [41] for mono-anionic systems as reported in our previous work of which the aspartic acid binds preferentially to lithium ion using amino nitrogen, α - and β -carbonyl oxygen atoms.

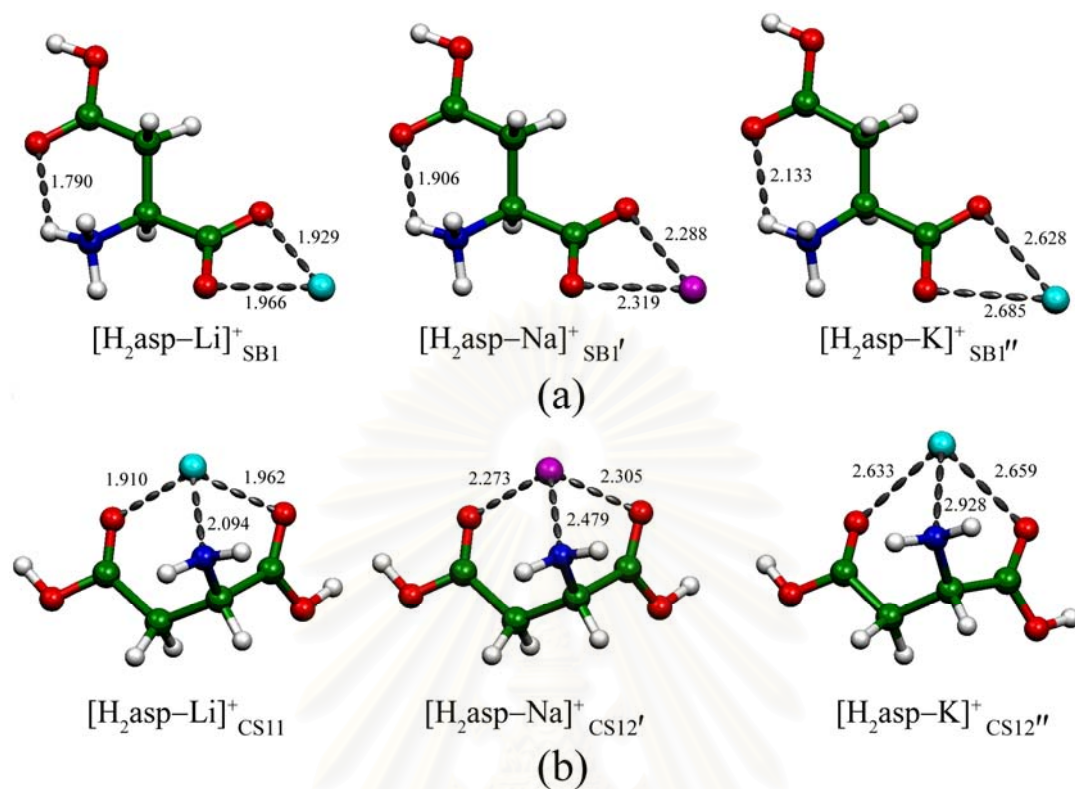


Figure 4.11 The most stable conformer of (a) SB and (b) CS structures of [H₂asp-M]⁺ (M = Li⁺, Na⁺, K⁺) complexes. Distances are in Å.

Table 4.20 Relative energies, MIAs and DPEs of the B3LYP/6–311++G(d,p)–optimized $[\text{H}_2\text{asp-M}]^+$ complex conformers

Complex	Aspartate conformation	Binding mode	ΔE_{rel}^a	MIAs ^a	DPE ^a
$[\text{H}_2\text{asp-Li}]^+$					
SB1	$\gamma_D [g^- g^+]^b$	S1	11.96	60.58	236.68
SB2	$\gamma_L [a g^+]^c$	S1	27.80	43.41	214.24
SB3	$\gamma_D [g^- a]^d$	S2	12.61	59.48	230.23
SB4	$\gamma_L [a a]^e$	S2	20.96	50.51	222.18
CS1	$\varepsilon_D [g^- g^-]^f$	C1	21.19	49.65	221.89
CS2	$\alpha_D [a g^-]^g$	C1	20.37	55.37	224.87
CS3	$\varepsilon_D [a a]^h$	C1	34.36	51.09	220.85
CS4	$\varepsilon_L [a a]^i$	C2	21.60	53.20	222.77
CS5	$\varepsilon_L [a a]^j$	C2	18.62	55.70	208.78
CS6	$\alpha_D [a g^-]^g$	C3	18.55	55.16	226.53
CS7	$\delta_D [g^- g^-]^j$	C3	13.02	60.17	232.07
CS8	$\varepsilon_D [a g^-]^k$	C4	7.02	65.69	237.27
CS9	$\varepsilon_D [a g^-]^k$	C4	9.43	63.43	234.86
CS10	$\gamma_D [g^- g^-]^b$	C5	9.84	63.08	237.84
CS11	$\gamma_D [g^+ g^-]^l$	C6	0.00	73.26	252.08
$[\text{H}_2\text{asp-Na}]^+$					
SB1'	$\gamma_D [g^- g^+]^{b1}$	S1	7.92	43.71	238.37
SB2'	$\gamma_L [a g^+]^{c1}$	S1	21.12	28.87	224.94
SB3'	$\gamma_D [g^- a]^{d1}$	S2	7.97	42.93	238.35
SB4'	$\gamma_L [a a]^{e1}$	S2	16.06	34.15	230.21
CS1'	$\varepsilon_D [g^- g^-]^{f1}$	C1	7.98	43.36	240.68
CS2'	$\alpha_D [a g^-]^{g1}$	C1	13.98	38.38	232.36
CS3'	$\varepsilon_D [a a]^{h1}$	C1	11.36	38.83	233.10
CS4'	$\gamma_D [g^- a]^{d1}$	C2	12.39	42.94	233.87
CS5'	$\varepsilon_L [a a]^{i1}$	C2	12.68	38.15	231.78
CS6'	$\varepsilon_L [a a]^{j1}$	C2	15.11	24.73	219.35
CS7'	$\alpha_D [a g^-]^{j1}$	C3	8.71	43.57	236.99
CS8'	$\delta_D [g^- g^-]^{k1}$	C3	9.68	41.94	236.02
CS9'	$\varepsilon_D [a g^-]^{l1}$	C4	5.90	45.30	232.38
CS10'	$\varepsilon_D [a g^-]^{l1}$	C4	7.46	39.80	238.39
CS11'	$\gamma_D [g^- g^-]^{b1}$	C5	7.72	43.97	238.24
CS12'	$\gamma_D [g^+ g^-]^{m1}$	C6	0.00	51.71	245.70
$[\text{H}_2\text{asp-K}]^+$					
SB1''	$\gamma_D [g^- g^+]^{b2}$	S1	5.56	30.43	237.05
SB2''	$\gamma_L [a g^+]^{c2}$	S1	17.02	17.85	225.59
SB3''	$\gamma_D [g^- a]^{d2}$	S2	4.65	31.02	243.81
SB4''	$\gamma_L [a a]^{e2}$	S2	13.15	21.92	235.31
CS1''	$\varepsilon_D [g^- g^-]^{f2}$	C1	8.65	27.91	242.13
CS2''	$\alpha_D [a g^-]^{g2}$	C1	7.72	29.39	242.93
CS3''	$\varepsilon_D [a a]^{h2}$	C1	18.25	16.49	229.11
CS4''	$\gamma_D [g^- a]^{d2}$	C2	3.62	31.98	244.85
CS5''	$\varepsilon_L [a a]^{i2}$	C2	6.60	28.41	241.86
CS6''	$\varepsilon_L [a a]^{j2}$	C2	8.75	31.71	239.71
CS7''	$\alpha_D [a g^-]^{g2}$	C3	9.35	27.92	241.64
CS8''	$\delta_D [g^- g^-]^{j2}$	C3	7.52	28.89	243.47
CS9''	$\varepsilon_D [a g^-]^{k2}$	C4	3.52	32.49	243.03
CS10''	$\varepsilon_D [a g^-]^{k2}$	C4	4.80	31.42	241.75
CS11''	$\gamma_D [g^- g^-]^{b2}$	C5	6.99	29.32	244.00
CS12''	$\gamma_D [g^+ g^-]^{m2}$	C6	0.00	36.45	250.99

^a In kcal/mol with ZPE correction. ^b Identical to $\gamma_D [g^- g^+]$. ^c Identical to $\gamma_L [a g^+]$. ^d Identical to $\gamma_D [g^- a]$. ^e Identical to $\gamma_L [a a]$. ^f Identical to $\varepsilon_D [g^- g^-]$. ^g Identical to $\alpha_D [a g^-]$. ^h Identical to $\varepsilon_D [a a]$. ⁱ Identical to $\varepsilon_L [a a]$. ^j Identical to $\delta_D [g^- g^-]$. ^k Identical to $\varepsilon_D [a g^-]$. ^l Identical to $\varepsilon_D [g^+ g^-]$. ^{b1} Identical to $\gamma_D [g^- g^+]$. ^{c1} Identical to $\gamma_L [a g^+]$. ^{d1} Identical to $\gamma_D [g^- a]$. ^{e1} Identical to $\gamma_L [a a]$. ^{f1} Identical to $\varepsilon_D [g^- g^-]$. ^{g1} Identical to $\alpha_D [a g^-]$. ^{h1} Identical to $\varepsilon_D [a a]$. ⁱ¹ Identical to $\varepsilon_L [a a]$. ^{j1} Identical to $\delta_D [g^- g^-]$. ^{k1} Identical to $\beta_L [g^- g^-]$. ^{l1} Identical to $\varepsilon_D [a g^-]$. ^{m1} Identical to $\varepsilon_D [g^+ g^-]$. ^{b2} Identical to $\gamma_D [g^- g^+]$. ^{c2} Identical to $\gamma_L [a g^+]$. ^{d2} Identical to $\gamma_D [g^- a]$. ^{e2} Identical to $\gamma_L [a a]$. ^{f2} Identical to $\varepsilon_D [g^- g^-]$. ^{g2} Identical to $\alpha_D [a g^-]$. ^{h2} Identical to $\varepsilon_D [a a]$. ⁱ² Identical to $\varepsilon_L [a a]$. ^{j2} Identical to $\delta_D [g^- g^-]$. ^{k2} Identical to $\beta_L [a g^+]$. ^{l2} Identical to $\varepsilon_D [a g^-]$. ^{m2} Identical to $\varepsilon_D [g^+ g^-]$.

The conformation structure of aspartic acid ligand in the $[\text{H}_2\text{asp-Li}]^+_{\text{CS11}}$ complex, γ_{D} is slightly different from those in the $[\text{asp-Li}]^-_9$ and $[\text{Hasp-Li}]_{19}$ complex conformers which possess the δ_{D} conformation. The binding preferences for lithium complexes in terms of MIAs are in decreasing order: $\text{C6} > \text{C4} > \text{C5} > \text{S1} \approx \text{S2} \approx \text{C3} > \text{C2} \approx \text{C1}$ as shown in Figure 4.12. It shows the same binding mode C6 lead to the highest MIAs values of H_2asp species for lithium, sodium and potassium. The relation between the MIAs of various species of aspartic acid for lithium, sodium and potassium against charge of their species as shown in Figure 3.20 shows that the MIAs of aspartic species for $[\text{H}_2\text{asp-Li}]^+_{\text{CS11}}$ (73.26 kcal/mol) is less favorable one and lower than that for $[\text{Hasp-Li}]_{19}$ (169.76 kcal/mol) [41] and $[\text{asp-Li}]^-_9$ (254.86 kcal/mol) [40] by 96.44 and 181.60 kcal/mol, respectively. Increasing orders of MIAs values of aspartic acid species of ether lithium or sodium or potassium are species are the same sequence as $\text{asp}^{2-} > \text{Hasp}^- > \text{H}_2\text{asp}$, see Figure 3.20. Based on the MIA of zwitterionic species H_2asp , the MIA for lithium ion of this work (73.26 kcal/mol) is seemly overestimated by approximately 20 kcal/mol as compared to the experimental result of which the MIA is 51.5 kcal/mol by kinetic method [18]; this experimental value is relatively close to the MIAs obtained by kinetic method of *N*-gly-asp (54.9 kcal/mol) and of *N*-acetyl-asp (54.9 kcal/mol). [19]

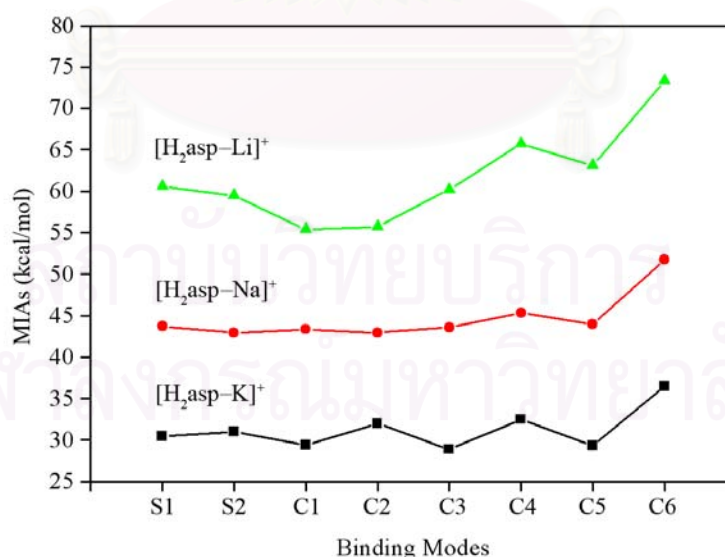


Figure 4.12 The MIAs of H_2asp for the complexation of $[\text{H}_2\text{asp-M}]^+$, M= lithium (\blacktriangle - \blacktriangle - \blacktriangle), sodium (\bullet - \bullet - \bullet) and potassium (\blacksquare - \blacksquare - \blacksquare) against binding mode.

4.2.3.2 Sodium Complexes

Sixteen $[\text{H}_2\text{asp}-\text{Na}]^+$ complex conformers obtained from structure optimization using the B3LYP/6-311++G(d,p) calculations are shown in Figure A33 and their relative energies are shown in Table 4.20. The most stable conformer for SB and CS structures of $[\text{H}_2\text{asp}-\text{Na}]^+$ complexes are shown in Figure 4.11. The most stable $[\text{H}_2\text{asp}-\text{Na}]^+$ complex conformer is the charge-solvated, **CS12'** conformer which is the only one of the tri-coordination structure. The MIAs of H_2asp , DPEs of $[\text{H}_2\text{asp}-\text{Na}]^+$ complex and their conformations are shown in Table 4.20. The relative stabilities of sodium complexes are in decreasing order, **CS12' > CS9' > CS10' > CS11' > SB1' \approx SB3' \approx CS1' > CS7' > CS8' > CS3' > CS4' > CS5' > CS2' > CS6' > SB4' > SB2'**. The most stable complex conformer **CS12'** is also found to possess the maximum values of MIA and DPE. The MIAs of H_2asp conformer and DPEs for all conformers of their sodium complexes are within the range of 24.73–51.71 and of 219.35–245.70 kcal/mol, respectively. The most stable complex conformer of $[\text{H}_2\text{asp}-\text{Na}]^+_{\text{CS12}'}$ possess the charge-solvated tri-coordination structure as same as the most stable conformers $[\text{asp}-\text{Na}]^-_{6'}$ [40] for di-anionic system and $[\text{Hasp}-\text{Na}]_{6'}$ [41] for mono-anionic systems as reported in our previous work.

All the conformation structures of aspartic acid ligand in the $[\text{H}_2\text{asp}-\text{Na}]^+_{\text{CS12}'}$, $[\text{asp}-\text{Na}]^-_{6'}$ and $[\text{Hasp}-\text{Na}]_{6'}$ complex conformers possess the same conformation, γ_{D} . The binding preferences for sodium complexes in terms of MIAs are in decreasing order: $\text{C6} > \text{C4} > \text{C5} > \text{S1} \approx \text{C3} \approx \text{C1} \approx \text{C2} \approx \text{S2}$ as shown in Figure 4.12. It shows the same binding mode C6 lead to the highest MIAs values of H_2asp species for lithium, sodium and potassium. The relation between the MIAs of various species of aspartic acid for lithium, sodium and potassium against charge of their species is shown in Figure 4.13. It shows that the MIAs of aspartic species for $[\text{H}_2\text{asp}-\text{Na}]^+_{\text{CS12}'}$ (51.71 kcal/mol) is less favorable one and lower than that for $[\text{Hasp}-\text{Na}]_{6'}$ (133.88 kcal/mol) [41] and $[\text{asp}-\text{Na}]^-_{6'}$ (219.40 kcal/mol) [40] by 82.17 and 167.69 kcal/mol, respectively. Increasing orders of MIAs values of aspartic acid species of either lithium or sodium or potassium are species are the same sequence as $\text{asp}^{2-} > \text{Hasp}^- > \text{H}_2\text{asp}$, see Figure 4.13. Based on the MIA of zwitterionic species H_2asp , the MIA for sodium ion of this work (51.71 kcal/mol) is

pretty close to the experimental result of which the MIA is 48.2 kcal/mol by kinetic method [16]; this experimental value is relatively close to the MIAs obtained by Cook method of *N*-gly-asp (38.5 kcal/mol) and of *N*-acetyl-asp (34.9 kcal/mol). [20]

4.2.3.3 Potassium Complexes

Sixteen $[\text{H}_2\text{asp-K}]^+$ complex conformers obtained from structure optimization using the B3LYP/6-311++G(d,p) calculations are shown in Figure A34 and their relative energies are shown in Table 4.20. The most stable conformer for SB and CS structures of $[\text{H}_2\text{asp-K}]^+$ complexes are shown in Figure 4.11. The most stable $[\text{H}_2\text{asp-K}]^+$ complex conformer is the charge-solvated, **CS12''** conformer which is the only one of the tri-coordination structure. The MIAs of H_2asp , DPEs of $[\text{H}_2\text{asp-K}]^+$ complex and their conformations are shown in Table 4.20. The relative stabilities of potassium complexes are in decreasing order: **CS12''** > **CS10''** > **CS4''** > **SB3''** > **CS11''** > **SB1''** > **CS5''** > **CS12''** > **CS2''** > **CS8''** > **CS1''** > **CS6''** > **CS7''** > **SB4''** > **SB2''** > **CS3''**. The most stable complex conformer **CS12''** also possess the maximum values of MIA and DPE. The MIAs of H_2asp conformer and DPEs for all conformers of their potassium complexes are within the range of 16.49–36.45 and of 225.59–250.99 kcal/mol, respectively. The most stable complex conformer of $[\text{H}_2\text{asp-K}]^+_{\text{CS12''}}$ possess the charge-solvated tri-coordination structure as same as the most stable conformers $[\text{asp-K}]_4^-$ [40] for di-anionic system and $[\text{Hasp-K}]_3$ [41] for mono-anionic systems as reported in our previous work.

All the conformation structures of aspartic acid ligand in the $[\text{H}_2\text{asp-K}]^+_{\text{CS12''}}$, $[\text{asp-K}]_3^-$ and $[\text{Hasp-K}]_4$ complex conformers possess the same conformation, γ_D . The binding preferences for potassium complexes in terms of MIAs are in decreasing order: $\text{C6} > \text{C4} > \text{C2} > \text{S2} \approx \text{S1} > \text{C1} \approx \text{C3} \approx \text{C5}$ as shown in Figure 4.12. It shows the same binding mode C6 lead to the highest MIAs values of H_2asp species for lithium, sodium and potassium. The relation between the MIAs of various species of aspartic acid for lithium, sodium and potassium against charge of their species is shown in Figure 4.13. It shows that the MIAs of aspartic species for $[\text{H}_2\text{asp-K}]^+_{\text{CS12''}}$ (36.45 kcal/mol) is less favorable one and lower than that for $[\text{Hasp-K}]_4$ (118.05 kcal/mol) [41] and $[\text{asp-K}]_3^-$

(197.09 kcal/mol) [40] by 81.60 and 160.64 kcal/mol, respectively. Increasing orders of MIAs values of aspartic acid species of ether lithium or sodium or potassium are species are the same sequence as $\text{asp}^{2-} > \text{Hasp}^- > \text{H}_2\text{asp}$, see Figure 4.13.

4.2.3.4 Comparative reactions of aspartate complexes

As consideration for binding modes S1, S2, C1, C2, C3, C4, C5 and C6, the binding preferences of aspartic acid species in terms of MIAs were obtained as shown in Figure 4.12. It shows that trend of their values are in order: $[\text{H}_2\text{asp-Li}]^+ > [\text{H}_2\text{asp-Na}]^+ > [\text{H}_2\text{asp-K}]^+$. Table 4.21 shows that complexation energies of charge-solvated aspartic acid conformers with lithium, sodium and potassium ions are larger than their salt-bridge conformers and their relative energies are in order: $[\text{H}_2\text{asp-Li}]^+ > [\text{H}_2\text{asp-Na}]^+ > [\text{H}_2\text{asp-K}]^+$. All the complexation of $[\text{H}_2\text{asp-M}]^+$ complexes are found as spontaneous reaction. Pre-organization energies for charge-solvated system are larger than those for salt-bridge system and relative values for pre-organization energies depend on sizes of alkaline metal ions namely $\text{Li}^+ > \text{Na}^+ > \text{K}^+$. Relation between charge of aspartic acid species in its corresponding complex with alkaline metal ions and the MIA shows remarkable linear trend as shown in Figure 4.13.

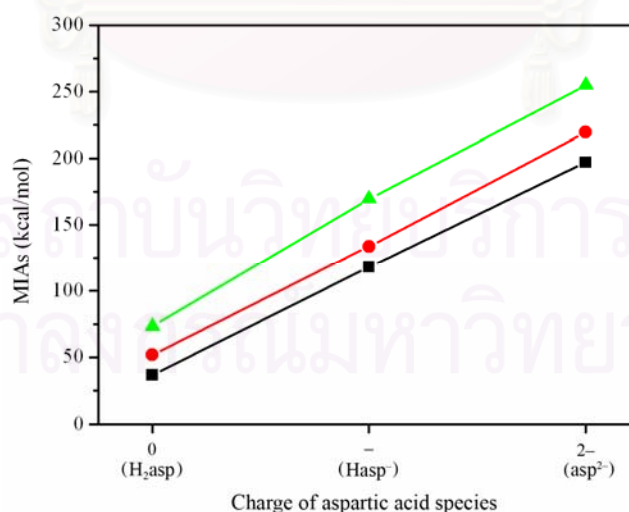


Figure 4.13 The MIAs of various species of aspartic acid of lithium (▲-▲-▲), sodium (●-●-●) and potassium (■-■-■) against charge of their species.

Table 4.21 Quantities for the formation reactions of the most stable conformers of salt–bridge and charge–solvated structures for $[\text{H}_2\text{asp}-\text{M}]^+$ complexes, and pre–organization for their corresponding aspartic acid structures

Reactions	$\Delta E^{a,b}$	$BSSE^a$	ΔE_{BSSE}^a	MIA ^a	$\Delta G_{298}^0{}^a$
<i>Complexation:</i>					
CS structures					
$[\text{H}_2\text{asp}]_{\delta_D[\text{g}^- \text{g}^+]5} + \text{Li}^+ \rightarrow [\text{H}_2\text{asp}-\text{Li}]_{\delta_D[\text{g}^- \text{g}^+]CS11}^+$	-71.78	1.4517	-70.33	73.26	-62.74
$[\text{H}_2\text{asp}]_{\delta_D[\text{g}^- \text{g}+]5} + \text{Na}^+ \rightarrow [\text{H}_2\text{asp}-\text{Na}]_{\delta_D[\text{g}^- \text{g}^+]CS12'}^+$	-50.84	1.3685	-49.47	51.71	-41.99
$[\text{H}_2\text{asp}]_{\delta_D[\text{g}^- \text{g}+]5} + \text{K}^+ \rightarrow [\text{H}_2\text{asp}-\text{K}]_{\delta_D[\text{g}^- \text{g}^+]CS13''}^+$	-35.86	0.3027	-35.56	36.45	-27.36
SB structures					
$[\text{H}_2\text{asp}]_{\sigma_D[\text{g}^- \text{g}^-]1} + \text{Li}^+ \rightarrow [\text{H}_2\text{asp}-\text{Li}]_{\sigma_D[\text{g}^- \text{g}^+]SB1}^+$	-58.51	0.5647	-57.95	59.29	-51.14
$[\text{H}_2\text{asp}]_{\sigma_D[\text{g}^- \text{g}^-]1} + \text{Na}^+ \rightarrow [\text{H}_2\text{asp}-\text{Na}]_{\sigma_D[\text{g}^- \text{g}^+]SB1'}^+$	-41.56	0.3765	-41.18	42.42	-33.32
$[\text{H}_2\text{asp}]_{\sigma_D[\text{g}^- \text{g}^-]1} + \text{K}^+ \rightarrow [\text{H}_2\text{asp}-\text{K}]_{\sigma_D[\text{g}^- \text{g}^+]SB1''}^+$	-28.99	0.2510	-28.04	29.14	-21.82
<i>Pre–organization:</i>					
CS structures					
$[\text{H}_2\text{asp}]_{\delta_D[\text{g}^- \text{g}^+]5} \rightarrow [\text{H}_2\text{asp}-\text{Li}]_{\delta_D[\text{g}^- \text{g}^+]CS11}^+$	13.78	–	–	12.18 ^c	16.56
$[\text{H}_2\text{asp}]_{\delta_D[\text{g}^- \text{g}^+]5} \rightarrow [\text{H}_2\text{asp}-\text{Na}]_{\delta_D[\text{g}^- \text{g}^+]CS12'}^+$	10.64	–	–	9.60 ^c	12.47
$[\text{H}_2\text{asp}]_{\delta_D[\text{g}^- \text{g}^+]5} \rightarrow [\text{H}_2\text{asp}-\text{K}]_{\delta_D[\text{g}^- \text{g}^+]CS13''}^+$	8.30	–	–	7.16 ^c	10.53
SB structures					
$[\text{H}_2\text{asp}]_{\sigma_D[\text{g}^- \text{g}^-]1} \rightarrow [\text{H}_2\text{asp}-\text{Li}]_{\sigma_D[\text{g}^- \text{g}^+]SB1}^+$	21.77	–	–	21.26 ^c	22.50
$[\text{H}_2\text{asp}]_{\sigma_D[\text{g}^- \text{g}^-]1} \rightarrow [\text{H}_2\text{asp}-\text{Na}]_{\sigma_D[\text{g}^- \text{g}^+]SB1'}^+$	18.17	–	–	18.11 ^c	18.19
$[\text{H}_2\text{asp}]_{\sigma_D[\text{g}^- \text{g}^-]1} \rightarrow [\text{H}_2\text{asp}-\text{K}]_{\sigma_D[\text{g}^- \text{g}^+]SB1''}^+$	14.54	–	–	14.07 ^c	15.07

^a In kcal/mol. ^b The ZPVE corrected energies. ^c Enthalpy in kcal/mol.

4.2.3.5 Relation between aspartic acid species and their complexes

Based on complexation and protonation processes of asp^{2-} and Hasp^- species as reported in our previous work [40,41], the $[\text{H}_2\text{asp}-\text{M}]^+$ complexes, $\text{M}=\text{Li}^+$, Na^+ and K^+ can be formed via reaction pathways as shown in Figure 4.14. The reactions at bottom and on top of each complexation processes in Figure 4.14 corresponds to the protonation of aspartic acid species and of their complexes with alkaline metal ions, respectively. As the Figure 4.14 presents reactions for relation between all three aspartic acid species (asp^{2-} , Hasp^- and H_2asp) and their complexes with three alkaline metal cations (Li^+ , Na^+ and K^+), this diagram is useful for description of their existing in relevant system. There

are three reaction pathways for complexation of alkaline metal reacting with dianion form of aspartic acid (asp^{2-}). The most preferable path is the protonation of asp^{2-} to form Hasp^- , Hasp^- to form H_2asp and complexation of H_2asp and M^+ to form $[\text{H}_2\text{asp-M}]^+$ complex. The second most preferable path is a sequence of protonation of asp^{2-} to Hasp^- , complexation of Hasp^- and M^+ to form $[\text{Hasp-M}]$, and protonation of $[\text{Hasp-M}]$ complex to form $[\text{H}_2\text{asp-M}]^+$. The third reaction pathway is therefore the least preferable path.

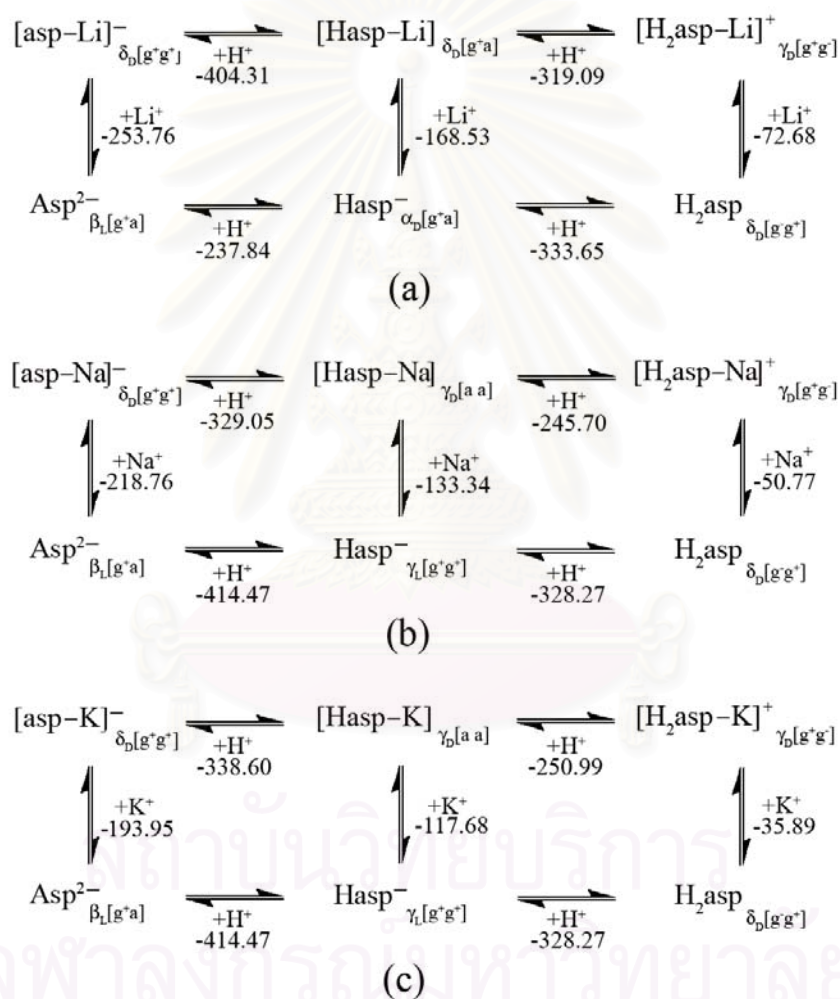


Figure 4.14 The reaction pathways for complexation and protonation of asp^{2-} and Hasp^- species to form $[\text{H}_2\text{asp-M}]^+$ complexes of (a) lithium (b) sodium and (c) potassium. Energies are in kcal/mol.

4.3 Aqueous acid–dissociation constants (pK_a) of aspartic acid

The B3LYP/6–31+G(d,p)–optimized geometries of bare and n –hydrated ($(H_2O)_n$, $n = 3$ to 6) structures of aspartic acid species H_3asp^+ , H_2asp , $Hasp^-$ and asp^{2-} were obtained and their superimposed structures are shown in Figure 4.15. The base structures for species H_2asp and $Hasp^-$ are not included in Figure 4.15, because their gas–phase structures are in the conformations of $\delta_L[a g^-]$ and $\gamma_L[a g^-]$ which are different from the aqueous phase. The acid dissociation equilibria of aspartic acid in gas phase as the bare and hydrated species are shown in Figure 4.16. It shows the conformations defined by Ramachandran [3] and IUPAC [4] nomenclatures of aspartic acid species in gas phase and aqueous systems which is represented by hexahydrated system. Conformations of the bare structures for the hydrated forms of aspartic acid species H_3asp^+ , H_2asp , $Hasp^-$ and asp^{2-} are $\delta_D[g^- g^+]$, $\delta_D[g^- a]$, $\delta_D[g^- g^+]$ and $\beta_L[g^- g^+]$, respectively.

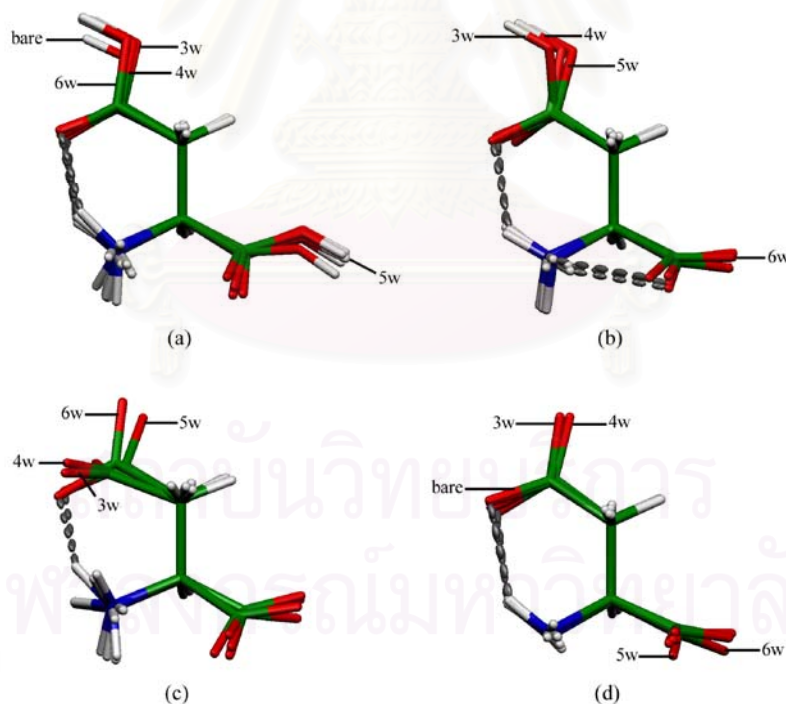


Figure 4.15 Superimposition of the B3LYP/6–31+G(d,p)–optimized structures of various states of the most stable species of aspartic acid as forms:(a) H_3asp^+ (b) H_2asp (c) $Hasp^-$ (d) asp^{2-} .

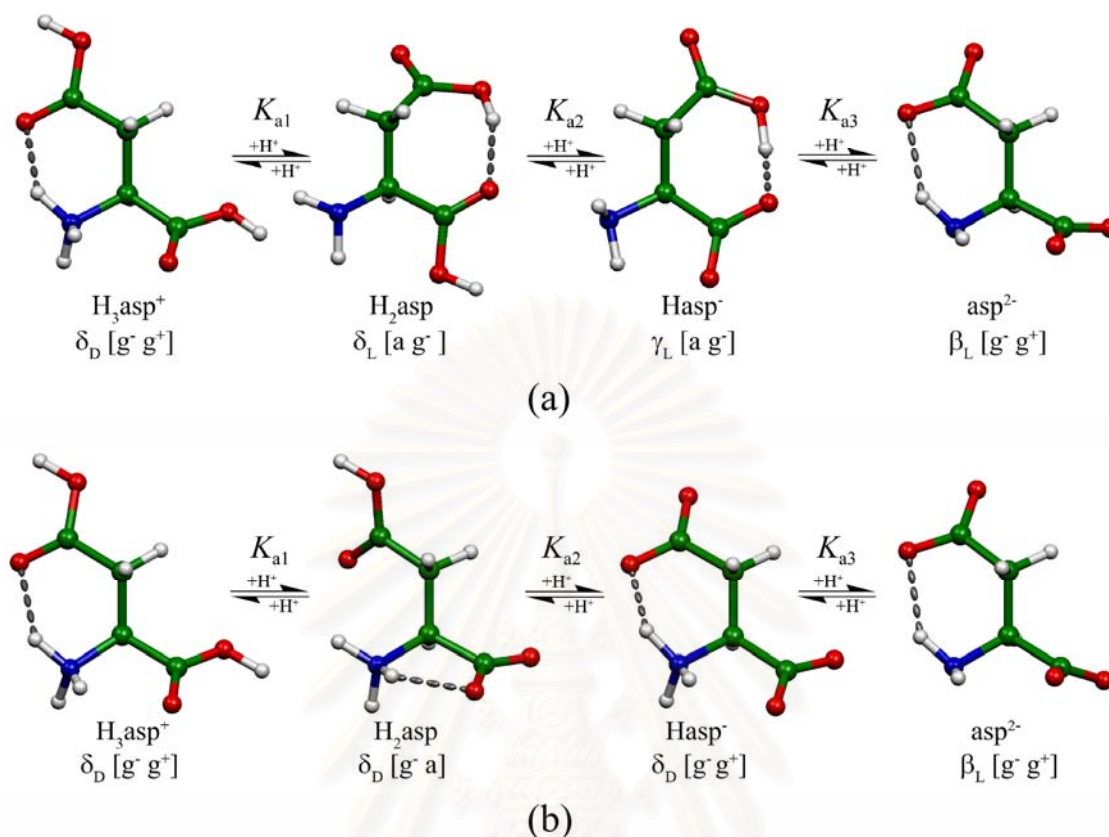


Figure 4.16 The acid–dissociation equilibria of aspartic acid in gas phase presented as (a) the bare structures and (b) hexahydrated species. For clarity, the six water molecules for hexahydrated species are not shown.

The conformations of free structures aspartic acid species H_3asp^+ , H_2asp , Hasp^- and asp^{2-} are the same conformations of their corresponding species of n -hydrated ($n = 3$ to 6) structures. The conformations of free forms of aspartic acid species H_2asp ($\delta_{\text{L}}[\text{a g}^-]$), and Hasp^- ($\gamma_{\text{L}}[\text{a g}^-]$) are different from their n -hydrated ($n = 3$ to 6) structures. All the n -hydrated structures of various species of aspartic acid and their equilibria are shown in Figure 4.17. The computed $\text{p}K_{\text{a}}$ values and Gibbs free energy contributions for corresponding acid dissociation equilibria of aspartic acid in gas phase of the bare, water-excluded hydrated and n -hydrated structures as shown in Scheme 3.3 are listed in Tables 4.22, 4.23 and 4.24, respectively.

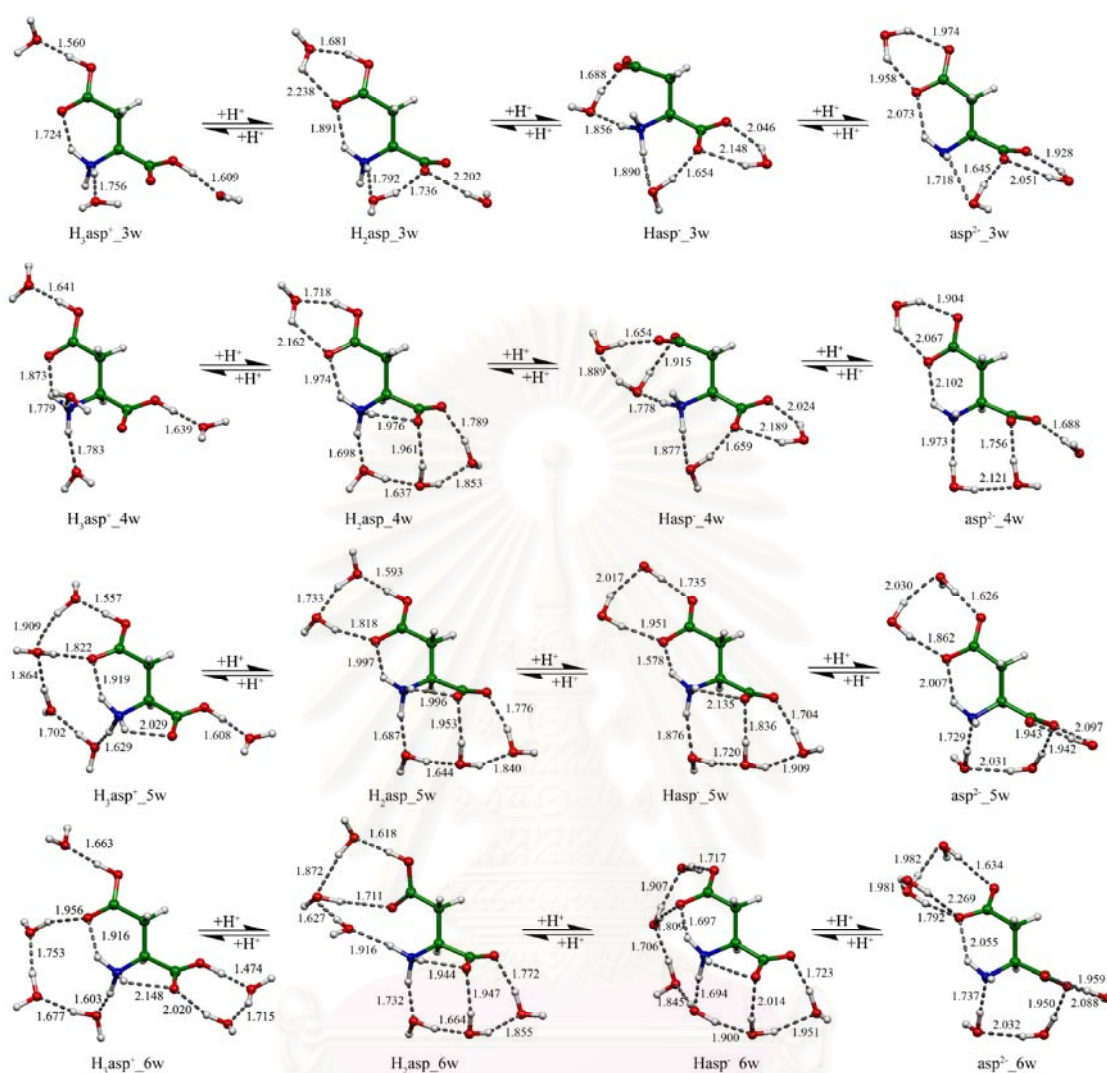


Figure 4.17 Acid-dissociation equilibria of aspartic acid based on their (a) tri- (b) tetra- (c) penta- (d) hexahydrated structures.

Based on the bare molecular system, the cavity models (UAKS and UAHF) cause different pK_a values, rather than the PCM models (CPCM and IEFPCM) and the PCM/UAHF model results the predicted pK_a values are very close to the experimental results, as shown in Table 4.22.

Table 4.22 Gibbs free energy contributions ΔG_{gas} , $\Delta\Delta G_{\text{solv}}$ and ΔG_{aq} (kcal/mol) for the acid dissociation equilibria of aspartic acid in gas phase

Deprotonation	ΔG_{gas}	CPCM		IEFPCM		$\text{p}K_{\text{a}}$		
		$\Delta\Delta G_{\text{solv}}^{\text{a}}$	$\Delta G_{\text{aq}}^{\text{b}}$	$\Delta\Delta G_{\text{solv}}^{\text{a}}$	$\Delta G_{\text{aq}}^{\text{b}}$	Calc. ^c	Calc. ^d	Exp. ^e
$\text{H}_3\text{asp}^+ \rightarrow \text{H}_2\text{asp} + \text{H}^+$	211.82	-208.66 (-208.83)	3.16 (2.99)	-208.66 (-208.83)	3.16 (2.99)	1.93 (1.42)	1.92 (1.42)	2.10
$\text{H}_2\text{asp} \rightarrow \text{Hasp}^- + \text{H}^+$	311.24	-304.49 (-304.10)	6.75 (7.14)	-304.49 (-304.10)	6.75 (7.14)	4.10 (5.18)	4.11 (5.19)	3.86
$\text{Hasp}^- \rightarrow \text{asp}^{2-} + \text{H}^+$	415.95	-399.91 (-404.42)	16.04 (11.53)	-399.91 (-404.42)	16.04 (11.53)	9.75 (9.18)	9.75 (9.17)	9.82

^aThe $\Delta\Delta G_{\text{solv}}$ values were obtained from single-point calculation at the B3LYP/6-31+G(d,p) level with UAKS and UAHF (in parenthesis) cavity models. ^bThe ΔG_{aq} values were computed according to the thermodynamic cycles as shown in Schemes 1, 2 and 3. ^cDue to the CPCM with UAKS and UAHF (in parenthesis) cavity models. ^dDue to the IEFPCM with UAKS and UAHF (in parenthesis) cavity models. ^eTaken from ref. 17.

The correlation coefficient (r^2) of the computed and measured $\text{p}K_{\text{a}}$ values of aspartic acid species are shown in Table B1, Appendix. As the high correlations of the computed $\text{p}K_{\text{a}}$ values for the bare structures of free form system with the experimental values taken from ref. 13 were considered, the small different $\text{p}K_{\text{a}}$ values, $\Delta\text{p}K_{\text{a}1} = -0.17$ (1.93–2.10), $\Delta\text{p}K_{\text{a}2} = 0.24$ (4.10–3.86) and $\Delta\text{p}K_{\text{a}3} = -0.07$ (9.75–9.82) with $r^2 = 0.9972$ for CPCM/UAHF model and $\Delta\text{p}K_{\text{a}1} = -0.18$ (1.92–2.10), $\Delta\text{p}K_{\text{a}2} = 0.25$ (4.11–3.86) and $\Delta\text{p}K_{\text{a}3} = -0.07$ (9.75–9.82) with $r^2 = 0.9970$ for IEFPCM/UAHF model. Based on the equilibrium systems of the water-excluded hydrated structures, the computed $\text{p}K_{\text{a}}$ values for the tri- and tetra-hydrated systems are mostly closed to the experimental values.

The different $\text{p}K_{\text{a}}$ values of water-excluded tri-hydrated system are $\Delta\text{p}K_{\text{a}1} = 0.09$ (2.19–2.10), $\Delta\text{p}K_{\text{a}2} = -0.14$ (3.72–3.86) and $\Delta\text{p}K_{\text{a}3} = 0.01$ (9.83–9.82) with $r^2 = 0.9992$ for CPCM/UAHF model and $\Delta\text{p}K_{\text{a}1} = -0.12$ (1.98–2.10), $\Delta\text{p}K_{\text{a}2} = 0.16$ (4.02–3.86) and $\Delta\text{p}K_{\text{a}3} = -0.04$ (9.78–9.82) with $r^2 = 0.9987$ for IEFPCM/UAHF model. The most accurate prediction of water-excluded tetra-hydrated system was found that the different $\text{p}K_{\text{a}}$ values are $\Delta\text{p}K_{\text{a}1} = 0.07$ (2.17–2.10), $\Delta\text{p}K_{\text{a}2} = -0.11$ (3.75–3.86) and $\Delta\text{p}K_{\text{a}3} = 0.01$ (9.83–9.82) with $r^2 = 0.9995$ for CPCM/UAHF model and $\Delta\text{p}K_{\text{a}1} = 0.07$ (2.17–2.10), $\Delta\text{p}K_{\text{a}2} = -0.09$ (3.77–3.86) and $\Delta\text{p}K_{\text{a}3} = 0.02$ (9.84–9.82) with $r^2 = 0.9996$ for IEFPCM/UAHF model.

Table 4.23 Gibbs free energy contributions ΔG_{gas} , $\Delta\Delta G_{\text{solv}}$ and ΔG_{aq} (kcal/mol) for the acid dissociation equilibria of aspartic acid of various water–cluster models in gas phase

Hydrated system/Reaction	ΔG_{gas}	CPCM			IEFPCM		
		$\Delta\Delta G_{\text{solv}}^{\text{a}}$	$\Delta G_{\text{aq}}^{\text{b}}$	$\text{p}K_{\text{a}}^{\text{c}}$	$\Delta\Delta G_{\text{solv}}^{\text{a}}$	$\Delta G_{\text{aq}}^{\text{b}}$	$\text{p}K_{\text{a}}^{\text{d}}$
<i>Tri-hydrated</i>							
$\text{H}_3\text{asp}^+(\text{H}_2\text{O})_3 \rightarrow \text{H}_2\text{asp}(\text{H}_2\text{O})_3 + \text{H}^+$	248.70	-234.92 (-235.63)	13.78 (13.07)	6.02 (7.84)	-234.93 (-235.65)	13.77 (13.05)	6.04 (4.75)
$\text{H}_2\text{asp}(\text{H}_2\text{O})_3 \rightarrow \text{Hasp}^-(\text{H}_2\text{O})_3 + \text{H}^+$	303.33	-294.93 (-297.54)	8.40 (5.79)	7.44 (2.50)	-294.91 (-297.50)	8.42 (5.83)	7.41 (6.51)
$\text{Hasp}^-(\text{H}_2\text{O})_3 \rightarrow \text{asp}^{2-}(\text{H}_2\text{O})_3 + \text{H}^+$	381.32	-361.33 (-360.60)	19.99 (20.72)	12.22 (13.44)	-361.56 (-360.70)	19.76 (20.62)	12.06 (12.46)
<i>Tetra-hydrated</i>							
$\text{H}_3\text{asp}^+(\text{H}_2\text{O})_4 \rightarrow \text{H}_2\text{asp}(\text{H}_2\text{O})_4 + \text{H}^+$	243.60	-231.02 (-232.76)	12.58 (10.84)	6.79 (6.20)	-231.00 (-232.74)	12.60 (10.86)	6.80 (5.26)
$\text{H}_2\text{asp}(\text{H}_2\text{O})_4 \rightarrow \text{Hasp}^-(\text{H}_2\text{O})_4 + \text{H}^+$	309.18	-297.42 (-299.51)	11.76 (9.67)	7.76 (5.34)	-297.44 (-299.51)	11.74 (9.67)	7.75 (6.58)
$\text{Hasp}^-(\text{H}_2\text{O})_4 \rightarrow \text{asp}^{2-}(\text{H}_2\text{O})_4 + \text{H}^+$	375.83	-358.08 (-357.90)	17.75 (17.93)	11.06 (11.40)	-358.20 (-358.03)	17.63 (17.80)	10.98 (11.02)
<i>Penta-hydrated</i>							
$\text{H}_3\text{asp}^+(\text{H}_2\text{O})_5 \rightarrow \text{H}_2\text{asp}(\text{H}_2\text{O})_5 + \text{H}^+$	240.14	-234.62 (-235.71)	5.52 (4.97)	1.16 (1.90)	-234.59 (-235.14)	5.55 (5.00)	1.17 (0.27)
$\text{H}_2\text{asp}(\text{H}_2\text{O})_5 \rightarrow \text{Hasp}^-(\text{H}_2\text{O})_5 + \text{H}^+$	303.15	-296.85 (-298.69)	6.30 (4.46)	4.36 (1.53)	-296.86 (-298.67)	6.29 (4.48)	4.36 (3.69)
$\text{Hasp}^-(\text{H}_2\text{O})_5 \rightarrow \text{asp}^{2-}(\text{H}_2\text{O})_5 + \text{H}^+$	377.74	-354.14 (-353.77)	23.60 (23.97)	15.22 (15.83)	-354.23 (-353.87)	23.51 (23.87)	15.15 (15.26)
<i>Hexa-hydrated</i>							
$\text{H}_3\text{asp}^+(\text{H}_2\text{O})_6 \rightarrow \text{H}_2\text{asp}(\text{H}_2\text{O})_6 + \text{H}^+$	243.05	-234.36 (-235.22)	8.69 (7.83)	3.02 (3.99)	-234.37 (-235.24)	8.68 (7.81)	3.03 (1.74)
$\text{H}_2\text{asp}(\text{H}_2\text{O})_6 \rightarrow \text{Hasp}^-(\text{H}_2\text{O})_6 + \text{H}^+$	301.60	-294.15 (-296.55)	7.45 (5.05)	5.79 (1.96)	-294.12 (-296.50)	7.48 (5.10)	5.79 (4.89)
$\text{Hasp}^-(\text{H}_2\text{O})_6 \rightarrow \text{asp}^{2-}(\text{H}_2\text{O})_6 + \text{H}^+$	374.44	-350.71 (-349.79)	23.73 (24.65)	15.17 (16.32)	-350.81 (-349.91)	23.63 (24.53)	15.11 (15.57)

^a The $\Delta\Delta G_{\text{solv}}$ values were obtained from single–point calculation at the B3LYP/6–31+G(d,p) level with UAKS and UAHF (in parenthesis) cavity models. ^b The ΔG_{aq} values were computed according to the thermodynamic cycles as shown in Schemes 1, 2 and 3. ^c Due to the CPCM with UAKS and UAHF (in parenthesis) cavity models. ^d Due to the IEFPCM with UAKS and UAHF (in parenthesis) cavity models.

Table 4.24 Gibbs free energy contributions ΔG_{gas} , $\Delta\Delta G_{\text{solv}}$ and ΔG_{aq} (kcal/mol) for the acid dissociation equilibria of aspartic acid of bare structure of different water cluster models in gas phase

Hydrated system/Reaction	ΔG_{gas}	CPCM			IEFPCM		
		$\Delta\Delta G_{\text{solv}}^{\text{a}}$	$\Delta G_{\text{aq}}^{\text{b}}$	pK_{a}^{c}	$\Delta\Delta G_{\text{solv}}^{\text{a}}$	$\Delta G_{\text{aq}}^{\text{b}}$	pK_{a}^{d}
<i>Tri-hydrated</i>							
$\text{H}_3\text{asp}^+ \rightarrow \text{H}_2\text{asp} + \text{H}^+$	233.23	-235.44 (-233.29)	-2.21 (-0.06)	1.74 (2.19)	-233.29 (-235.44)	-0.06 (-2.21)	1.67 (1.98)
$\text{H}_2\text{asp} \rightarrow \text{Hasp}^- + \text{H}^+$	314.74	-311.12 (-307.89)	3.62 (6.85)	4.18 (3.72)	-307.89 (-311.12)	6.85 (3.62)	4.54 (4.02)
$\text{Hasp}^- \rightarrow \text{asp}^{2-} + \text{H}^+$	390.34	-370.29 (-371.37)	20.05 (18.97)	9.24 (9.83)	-371.37 (-370.29)	18.97 (20.05)	9.57 (9.78)
<i>Tetra-hydrated</i>							
$\text{H}_3\text{asp}^+ \rightarrow \text{H}_2\text{asp} + \text{H}^+$	228.29	-230.11 (-228.02)	-1.82 (0.27)	1.83 (2.17)	-228.02 (-230.11)	0.27 (-1.82)	1.84 (2.17)
$\text{H}_2\text{asp} \rightarrow \text{Hasp}^- + \text{H}^+$	320.63	-317.62 (-314.28)	3.01 (6.35)	4.21 (3.75)	-314.28 (-317.62)	6.35 (3.01)	4.21 (3.77)
$\text{Hasp}^- \rightarrow \text{asp}^{2-} + \text{H}^+$	389.62	-368.25 (-369.44)	21.37 (20.18)	9.69 (9.83)	-369.44 (-368.25)	20.18 (21.37)	9.61 (9.84)
<i>Penta-hydrated</i>							
$\text{H}_3\text{asp}^+ \rightarrow \text{H}_2\text{asp} + \text{H}^+$	226.79	-231.75 (-229.50)	-4.96 (-2.71)	2.52 (2.67)	-229.50 (-231.75)	-2.71 (-4.96)	2.52 (2.67)
$\text{H}_2\text{asp} \rightarrow \text{Hasp}^- + \text{H}^+$	304.43	-306.82 (-303.69)	-2.39 (0.74)	3.38 (3.24)	-303.69 (-306.82)	0.74 (-2.39)	3.38 (3.24)
$\text{Hasp}^- \rightarrow \text{asp}^{2-} + \text{H}^+$	404.42	-376.35 (-377.54)	28.07 (26.88)	9.87 (9.87)	-377.54 (-376.35)	26.88 (28.07)	9.88 (9.87)
<i>Hexa-hydrated</i>							
$\text{H}_3\text{asp}^+ \rightarrow \text{H}_2\text{asp} + \text{H}^+$	229.46	-233.79 (-231.44)	-4.33 (-1.98)	2.65 (2.78)	-231.44 (-233.79)	-1.98 (-4.33)	2.66 (2.78)
$\text{H}_2\text{asp} \rightarrow \text{Hasp}^- + \text{H}^+$	304.19	-306.88 (-303.79)	-2.69 (0.40)	3.26 (3.14)	-303.79 (-306.88)	0.40 (-2.69)	3.25 (3.14)
$\text{Hasp}^- \rightarrow \text{asp}^{2-} + \text{H}^+$	402.13	-373.73 (-375.09)	28.40 (27.04)	9.87 (9.86)	-375.09 (-373.73)	27.04 (28.40)	9.87 (9.86)

^aThe $\Delta\Delta G_{\text{solv}}$ values were obtained from single-point calculation at the B3LYP/6-31+G(d,p) level with UAKS and UAHF (in parenthesis) cavity models. ^bThe ΔG_{aq} values were computed according to the thermodynamic cycles as shown in Schemes 1, 2 and 3. ^cDue to the CPCM with UAKS and UAHF (in parenthesis) cavity models. ^dDue to the IEFPCM with UAKS and UAHF (in parenthesis) cavity models.

Complete sets of the computed pK_{a} values for n -hydrated systems (Table 4.24) are really different from the experimental results. This must be the limitation of these two cavity models of solvent-effect calculation on the water-added system. Deviation of the pK_{a} values of all sets of the hydrated structures of various aspartic acid species from their experimental values corresponds to the inaccurate results of solvent-effect calculation for the tri-hydrated system of 5-hydroxytryptamine as reported in ref. 56.

CHAPTER V

CONCLUSIONS

5.1 Conformational study of cationic, zwitterionic and anionic species of aspartic acid and their water-added forms

The potential energy surfaces for the bare structures of species H_3asp^+ and asp^{2-} and for the trihydrated structures of species H_2asp and Hasp^- of aspartic acid have been performed at the DFT/B3LYP/6-31G(d) level of theory. Conformations of 34, 11, 9 and 3 were found from 324, 162, 81 and 81 possible conformers for species H_3asp^+ , H_2asp , Hasp^- and asp^{2-} , respectively. Based on the B3LYP/6-31+G(d,p) computations of different structural models (the bare, trihydrated and tetrahydrated structures), the conformation for the species H_3asp^+ ($\gamma_{\text{D}}[\text{g}^- \text{g}^+]$), H_2asp ($\alpha_{\text{L}}[\text{a} \text{g}^-]$), Hasp^- ($\epsilon_{\text{L}}[\text{g}^+ \text{a}]$) and asp^{2-} ($\beta_{\text{L}}[\text{g}^+ \text{a}]$) are not changed. In gas phase, the species H_2asp and Hasp^- must be stabilized by at least three water molecules but the bare structures of the species H_3asp^+ and asp^{2-} are stable. Three protonation steps due to the tetrahydrated species of asp^{2-} , Hasp^- and H_2asp of aspartic acid computed at B3LYP/6-31+G(d,p) level of theory with zero-point vibrational energy corrections are exothermic reactions and their stabilization energies of the stepwise protonation are -244.68 , -308.57 and -379.97 kcal/mol, respectively.

5.2.1 Conformational analysis of alkali metal complexes of dianionic species of aspartic acid

The B3LYP/6-311++G(d,p)-optimized structures of mono and dinuclear complexes of dianionic species (asp^{2-}) of aspartic acid with Li^+ , Na^+ and K^+ cations were obtained. The most stable conformers mono- and dinuclear complexes of asp^{2-} with Li^+ , Na^+ and K^+ are **9** and **16**, **6'** and **11'** and **4''** and **9''**, respectively. The metal ion affinities of the most stable complex conformers are $\text{MIA}(1) = 254.86$ and $\text{MIA}(2) = 155.88$ kcal/mol for the $\text{asp}^{2-}/\text{Li}^+$ complex system, $\text{MIA}(1) = 219.40$ and $\text{MIA}(2) = 144.46$ kcal/mol for the $\text{asp}^{2-}/\text{Na}^+$ complex system, and $\text{MIA}(1) = 197.09$ and $\text{MIA}(2) = 126.04$ kcal/mol for the $\text{asp}^{2-}/\text{K}^+$ complex system. The asp^{2-} complex

components of the most stable complex conformer exist as $\delta_D [g^+ g^+]$ conformation. The relative energies of complexation reaction of $[\text{asp-M}]^-$ and $[\text{asp-M}_2]$ are in decreasing order: $[\text{asp-Li}]^- > [\text{asp-Na}]^- > [\text{asp-K}]^-$ and $[\text{asp-Li}_2] > [\text{asp-Na}_2] > [\text{asp-K}_2]$, respectively. The relative reactivities of $[\text{asp-M}]^-$ and $[\text{asp-M}_2]$ complexes are in order: $[\text{asp-K}]^- > [\text{asp-Na}]^- > [\text{asp-Li}]^-$ and $[\text{asp-K}_2] > [\text{asp-Na}_2] > [\text{asp-Li}_2]$, respectively, but their absolute values are not very different. As the energy gap for K^+ and Na^+ cations are, respectively, lower than Na^+ and Li^+ cations by 0.38 and 0.88 eV, their relative reactivities are correspondingly in decreasing order: $\text{K}^+ > \text{Na}^+ > \text{Li}^+$.

5.2.2 Conformational analysis of alkali metal complexes of anionic species of aspartic acid

The B3LYP/6-311++G(d,p)-optimized structures of all conformers of α - and β -[Hasp-M] complexes were obtained. Numbers of 39 conformers for [Hasp-Li], 23 conformers for [Hasp-Na] and 22 conformers for [Hasp-K] complexes were found. Based on their single-step interconversions, numbers of 28 equilibria for [Hasp-Li], 13 equilibria for [Hasp-Na] and 12 equilibria for [Hasp-Li] complex systems were found and their corresponding transition-state structures were obtained. The most stable conformers of [Hasp-M] complexes are α -[Hasp-Li]₁₉, α -[Hasp-Na]₆ and α -[Hasp-K]₃, of which binding energies are -168.53, -133.34 and -117.68 kcal/mol, respectively. Relative stabilities and reactivities of [Hasp-M] complexes are in orders: [Hasp-Li] > [Hasp-Na] > [Hasp-K] and [Hasp-Li] > [Hasp-K] > [Hasp-Na], respectively. Magnitudes of MIAs of [Hasp-M]-aspartate ligands are in order: [Hasp-Li]-aspartate > [Hasp-Na]-aspartate > [Hasp-K]-aspartate. Relative reactivities of seven conformers of [Hasp⁻]-ligands are in decreasing order: Hasp_{IV}⁻ > Hasp_V⁻ > Hasp_I⁻ > Hasp_{II}⁻ > Hasp_{VII}⁻ > Hasp_{VI}⁻ > Hasp_{III}⁻. The average bond-distances of M^+ -O bonds of the [Hasp-M] complexes are in order: [Hasp-K]-bond > [Hasp-Na]-bond > [Hasp-Li]-bond. The most stable complex conformer as a tri-coordinated form for aspartate complex with Li^+ and bi-coordinated form for aspartate complexes with Na^+ and K^+ were found.

5.2.3 Conformational analysis of alkali metal complexes of zwitterionic species of aspartic acid

The B3LYP/6-311++G(d,p)-optimized structures of $[\text{H}_2\text{asp-M}]^+$ where $M=\text{Li}^+$, Na^+ , K^+ were obtained. Numbers of $[\text{H}_2\text{asp-Li}]^+$, $[\text{H}_2\text{asp-Na}]^+$ and $[\text{H}_2\text{asp-K}]^+$ conformers of 11, 12 and 12 were obtained respectively and their structures as charge-solvated and salt-bridge structures were found. The most stable form of all $[\text{H}_2\text{asp-M}]^+$ complex conformers are charge-solvated tri-coordination structures in which M^+ alkali metal cation is preferably coordinated to amino nitrogen, α - and β -carbonyl oxygen atoms of aspartic acid. MIAs of aspartic acid conformers are in order: $[\text{H}_2\text{asp-Li}]^+ > [\text{H}_2\text{asp-Na}]^+ > [\text{H}_2\text{asp-K}]^+$. Complexation energies of charge-solvated aspartic acid conformers with lithium, sodium and potassium ions are larger than their salt-bridge conformers and their relative energies are in order: $[\text{H}_2\text{asp-Li}]^+ > [\text{H}_2\text{asp-Na}]^+ > [\text{H}_2\text{asp-K}]^+$. All the complexation of $[\text{H}_2\text{asp-M}]^+$ complexes are found as spontaneous reaction. Pre-organization energies for charge-solvated system are larger than those for salt-bridge system and relative values for pre-organization energies depend on sizes of alkali metal ions namely $\text{Li}^+ > \text{Na}^+ > \text{K}^+$.

5.3 Aqueous acid-dissociation constants ($\text{p}K_a$) of aspartic acid

Acid dissociation constants of aspartic acid in aqueous solution were determined using the DFT with two different solvation models of CPCM and IEFPCM based on two different cavity models of UAKS and UAHF. We found that the $\text{p}K_a$ values derived from the CPCM and IEFPCM with UAHF cavity model of the bare B3LYP/6-31+G(d,p)-optimized structures of tetra-hydrated aspartic acid species are mostly closed to the experimental $\text{p}K_a$ values. These two different solvation models of CPCM and IEFPCM are excellent methods for determination of acid dissociation constants of the system of bare structures of aspartic acid as the conformations of $\delta_{\text{D}}[\text{g}^- \text{g}^+]$ for H_3asp^+ , $\delta_{\text{D}}[\text{g}^- \text{a}]$ for H_2asp , $\delta_{\text{D}}[\text{g}^- \text{g}^+]$ for Hasp^- and $\beta_{\text{L}}[\text{g}^- \text{g}^+]$ for asp^{2-} species.

REFERENCES

- [1] Hecht, S. M. Bioorganic chemistry: Peptides and Proteins. New York: Oxford University Press, 1998.
- [2] Perczel, A.; McAllister, Császár, M. A. P.; Csizmadia, I. G. Peptide models 6. New .beta.–turn conformations from ab initio calculations confirmed by x–ray data of proteins, *J. Am. Chem. Soc.* 115 (1993) :4849–4858.
- [3] Chakrabarti, P.; Pal, D. The interrelationships of side–chain and main–chain conformations in proteins, *Prog. Biophys. Mol. Biol.* 76 (2001) :1–102.
- [4] IUPAC–IUB Commission on biochemical nomenclature. Abbreviations and symbols for the description of the conformation of polypeptide chains. Tentative rules (1969). *Biochemistry.* 9 (1970) :3471–3479.
- [5] Onufriev, A.; Case, D. A.; Ullmann, G. M. A novel view of pH titration in biomolecules, *Biochemistry.* 40 (2001) :3413–3419.
- [6] Lippard, S A.; Berg, J. M. Principle of organic chemistry, University Science Books. California: Mill Valley, 1994.
- [7] Hughes, M. N. The inorganic chemistry of biological process, 2nd ed. Chichester: John Wiley and Sons, 1981.
- [8] Dougherty, D. A. Cation intractions in chemistry and biology: a new view of benzene, Phe, Tyr and Trp, *Science.* 271 (1996) :163–168.
- [9] Freiser, B. S. Organometallic ion chemistry, Kluwer: Dordrecht, 1996.
- [10] Kaim, W.; Schwederski, B. Bioinorganic chemistry: Inorganic Elements in Chemistry of Life, Chichester: John Wiley & Sons, 1994.
- [11] Chu, I. K.; Guo, X.; Lau, T–C. ; Siu, K. W. M. Sequencing of argintinated peptides by means of electrospray tandem mass spectrometry, *Anal chem.* 71 (1999) :2364–2372.
- [12] Lee, S–W.; Kim, H. S.; Beauchamp, J. L. Salt bridge chemistry applied to gas–phase peptide sequencing: Selective fragmentation of sodiated gas–phase peptide ions adjacent to aspartic acid residues, *J. Am. Chem. Soc.* 120 (1998) :3188–3195.
- [13] Lin, T.; Glish, G. L. C–Terminal peptide sequencing via multistage mass spectrometry, *Anal. Chem.* 70 (1998) :5162–5165.

- [14] Edsall, J. T.; Blanchard, M. H. The activity ratio of zwitterions and uncharged molecules in ampholyte solutions. The dissociation constants of amino acid esters, *J. Am. Chem. Soc.* 55 (1933) :2337–2353.
- [15] Noszál, B. Microspeciation of polypeptides, *Phys. chem.* 90 (1986) :6345–6349.
- [16] Tananaeva, N. N.; Gorokhovatskaya, M. Ya.; Tikhonova, R. V.; Kostromina, N.A. Investigation of the conformation of aspartic acid by the NMR method, *Theor. Exp. Chem.* 21 (1985) :471–475.
- [17] Ruangpornvisuti, V.; Tomapatanaget, B. Determination of acidity and basicity constants of polyaspartic acids by potentiometric titrations, *ScienceAsia.* 29 (2003) :45–49.
- [18] Feng, W. Y.; Gronert, S.; Lebrilla, C. The lithium cation binding energies of gaseous amino acids, *J. Phys. Chem A.* 107 (2003) :405–410.
- [19] Feng, W. Y.; Gronert, S.; Lebrilla, C. B. Lithium and sodium ion binding energies of N-acetyl and N-glycyl amino acids, *J. Am. Chem. Soc.* 121 (1999) :1365–1371.
- [20] Kish, M. M., Wesdemiotis, C., Ohanessian, G. The Na⁺ affinities of α -amino acids: Side-chain substituent effects, *Int. J. Mass. Spectrom.* 227 (2003) :509–524.
- [21] Bukietyńska, K.; Podsiadły, H.; Karwecka, Z. Complexes of vanadium (III) with L-alanine and L-aspartic acid, *J. Inorg. Biochem.* 94 (2003) :317–325.
- [22] Massa, M. B.; Dalosto, S. D.; Graciela, F. M.; Labadie, G.; Calvo, R. Vibronic Behavior and Single-Crystal EPR Spectra of Cu(II) in Copper-Doped Diaqua(L-aspartato)zinc(II) Hydrate, *J. Phys. Chem. A.* 103 (1999) :2606–2617.
- [23] Battaglia, L. P.; Bonamartini, C. A.; Antolini, L.; Marcotrigiano, G.; Menabue, L.; Pellacani, G. C. Coordination behavior of L-aspartic acid: Ternary nickel(II) complexes with imidazoles. Crystal and molecular structure of (L-aspartate)tris(imidazole)nickel(II), *J. Am. Chem. Soc.* 104 (1982) :2407–2411.
- [24] Antolini, L.; Battaglia, L. P.; Bonamartini, C. A.; Marcotrigiano, G.; Menabue, L.; Pellacani, G. C.; Saladini, M.; Sola, M. Tridentate facially coordinated L-aspartate ion complexation with the copper(II) ion: Spectroscopic and

- structural properties of aqua(L-aspartato)(1,10-phenanthroline)copper(II) tetrahydrate, *Inorg. Chem.* 25 (1986) :2901–2904.
- [25] Koo, J. C. P.; Lam, J. S. W.; Chass, G. A.; Torday, L. L.; Varro A.; Papp, J. G. Conformational dependence of the intrinsic acidity of the aspartic acid residue sidechain in *N*-acetyl-L-aspartic acid-*N'*-methanamide, *J. Mol. Struct (Theochem)* 620 (2003) :231–255.
- [26] Salpietro, S. J.; Perczel, A.; Farkas, Ö.; Enriz R. D.; and Csizmadia. I. G. Peptide models XXV. Side-chain conformational potential energy surface, $E=E(\chi_1, \chi_2)$ of *N*-formyl-L-aspartic acidamide and its conjugate base *N*-formyl-L-aspartatamide in their γ_L backbone conformations, *J. Mol. Struct (Theochem)* 497 (2000) :39–96.
- [27] Grant, G. H.; Richards, W. G. Computational chemistry, New York: Oxford university press, 1995.
- [28] Jensen, F. Introduction to computational chemistry, Chichester: John Wiley and Sons, 1999.
- [29] Cramer, C. J. Essentials of computational chemistry, Chichester: John Wiley and Sons, 2001.
- [30] Lewars, E. Computational chemistry: Introduction to theory and applications of molecular and quantum mechanics, Massachusetts: Kluwer academic publisher, 2003.
- [31] Sabin, J. R.; Trickey, S. B.; Apell, S. P.; Oddershede, J.; Molecular Shape, Capacitance, and Chemical Hardness, *J. Quant. Chem.* 77 (2000) :358–366.
- [32] Tomasi, J.; Mennucci, B.; Cammi, R. Quantum Mechanical Continuum Solvation Models, *Chem. Rev.* 105 (2005) :2999–3094.
- [33] Becke, A. D. Density-Functional Thermochemistry. III. The role of exact exchange, *J. Chem. Phys.* 98 (1993) :5648–5652.
- [34] Lee, C.; Yang, W.; Parr, R. G. Development of the colle-salvetti correlation-energy formula into a functional of the electron density, *Phys. Rev B.* 37 (1988) :785–789.
- [35] Frisch, M. J.; Trucks, G. W.; Schlegel, H. B., Scuseria, G. E.; Robb, M. A.; Cheeseman, J. R.; Montgomery, Jr., Vreven, T.; Kudin, K. N.; Burant, J. C.; Millam, J. M.; Iyengar, S. S., Tomasi, J.; Barone, V.; Mennucci, B.; Cossi, M.; Scalmani, G.; Rega, N.; Petersson, G. A.; Nakatsuji, H.; Hada,

- M.; Ehara, M.; Toyota, K.; Fukuda, R.; Hasegawa, J.; Ishida, M.; Nakajima, T.; Honda, Y.; Kitao, O.; Nakai, H.; Klene, M.; Li, X.; Knox, J. E.; Hratchian, H. P.; Cross, J. B.; Adamo, C.; Jaramillo, J.; Gomperts, R.; Stratmann, R. E.; Yazyev, O.; Austin, A. J.; Cammi, R.; Pomelli, C.; Ochterski, J. W.; Ayala, P. Y.; Morokuma, K.; Voth, G. A.; Salvador, P.; Dannenberg, J. J.; Zakrzewski, V. G.; Dapprich, S.; Daniels, A. D.; Strain, M. C.; Farkas, O.; Malick, D. K.; Rabuck, A. D.; Raghavachari, K.; Foresman, J. B.; Ortiz, J. V.; Cui, Q.; Baboul, A. G.; Clifford, S.; Cioslowski, J.; Stefanov, B. B.; Liu, G.; Liashenko, A.; Piskorz, P.; Komaromi, I.; Martin, R. L.; Fox, D. J.; Keith, T.; Al-Laham, M. A.; Peng, C. Y.; Nanayakkara, A.; Challacombe, M.; Gill, P. M. W.; Johnson, B.; Chen, W.; Wong, M. W.; Gonzalez, C.; Pople, J. A. Gaussian 03; Revision B.03; Gaussian, Inc.: Pittsburgh PA, 2003.
- [36] Flükiger, P.; Lüthi, H. P.; Portmann S.; Weber, J. MOLEKEL 4.3, Swiss Center for Scientific Computing, Manno (Switzerland), 2000.
- [37] Sang-aaron, W.; Ruangpornvisuti, V. Conformational study of cationic, zwitterionic, anionic species of aspartic acid, water-added forms and their protonation. A DFT method, *J. Mol. Struct (Theochem)* 758 (2006) :181–187.
- [38] Frisch, M. J.; Del Bene, J. E.; Binkley, J. S.; Schaefer III, H. F. Extensive theoretical studies of the hydrogen-bonded complexes $(\text{H}_2\text{O})_2$, $(\text{H}_2\text{O})_2\text{H}^+$, $(\text{HF})_2$, $(\text{HF})_2\text{H}^+$, F_2H^- , and $(\text{NH}_3)_2$, *J. Chem. Phys.* 84 (1986) :2279–2289.
- [39] Schwenke, D. W.; Truhlar, D. G. Systematic study of basis set superposition errors in the calculated interaction energy of two HF molecules, *J. Chem. Phys.* 82 (1985) :2418–2426.
- [40] Sang-aaron, W.; Ruangpornvisuti, V. Conformational analysis of alkali metal complexes of aspartate dianion and their interactions in gas phase, *J. Mol. Graph. Model.* 26 (2007) :342–351.
- [41] Sang-aaron, W.; Ruangpornvisuti, V. Conformational analysis of alkali metal complexes of anionic species of aspartic acid, their interconversion and deprotonation, A DFT investigation, *J. Mol. Graph. Model.* 26 (2007) :982–990.

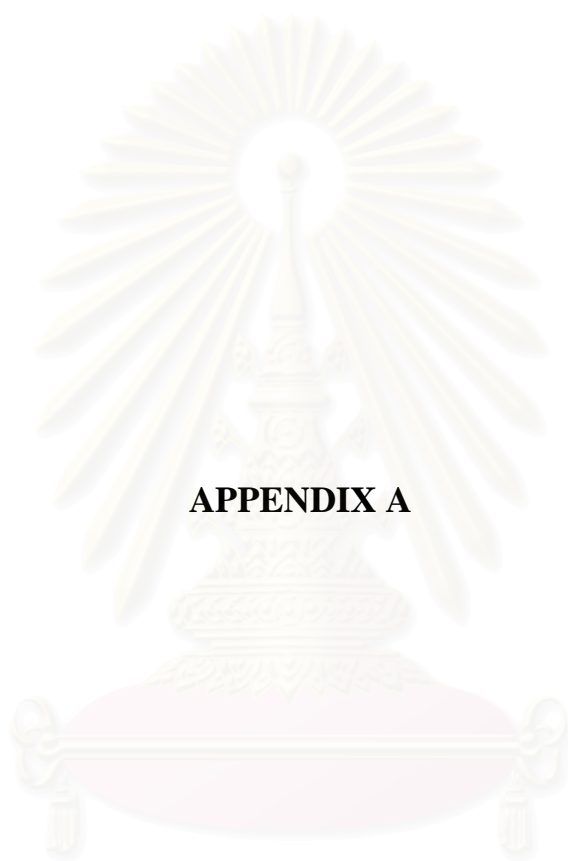
- [42] Sang-aaron, W.; Ruangpornvisuti, V. Determination of aqueous acid-dissociation constants of aspartic acid using PCM/DFT method, *Int. J. Quant. Chem.* 108 (2008) :1181–1188.
- [43] Cancès, E.; Mennucci, B.; Tomasi, J. A new integral equation formalism for the polarizable continuum model: Theoretical background and applications to isotropic and anisotropic dielectrics, *J. Chem. Phys.* 107 (1997) :3032–3041.
- [44] Mennucci, B.; Tomasi, J. Continuum solvation models: A new approach to the problem of solute's charge distribution and cavity boundaries, *J. Chem. Phys.* 106 (1997) :5151–5158.
- [45] Cossi, M.; Barone, V.; Mennucci, B.; Tomasi, J. Ab initio study of ionic solutions by a polarizable continuum dielectric model, *Chem. Phys. Lett.* 286 (1998) :253–260.
- [46] Barone, V.; Cossi, M.; Tomasi, J. Geometry optimization of molecular structures in solution by the polarizable continuum model, *J. Comput. Chem.* 19 (1998) :404–417.
- [47] Barone, V.; Cossi, M.; Tomasi, J. A new definition of cavities for the computation of solvation free energies by the polarizable continuum model, *J. Chem. Phys.* 107 (1997) :3210–3221.
- [48] Cossi, M.; Barone, V.; Cammi, R.; Tomasi, J. Ab initio study of solvated molecules: A new implementation of the polarizable continuum model, *Chem. Phys. Lett.* 255 (1996) :227–235.
- [49] Cossi, M.; Rega, N.; Scalmani, G.; Barone, V. Energies, structures, and electronic properties of molecules in solution with the C-PCM solvation model, *J. Comput. Chem.* 24 (2003) :669–681.
- [50] Cossi, M.; Barone, V. Analytical second derivatives of the free energy in solution by polarizable continuum models, *J. Chem. Phys.* 109 (1998) :6246–6254.
- [51] Barone, V.; Cossi, M. Quantum calculation of molecular energies and energy gradients in solution by a conductor solvent model, *J. Phys. Chem. A.* 102 (1998) :1995–2001.
- [52] Mennucci, B.; Cancès, E.; Tomasi, J. Evaluation of solvent effects in isotropic and anisotropic dielectrics and in ionic solutions with a unified integral

- equation method: Theoretical bases, computational implementation, and numerical applications, *J. Phys. Chem B.* 101 (1997) :10506–10517.
- [53] Kelly, C. P.; Cramer, C. J.; Truhlar, D. G. Adding explicit solvent molecules to continuum solvent calculations for the calculation of aqueous acid dissociation constants, *J. Phys. Chem A.* 110 (2006) :2493–2499.
- [54] Topol, I. A.; Tawa, G. J.; Burt, S. K.; Rashin, A. A. On the structure and thermodynamics of solvated monoatomic ions using a hybrid solvation model, *J. Chem. Phys.* 111 (1999) :10998–11014.
- [55] Liptak, M. D.; Shields, G. C. Accurate pK_a calculations for carboxylic acids using Complete Basis Set and Gaussian- n models combined with CPCM continuum solvation methods, *J. Am. Chem. Soc.* 123 (2001) :7314–7319.
- [56] Pratuangdejkul, J.; Nosoonngnoen, W.; Guerin, G.-A.; Loric, S.; Conti, M.; Launay, J.-M.; Manivet, P. Conformational dependence of serotonin theoretical pK_a prediction, *Chem. Phys. Lett.* 420 (2006) :420. 538–544.



APPENDICES

สถาบันวิทยบริการ
จุฬาลงกรณ์มหาวิทยาลัย



APPENDIX A

สถาบันวิทยบริการ
จุฬาลงกรณ์มหาวิทยาลัย

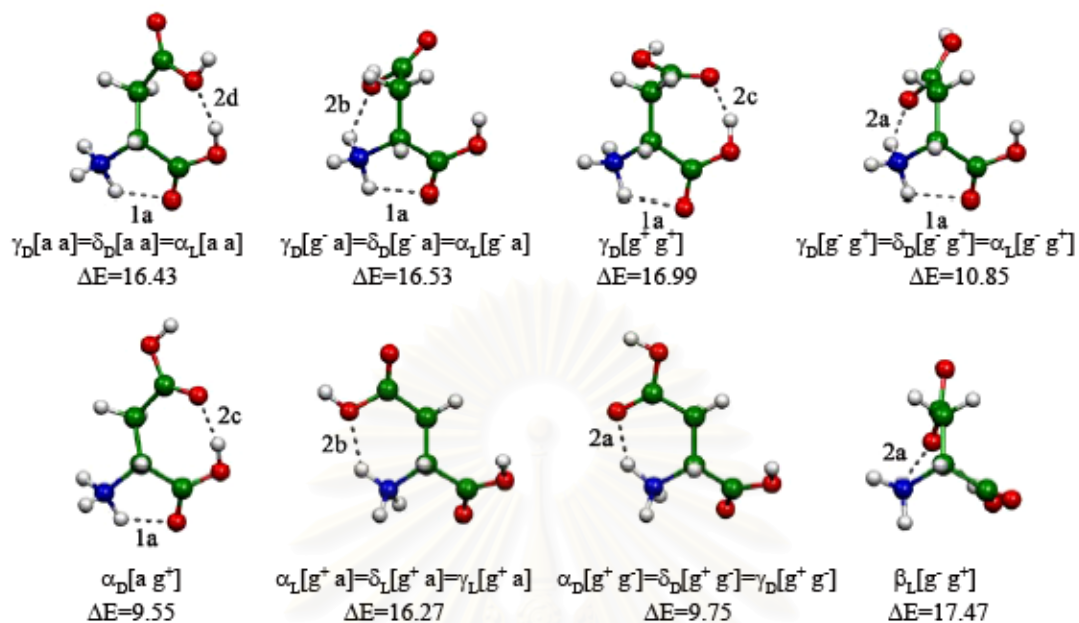


Figure A1: B3LYP/6-31G(d) optimized structures of species $H_3asp^+-endo-E$ and their conformations. Relative energy, ΔE is relative to the most stable species of H_3asp^+ ($\alpha_D [g^+ g^-] = \gamma_L [g^+ g^-] = \delta_L [g^+ g^-]$), in kcal/mol.

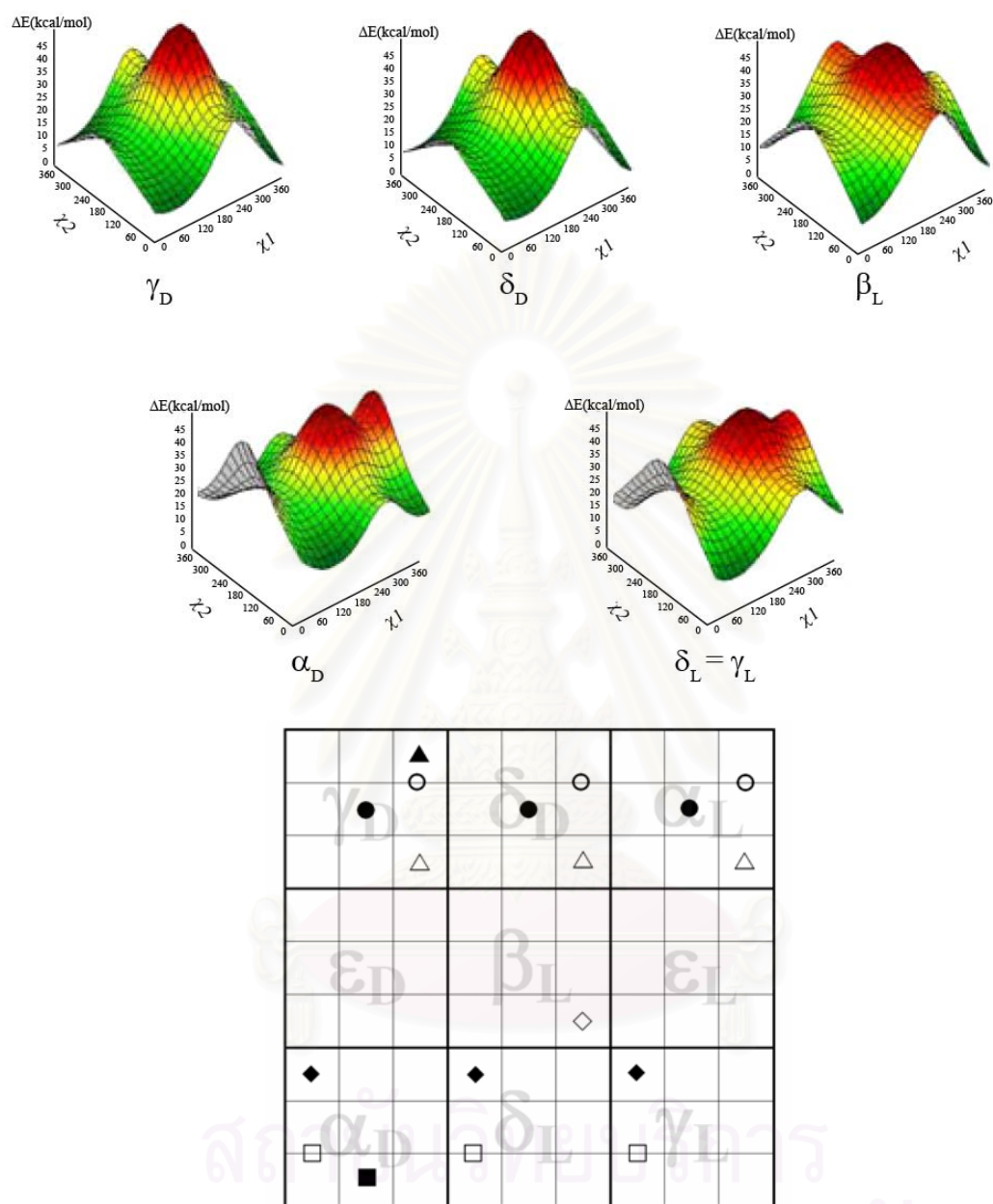


Figure A2: Landscape representations (top) of the side-chain conformational PESs, $E=E(\chi_1, \chi_2)$ associated with a backbone conformations of $H_3asp^+-endo-E$ and integrated scatter-plot diagram of their PESs (bottom) (● = γ_D [a a] = δ_D [a a] = α_L [a a], ○ = γ_D [g^- a] = δ_D [g^- a] = α_L [g^- a], ▲ = γ_D [g^- g^-], △ = γ_D [g^- g^+] = δ_D [g^- g^+] = α_L [g^- g^+], ■ = α_D [a g^+], □ = α_D [g^+ a] = δ_L [g^+ a] = γ_L [g^+ a], ◆ = α_D [g^+ g^-] = γ_L [g^+ g^-] = δ_L [g^+ g^-], ◇ = β_L [g^- g^+]).

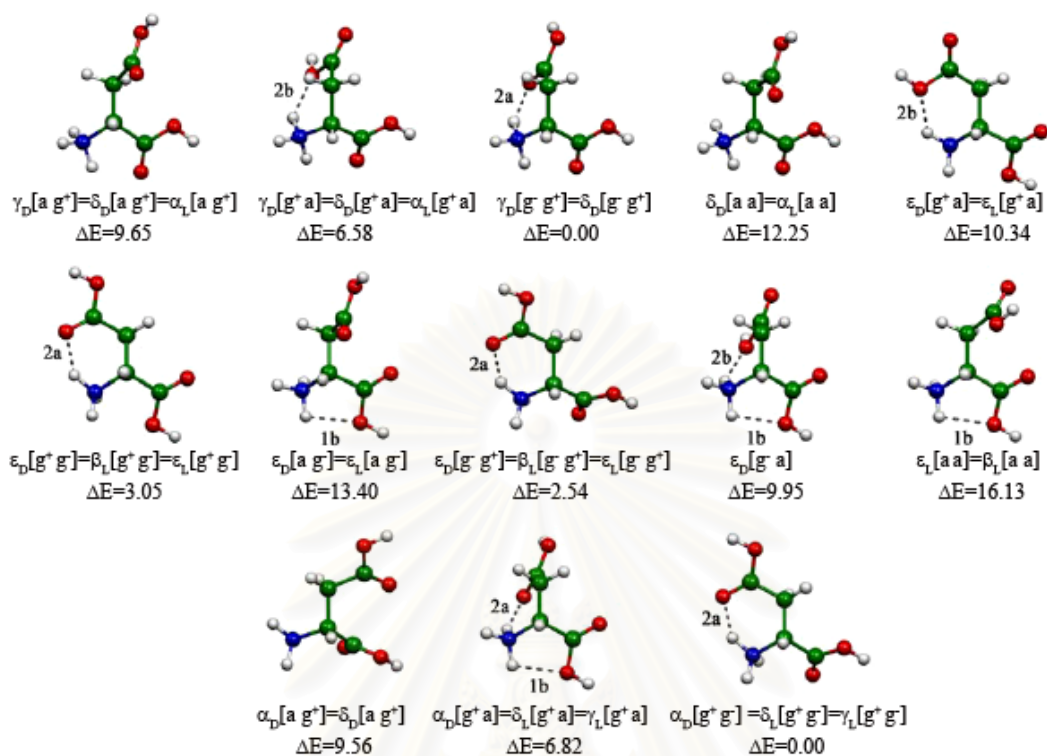


Figure A3: B3LYP/6-31G(d) optimized structures of species $H_3asp^+ -endo-E$ and their conformations. Relative energy, ΔE is relative to the most stable species of H_3asp^+ ($\alpha_D [g^+ g^-] = \gamma_L [g^+ g^-] = \delta_L [g^+ g^-]$), in kcal/mol.

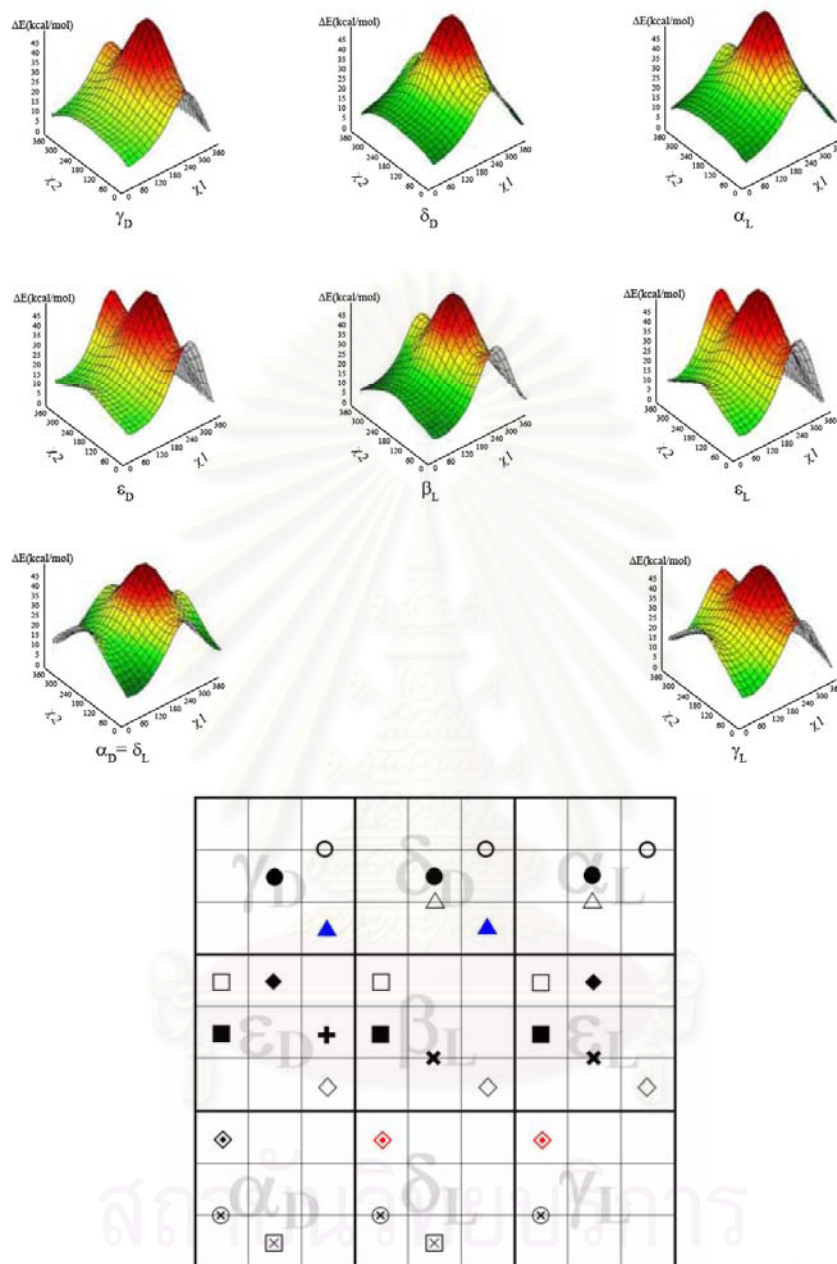


Figure A4: Landscape representations (top) of the side-chain conformational PESs, $E=E(\chi_1, \chi_2)$ associated with a backbone conformations of $H_3asp^+endo-Z$ and integrated scatter-plot diagram of their PESs (bottom) (● = $\gamma_D [a g^-] = \delta_D [a g^-] = \alpha_L [a g^-]$, ○ = $\gamma_D [g^- a] = \delta_D [g^- a] = \alpha_L [g^- a]$, ▲ = $\gamma_D [g^- g^+] = \delta_D [g^- g^+]$, △ = $\delta_D [a a] = \alpha_L [a a]$, ■ = $\epsilon_D [g^+ a] = \epsilon_L [g^+ a] = \beta_L [g^+ a]$, □ = $\epsilon_D [g^+ g^-] = \beta_L [g^+ g^-] = \epsilon_L [g^+ g^-]$, ◆ = $\epsilon_D [a g^-] = \epsilon_L [a g^-]$, ◇ = $\epsilon_D [g^- g^+] = \beta_L [g^- g^+] = \epsilon_L [g^- g^+]$, + = $\epsilon_D [g^- a]$, × = $\epsilon_L [a a] = \beta_L [a a]$, ⊗ = $\alpha_D [a g^+] = \delta_L [a g^+] = \gamma_L [g^+ a]$, ⊙ = $\alpha_D [g^+ g^-] = \delta_L [g^+ g^-] = \gamma_L [g^+ g^-]$).

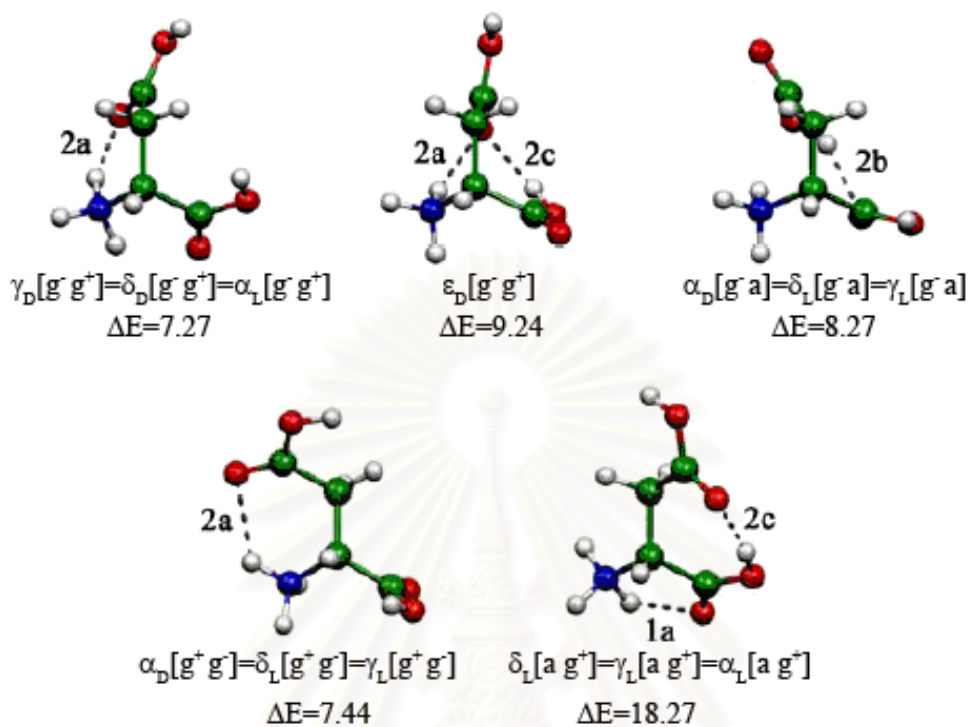


Figure A5: B3LYP/6-31G(d) optimized structures of species $H_3asp^+ -exo-E$ and their conformations. Relative energy, ΔE is relative to the most stable species of H_3asp^+ ($\alpha_D [g^+ g^-] = \gamma_L [g^+ g^-] = \delta_L [g^+ g^-]$), in kcal/mol.

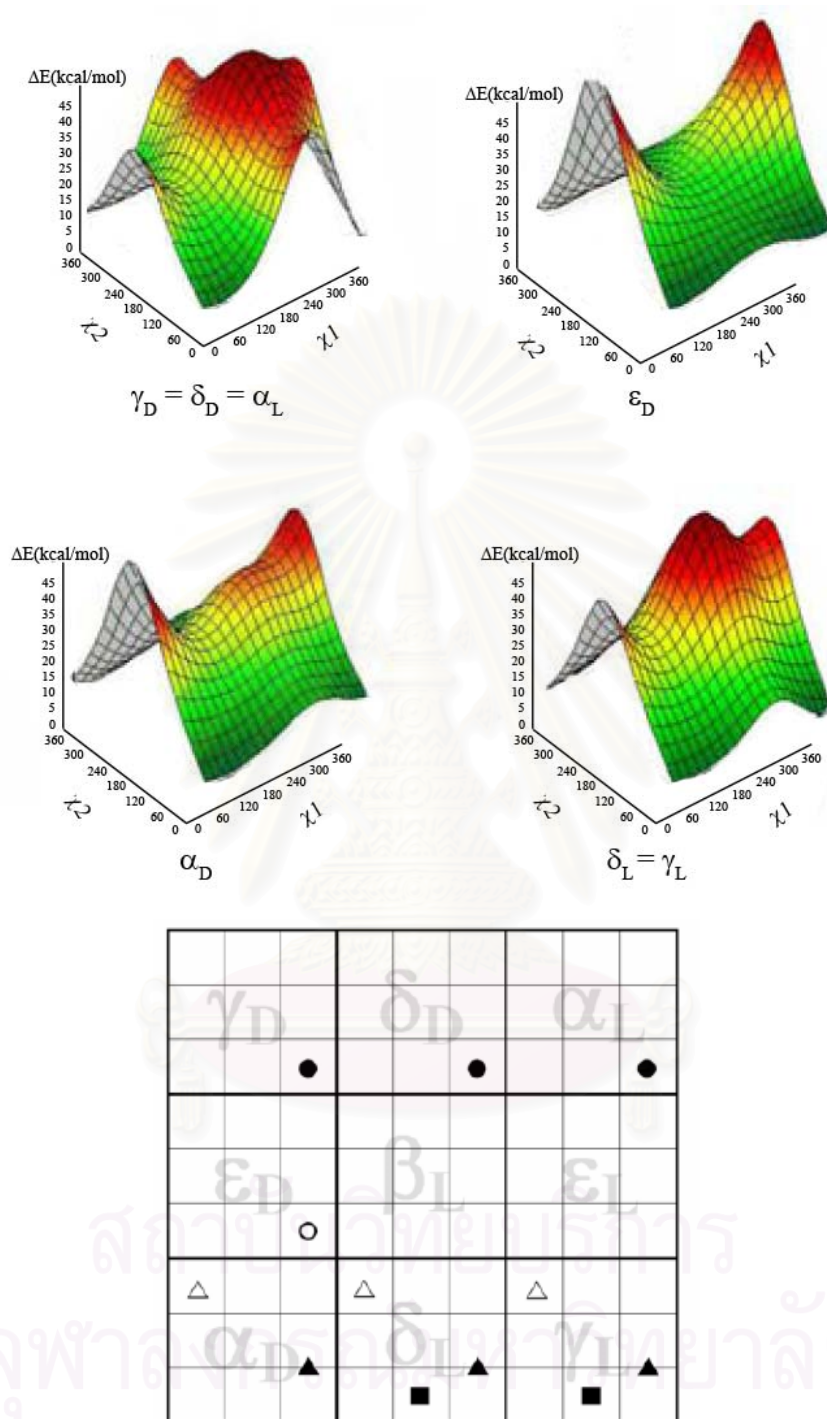


Figure A6: Landscape representations (top) of the side-chain conformational PESs, $E=E(\chi_1, \chi_2)$ associated with a backbone conformations of $\text{H}_3\text{asp}^+ \text{-exo-E}$ and integrated scatter-plot diagram of their PESs (bottom) (● = $\gamma_D [g^- g^+] = \delta_D [g^- g^+] = \alpha_L [g^- g^+]$, ○ = $\epsilon_D [g^- g^+]$, ▲ = $\alpha_D [g^- a] = \delta_L [g^- a] = \gamma_L [g^- a]$, △ = $\alpha_D [g^+ g^-] = \delta_L [g^+ g^-] = \gamma_L [g^+ g^-]$, ■ = $\delta_L [a g^+] = \gamma_L [a g^+]$).

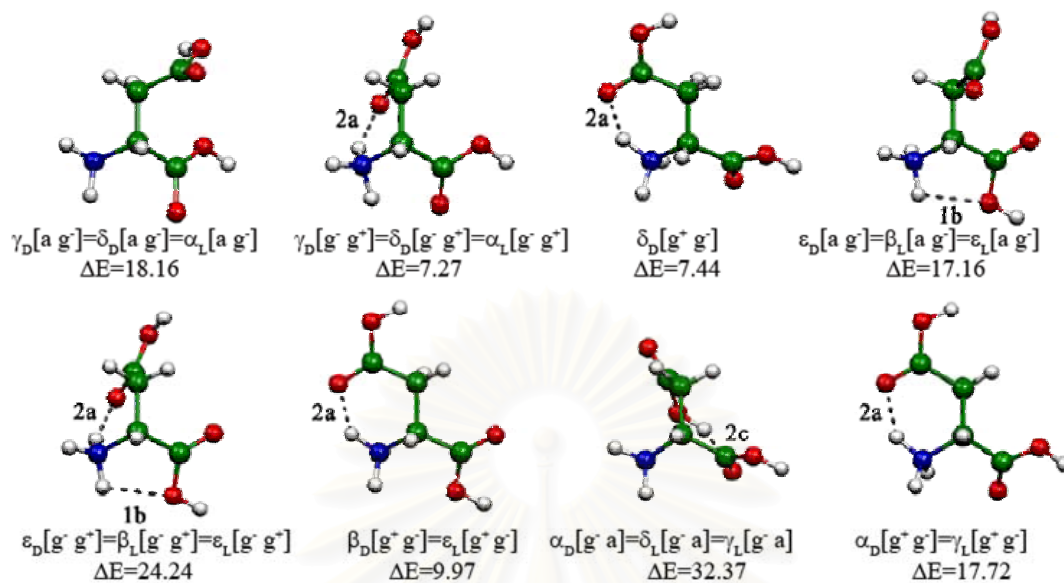


Figure A7: B3LYP/6-31G(d) optimized structures of species $H_3asp^+-exo-Z$ and their conformations. Relative energy, ΔE is relative to the most stable species of $H_3asp^+(\alpha_D [g^+g^-] = \gamma_L [g^+g^-] = \delta_L [g^+g^-])$, in kcal/mol.

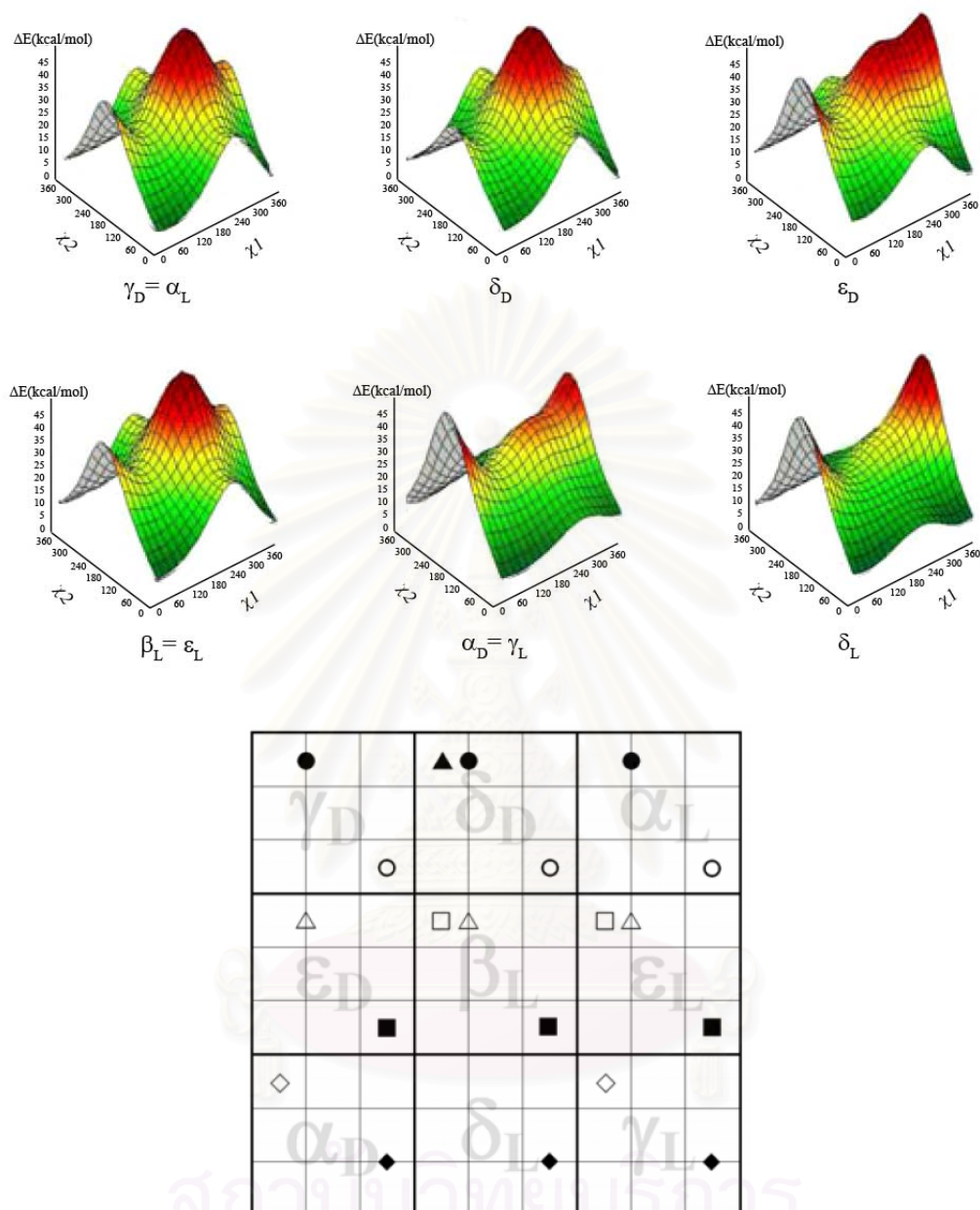


Figure A8: Landscape representations (top) of the side-chain conformational PESs, $E=E(\chi_1, \chi_2)$ associated with a backbone conformations of H_3asp^+exo-Z and integrated scatter-plot diagram of their PESs (bottom) (● = $\gamma_D [a g^-] = \delta_D [a g^-] = \alpha_L [a g^-]$, ○ = $\gamma_D [g^- g^+] = \delta_D [g^- g^+] = \alpha_L [g^- g^+]$, ▲ = $\delta_D [g^+ g^-]$, △ = $\epsilon_D [a g^-] = \beta_L [a g^-] = \epsilon_L [a g^-]$, ■ = $\epsilon_D [g^- g^+] = \beta_L [g^- g^+] = \epsilon_L [g^- g^+]$, □ = $\beta_L [g^+ g^-] = \epsilon_L [g^+ g^-]$, ◆ = $\alpha_D [g^- a] = \delta_L [g^- a] = \gamma_L [g^- a]$, ◇ = $\alpha_D [g^+ g^-] = \gamma_L [g^+ g^-]$).

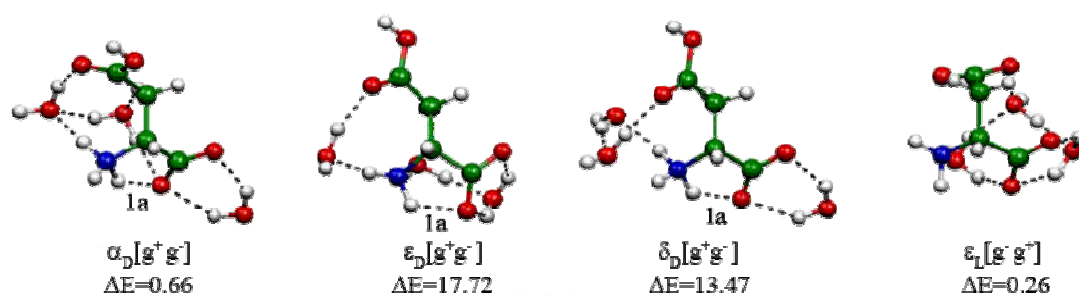


Figure A9: B3LYP/6–31G(d) optimized structures of trihydrated form of H₂asp–*endo* species and their conformations. Relative energy, ΔE is relative to the most stable species of H₂asp ($\alpha_L[a g^-]$), in kcal/mol.

สถาบันวิทยบริการ
 จุฬาลงกรณ์มหาวิทยาลัย

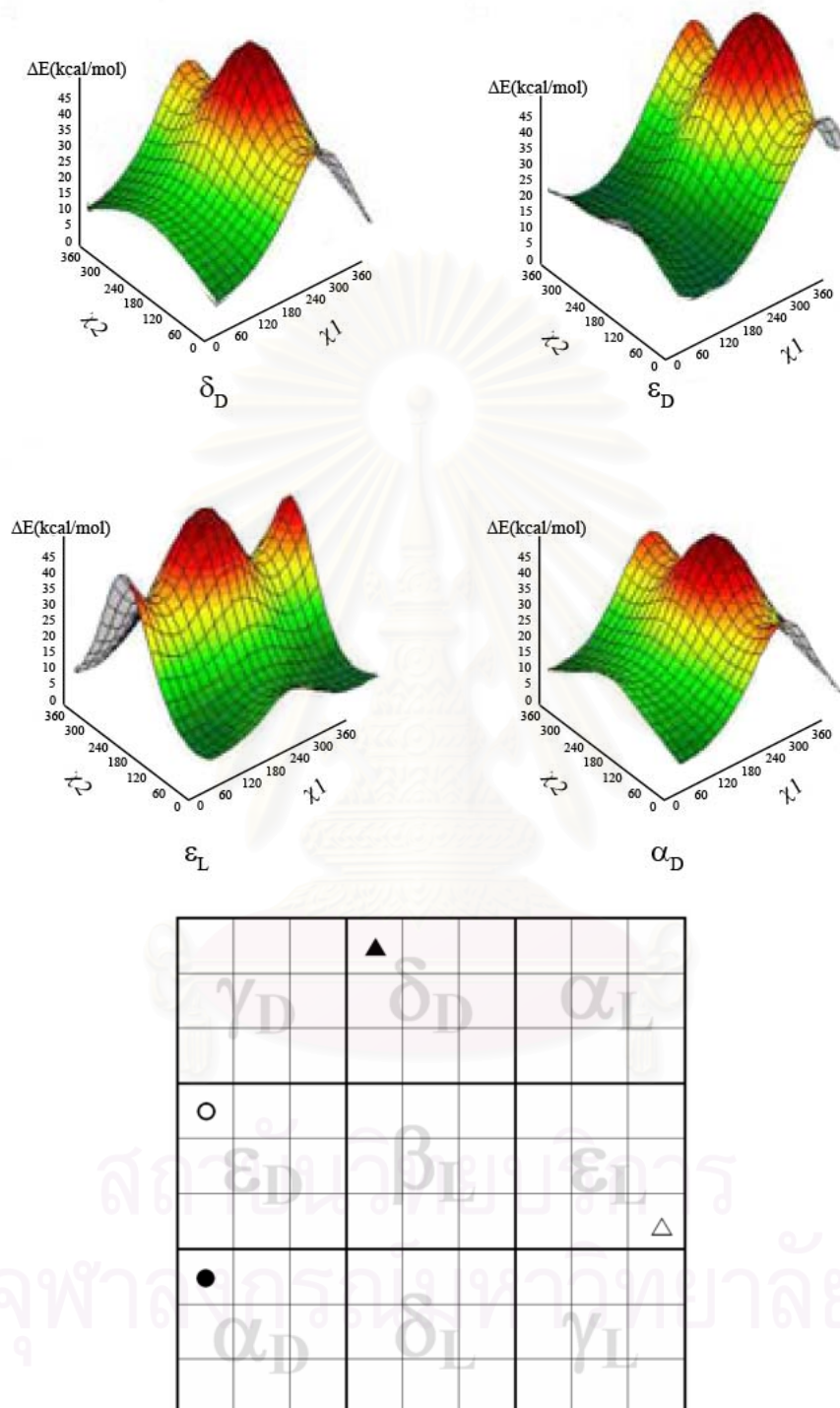


Figure A10: Landscape representations (top) of the side-chain conformational PESs, $E=E(\chi_1, \chi_2)$ associated with a backbone conformations of trihydrated form of $H_2asp-endo$ species and integrated scatter-plot diagram of their PESs (bottom) (● = $\epsilon_D [g^+ g^-]$, ○ = $\alpha_D [g^+ g^-]$, ▲ = $\delta_D [g^+ g^-]$, △ = $\epsilon_L [g^- g^+]$).

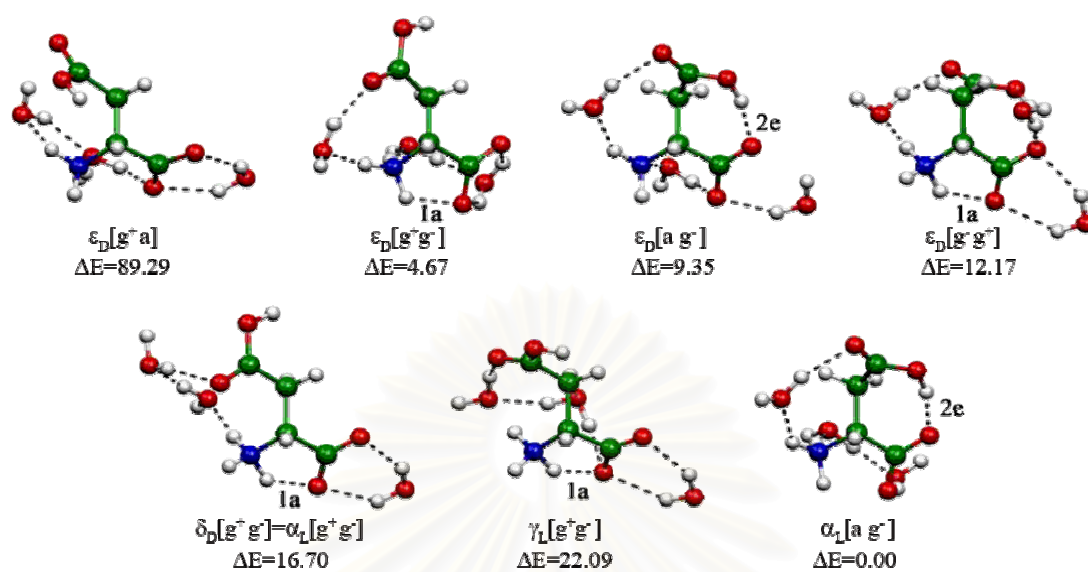


Figure A11: B3LYP/6-31G(d) optimized structures of trihydrated form of H₂asp-*exo* species and their conformations. Relative energy, ΔE is relative to the most stable species of H₂asp (α_L [a g⁻]), in kcal/mol.

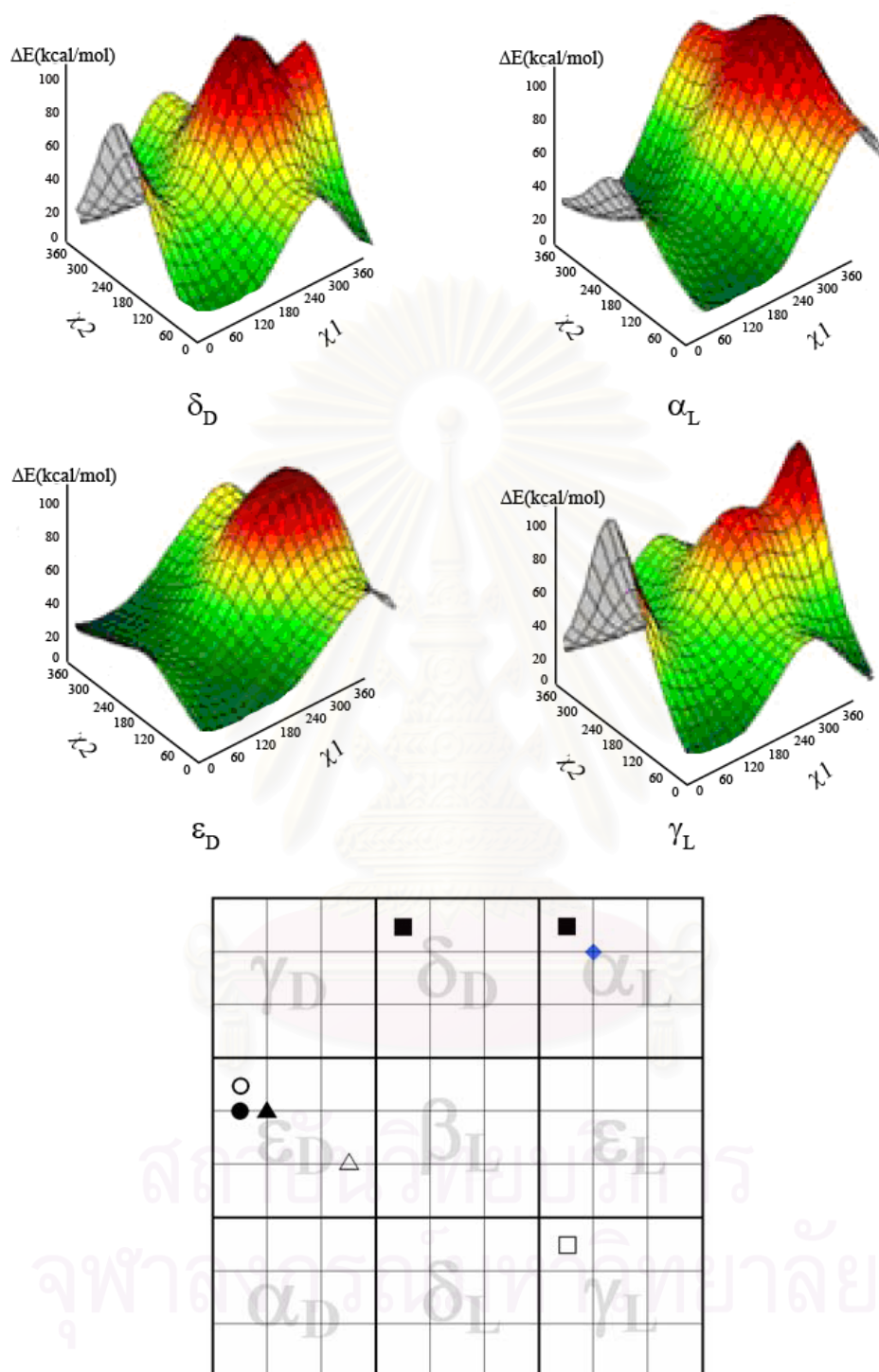


Figure A12: Landscape representations (top) of the side-chain conformational PESs, $E=E(\chi_1, \chi_2)$ associated with a backbone conformations of trihydrated form of $H_2asp-exo$ species and integrated scatter-plot diagram of their PESs (bottom) ($\bullet = \epsilon_D [g^+ a]$, $\circ = \epsilon_D [g^+ g^-]$, $\blacktriangle = \epsilon_D [a g^-]$, $\triangle = \epsilon_D [g^- g^+]$, $\blacksquare = \delta_D [g^+ g^-] = \alpha_L [g^+ g^-]$, $\square = \gamma_L [g^+ g^-]$, $\blacklozenge = \alpha_L [a g^-]$).

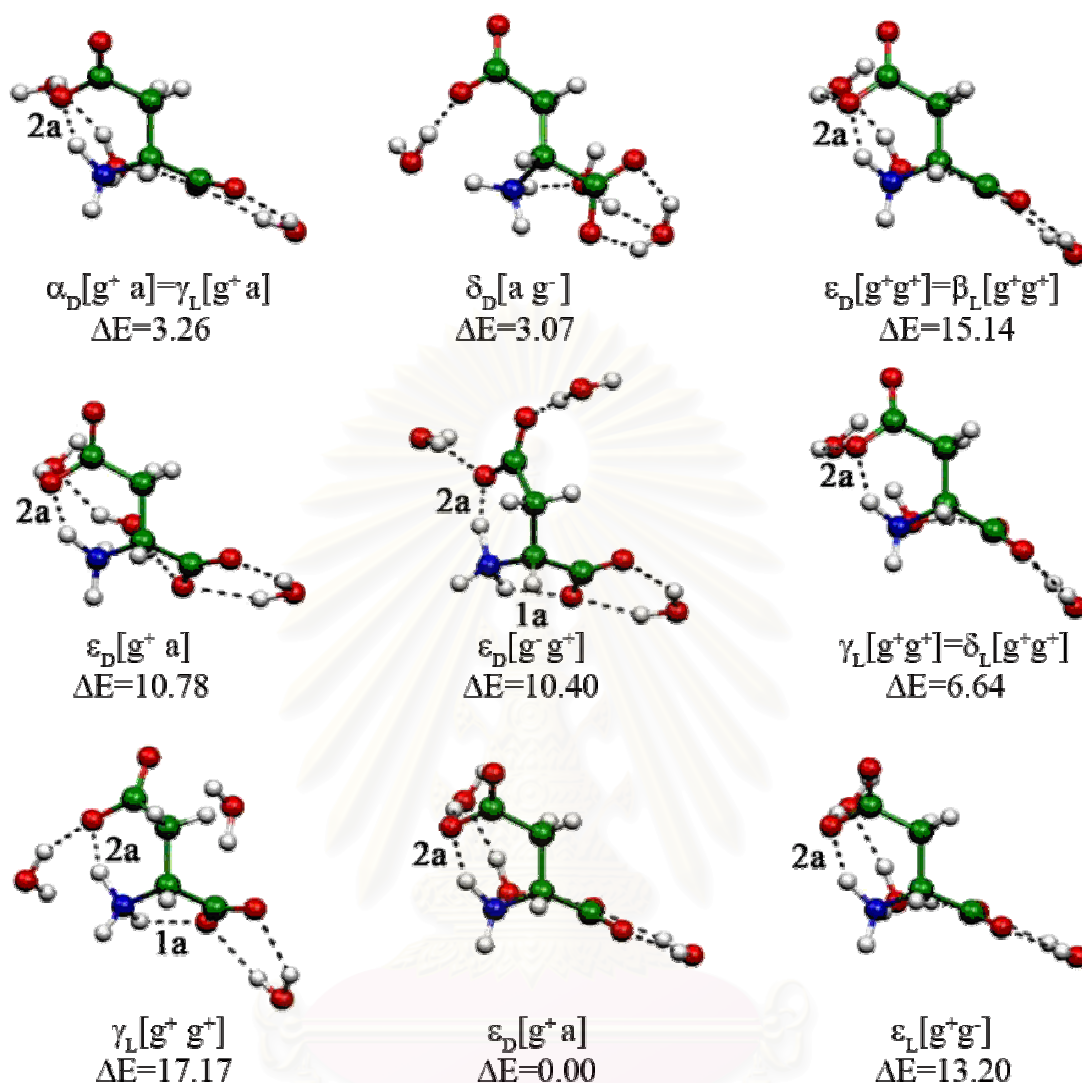


Figure A13: B3LYP/6-31G(d) optimized structures of trihydrated form of Hasp⁻ species and their conformations. Relative energy, ΔE is relative to the most stable species of Hasp⁻ ($\epsilon_L[g^+ a]$), in kcal/mol.

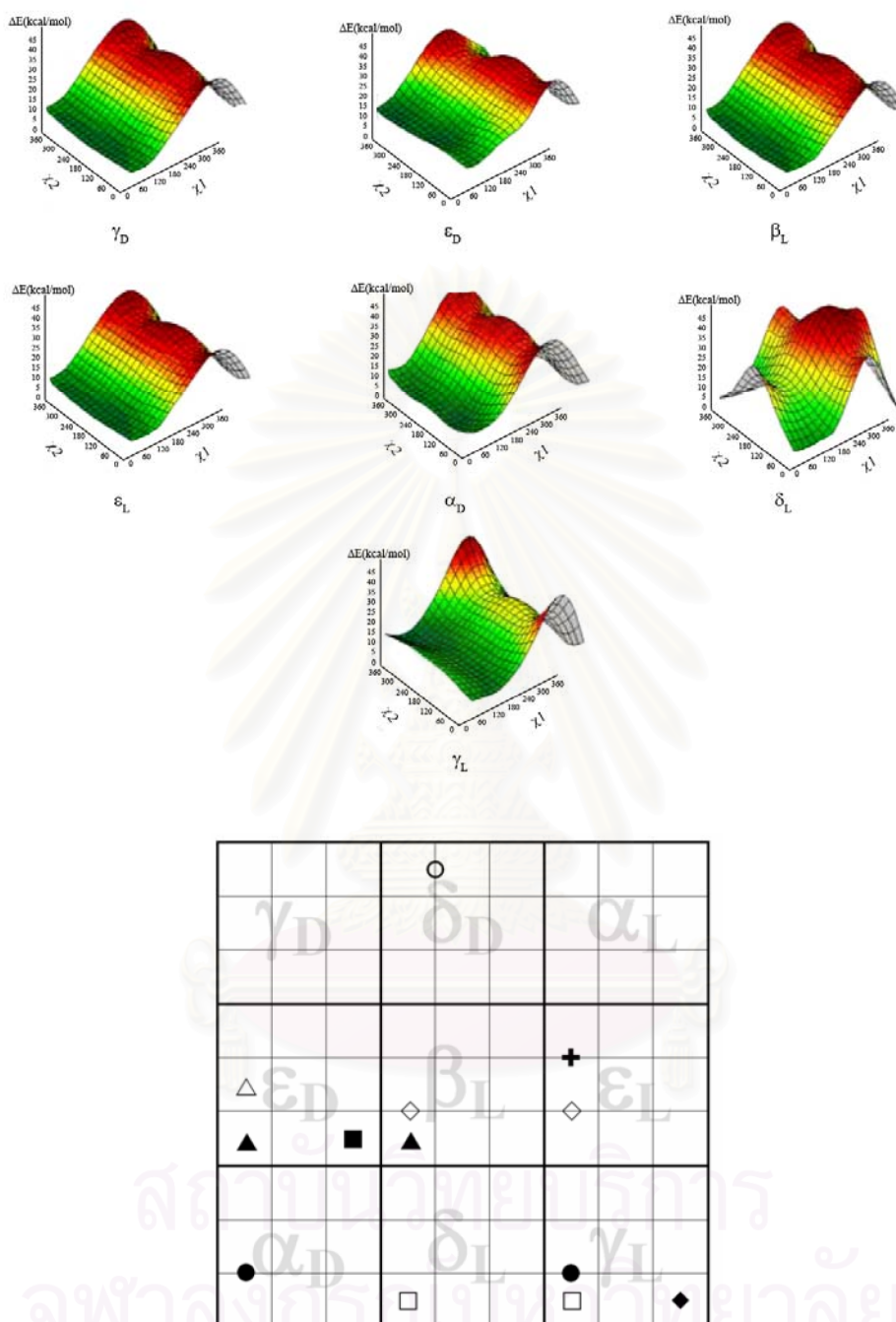


Figure A14: Landscape representations (top) of the side-chain conformational PESs, $E=E(\chi_1, \chi_2)$ associated with a backbone conformations of trihydrated form of Hasp^- species and integrated scatter-plot diagram of their PESs (bottom) ($\bullet = \alpha_D [g^+ a] = \gamma_L [g^+ a]$, $\circ = \delta_D [a g^-]$, $\blacktriangle = \epsilon_D [g^+ g^+] = \beta_L [g^+ g^+]$, $\triangle = \epsilon_D [g^+ a]$, $\blacksquare = \epsilon_D [g^- g^+]$, $\square = \gamma_L [g^+ g^+] = \delta_L [g^+ g^+]$, $\blacklozenge = \gamma_L [g^- g^+]$, $\diamond = \epsilon_L [g^+ a] = \beta_L [g^+ a]$, $\times = \epsilon_L [g^+ g^-]$).

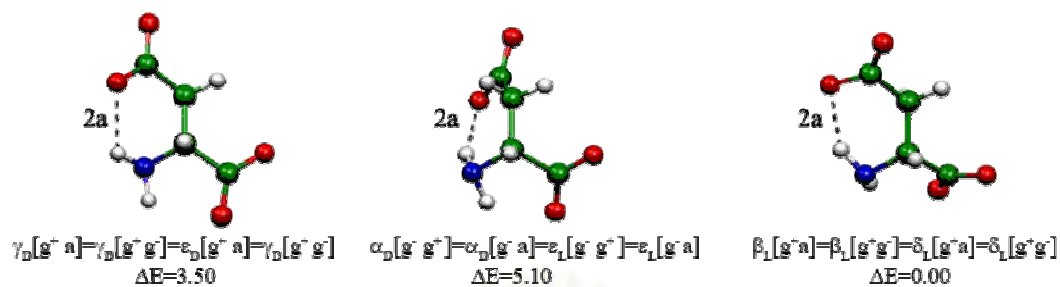


Figure A15: B3LYP/6-31G(d) optimized structures of species asp^{2-} and their conformations. Relative energy, ΔE is relative to the most stable species of asp^{2-} ($\beta_{\text{L}}[\text{g}^+ \text{a}]$), in kcal/mol.

สถาบันวิทยบริการ
จุฬาลงกรณ์มหาวิทยาลัย

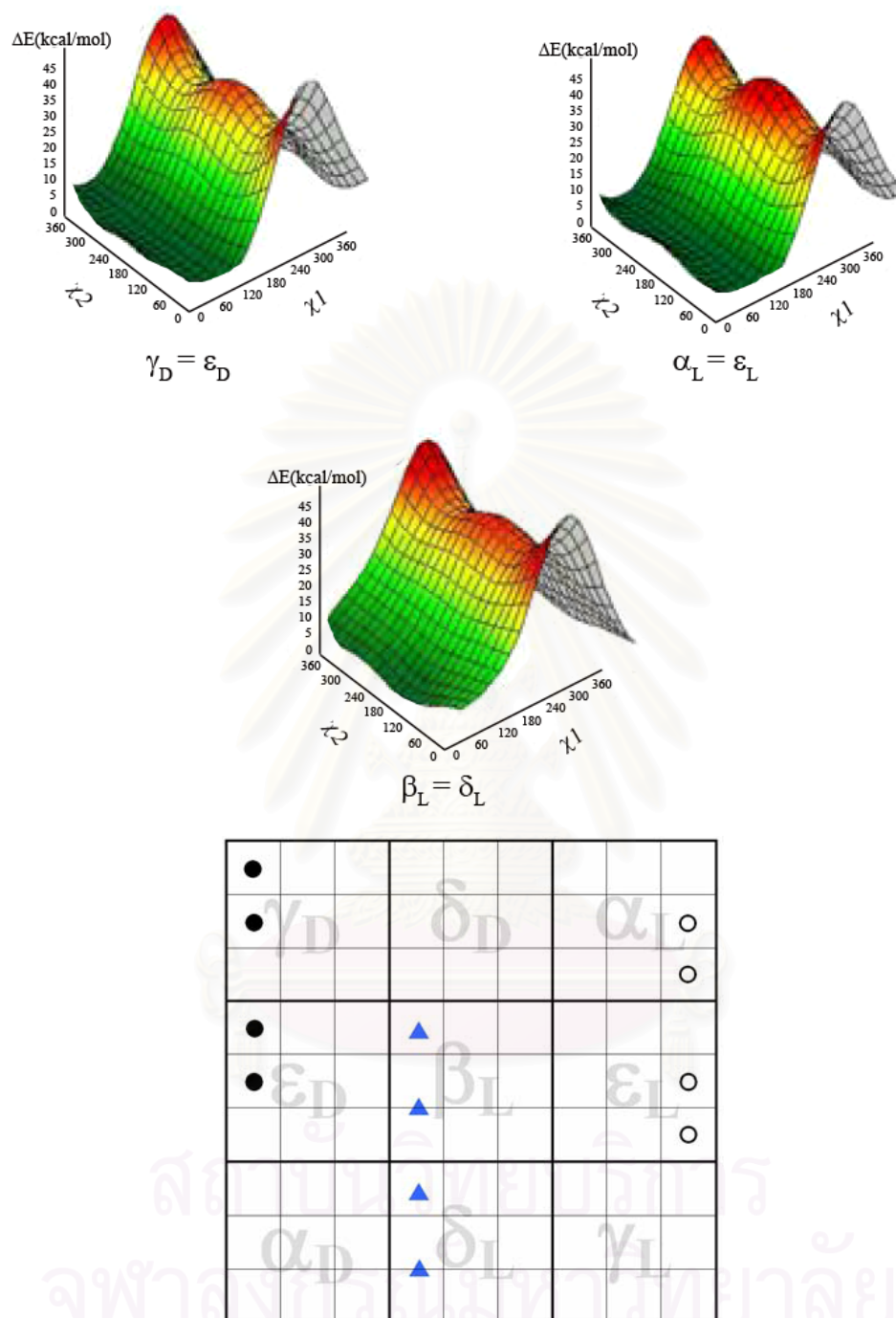


Figure A16: Landscape representations (top) of the side-chain conformational PESs, $E=E(\chi_1, \chi_2)$ associated with a backbone conformations of asp²⁻ and integrated scatter-plot diagram of their PESs (bottom) (● = $\gamma_D [g^+ a] = \gamma_D [g^+ g^-] = \epsilon_D [g^+ a] = \epsilon_D [g^+ g^-]$, ○ = $\alpha_L [g^- g^+] = \alpha_L [g^- a] = \epsilon_L [g^- g^+] = \epsilon_L [g^- a]$, ▲ = $\beta_L [g^+ a] = \beta_L [g^+ g^-] = \delta_L [g^+ a] = \delta_L [g^+ g^-]$).

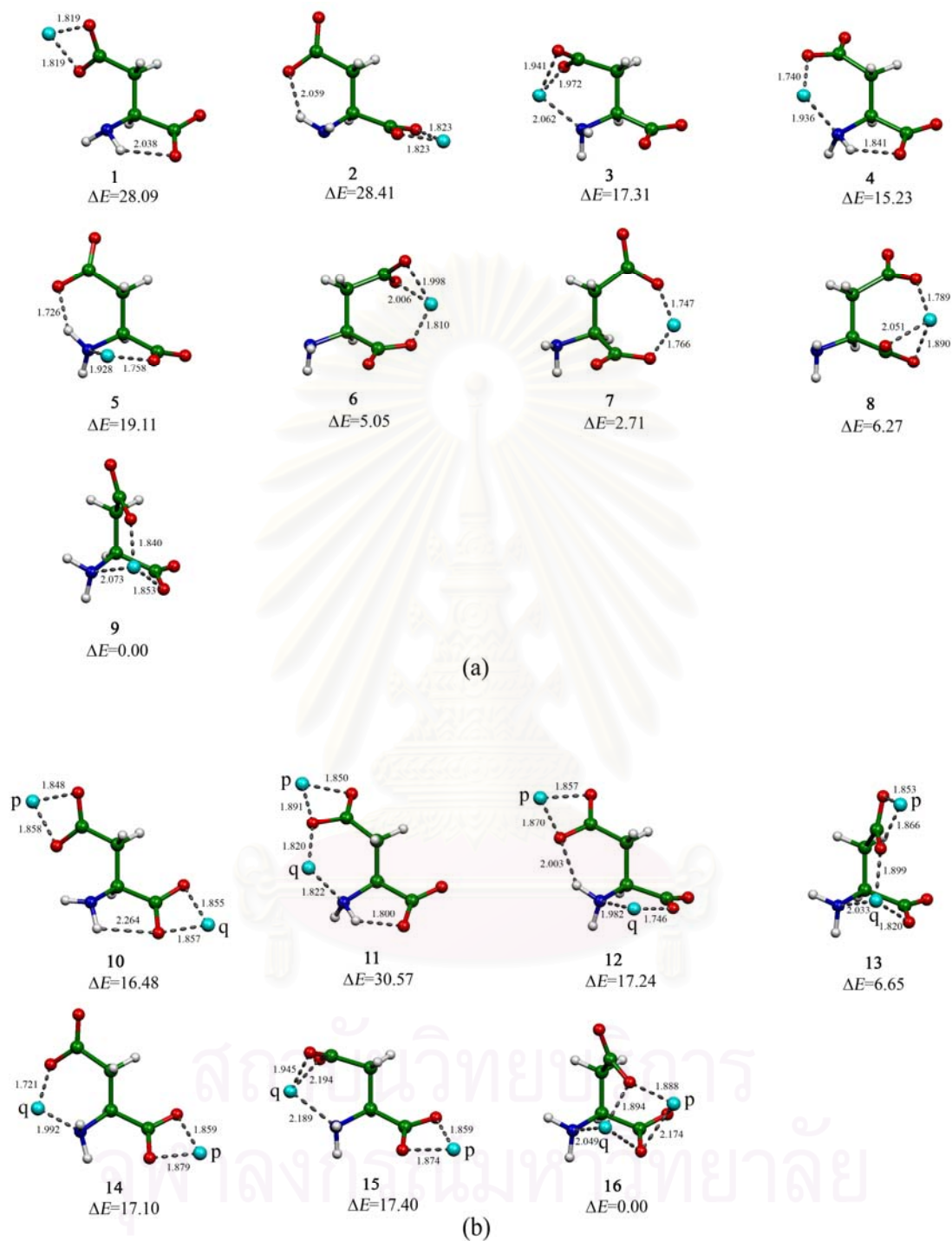


Figure A17: The B3LYP/6-311++G(d,p)-optimized structures of (a) $[\text{asp-Li}]^-$ and (b) $[\text{asp-Li}_2]$ complexes. Bond distances are in Å.

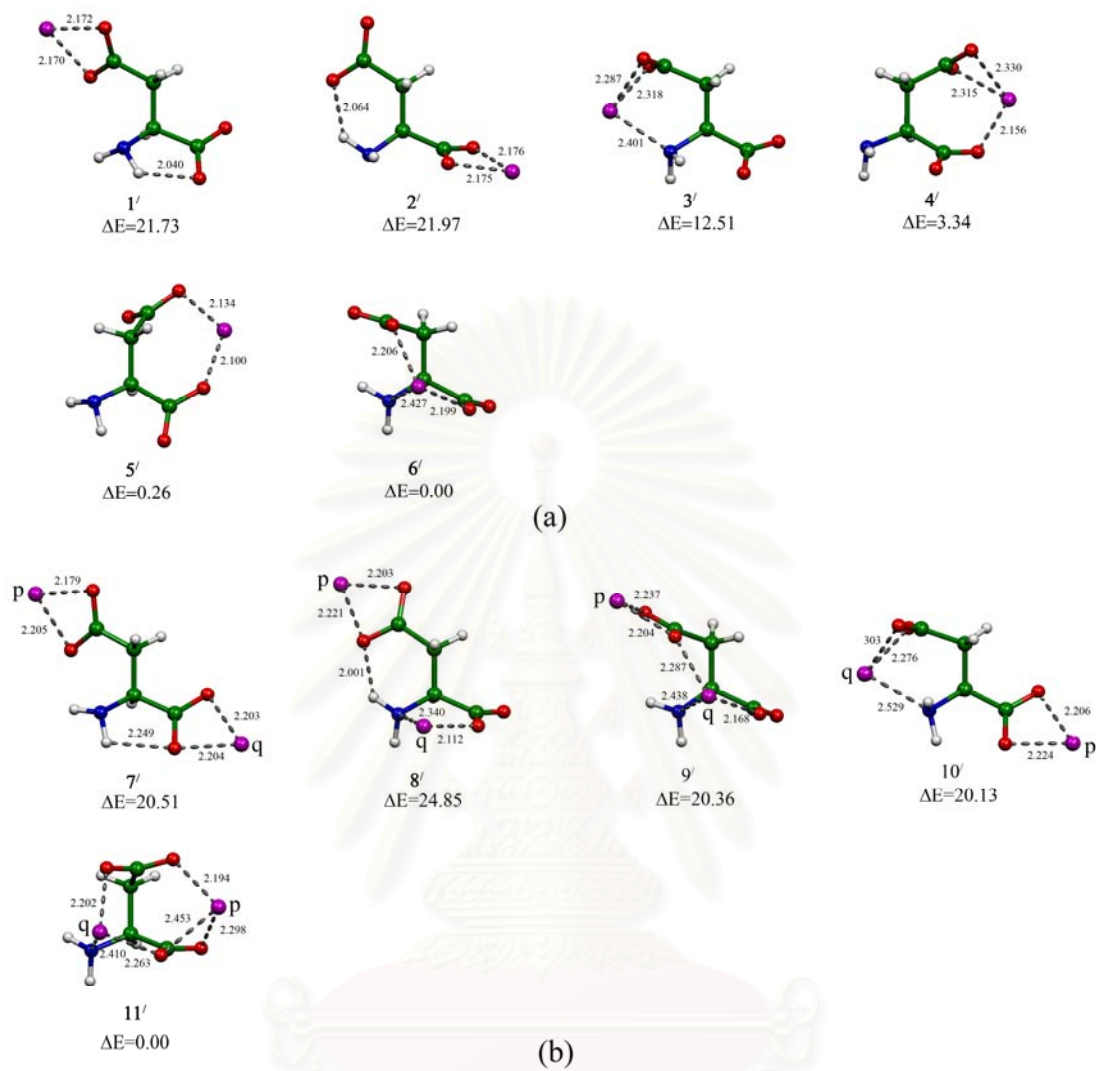


Figure A18: The B3LYP/6-311++G(d,p)-optimized structures of (a) $[\text{asp-Na}]^-$ and (b) $[\text{asp-Na}_2]$ complexes. Bond distances are in Å.

สถาบันวิทยบริการ
จุฬาลงกรณ์มหาวิทยาลัย

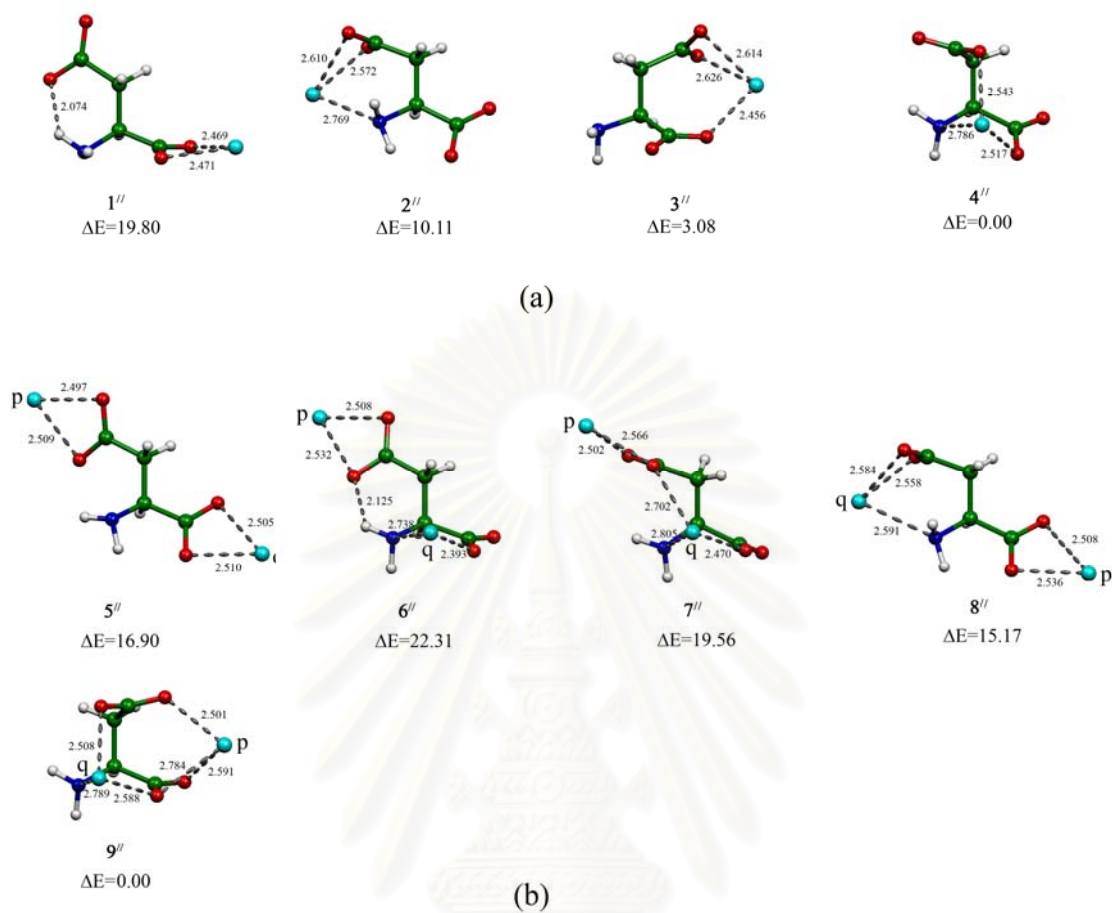


Figure A19: The B3LYP/6-311++G(d,p)-optimized structures of (a) [asp-K]⁻ and (b) [asp-K₂] complexes. Bond distances are in Å.

สถาบันวิทยบริการ
จุฬาลงกรณ์มหาวิทยาลัย

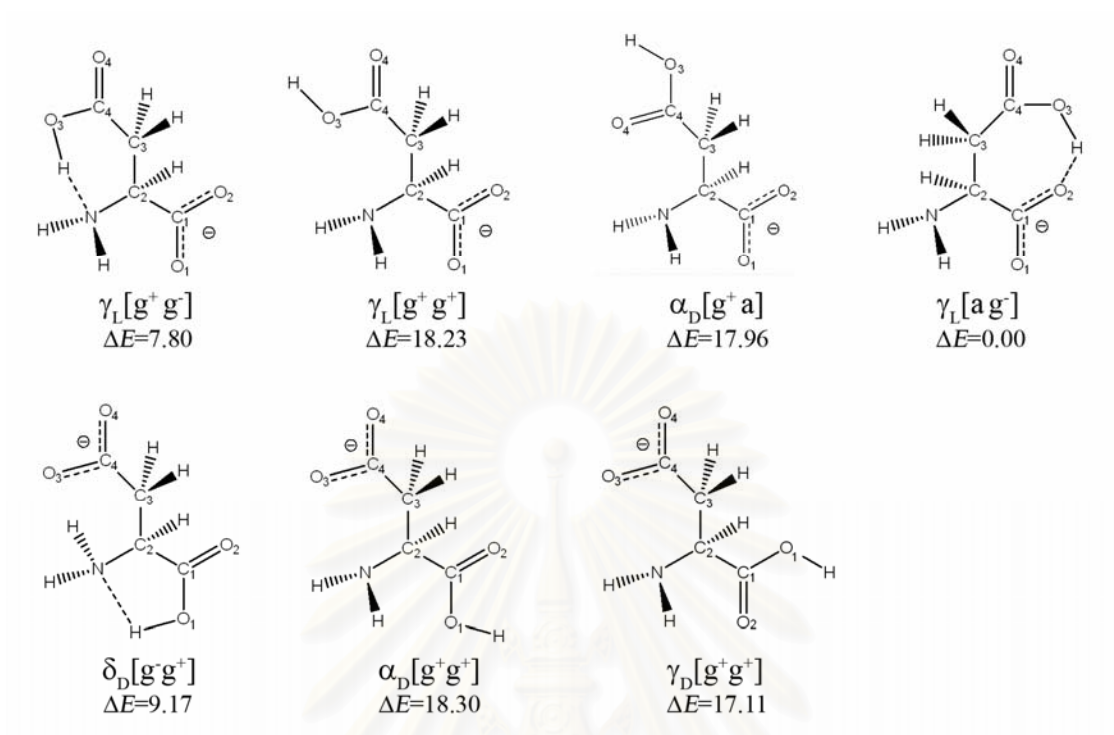


Figure A20: The B3LYP/6-311++G(d,p)-optimized structures of Hasp⁻ ligand.

สถาบันวิทยบริการ
จุฬาลงกรณ์มหาวิทยาลัย

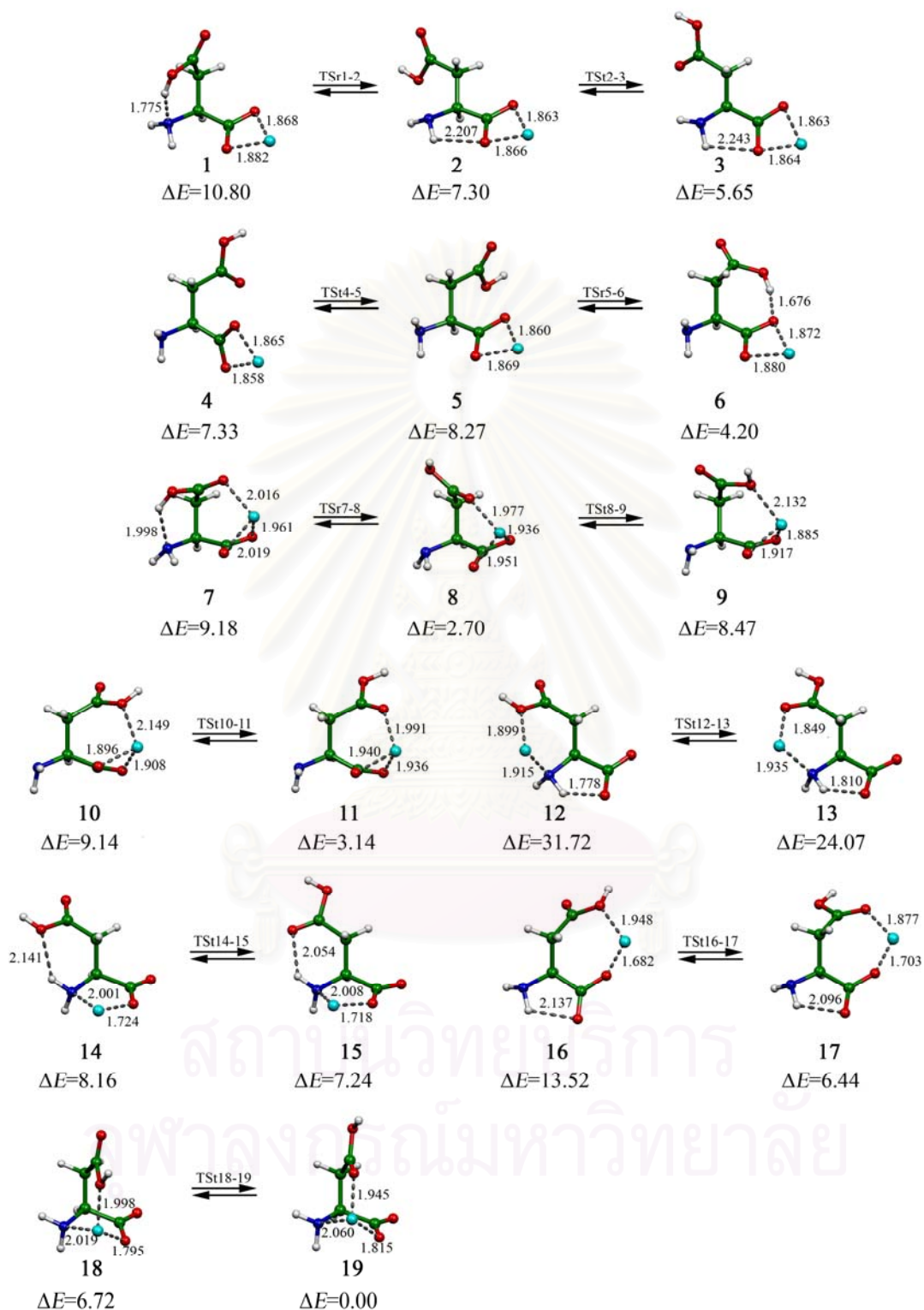


Figure A21: The B3LYP/6-311++G(d,p)-optimized structures of α -[Hasp-Li] complexes. Bond distances are in Å.

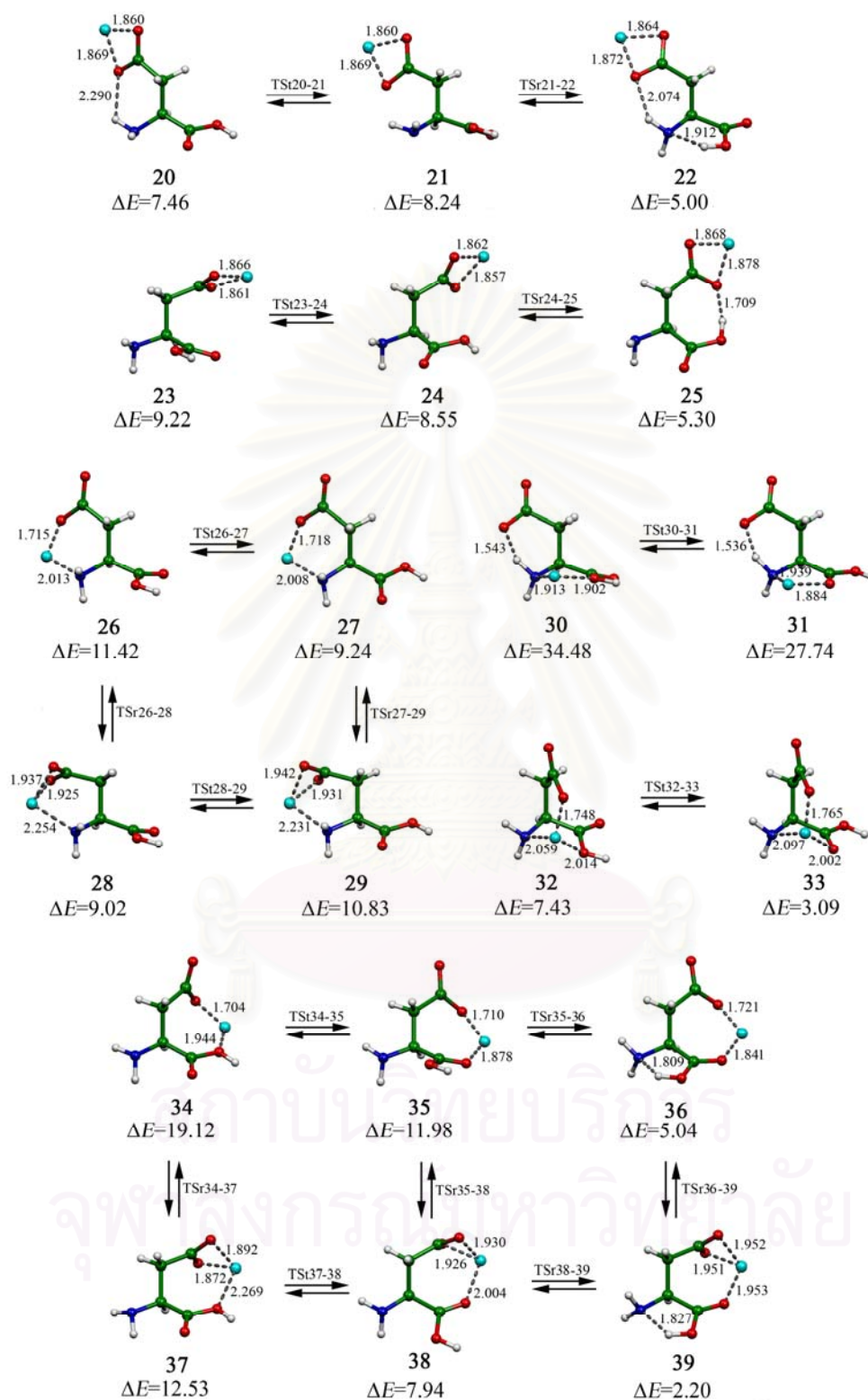


Figure A22: The B3LYP/6-311++G(d,p)-optimized structures of β -[Hasp-Li] complexes. Bond distances are in Å.

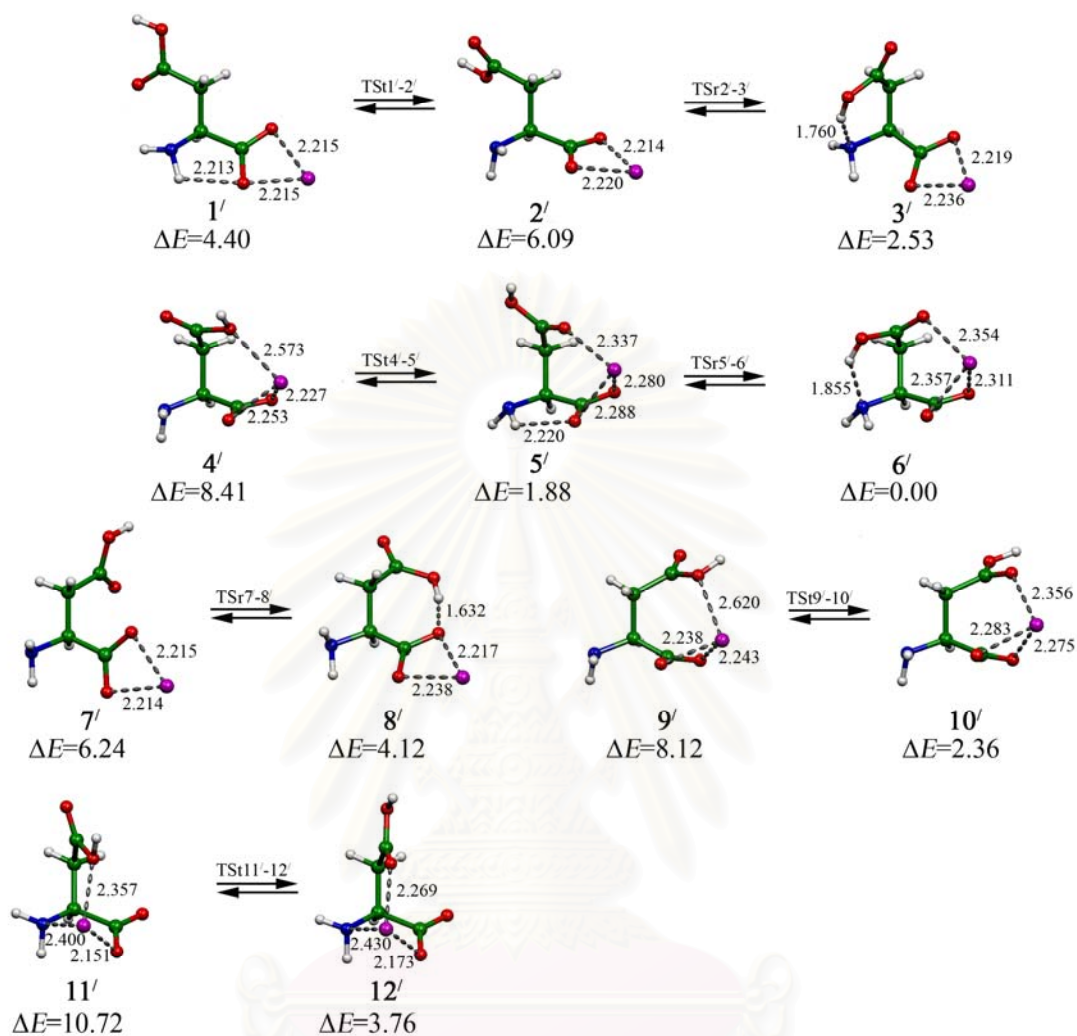


Figure A23: The B3LYP/6-311++G(d,p)-optimized structures of α -[Hasp-Na] complexes. Bond distances are in Å.

สถาบันวิทยบริการ
จุฬาลงกรณ์มหาวิทยาลัย

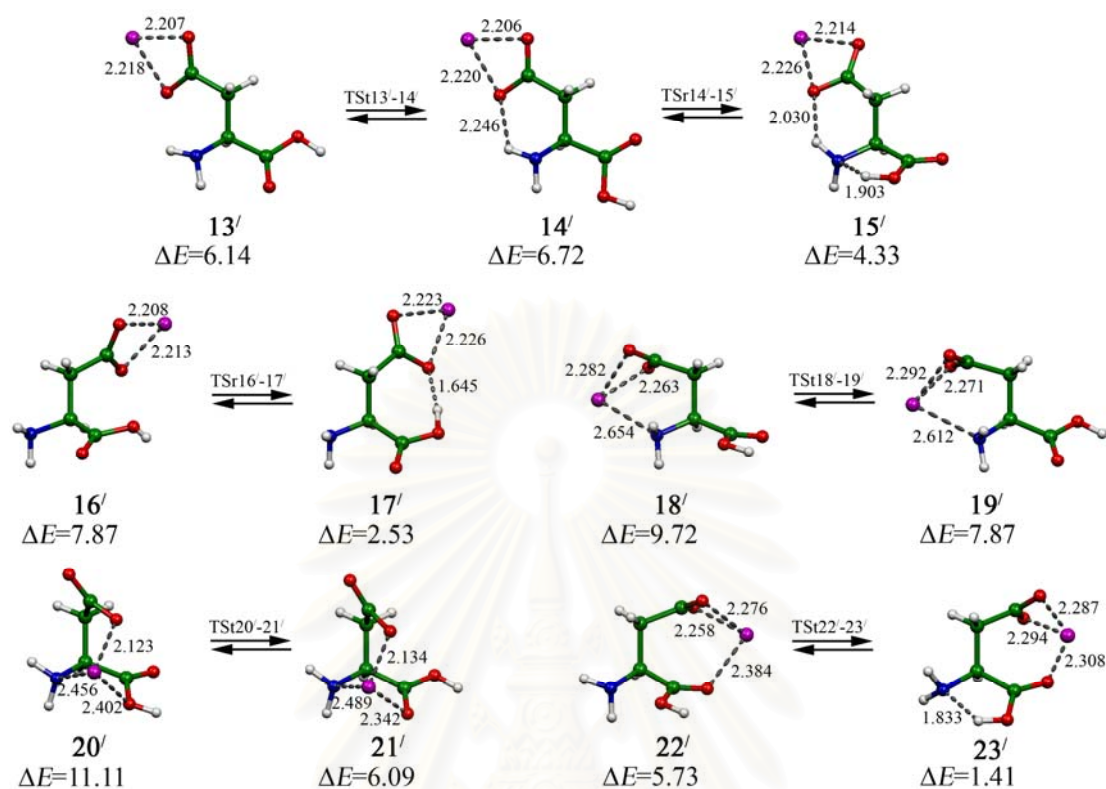


Figure A24: The B3LYP/6-311++G(d,p)-optimized structures of β -[Hasp-Na] complexes. Bond distances are in Å.

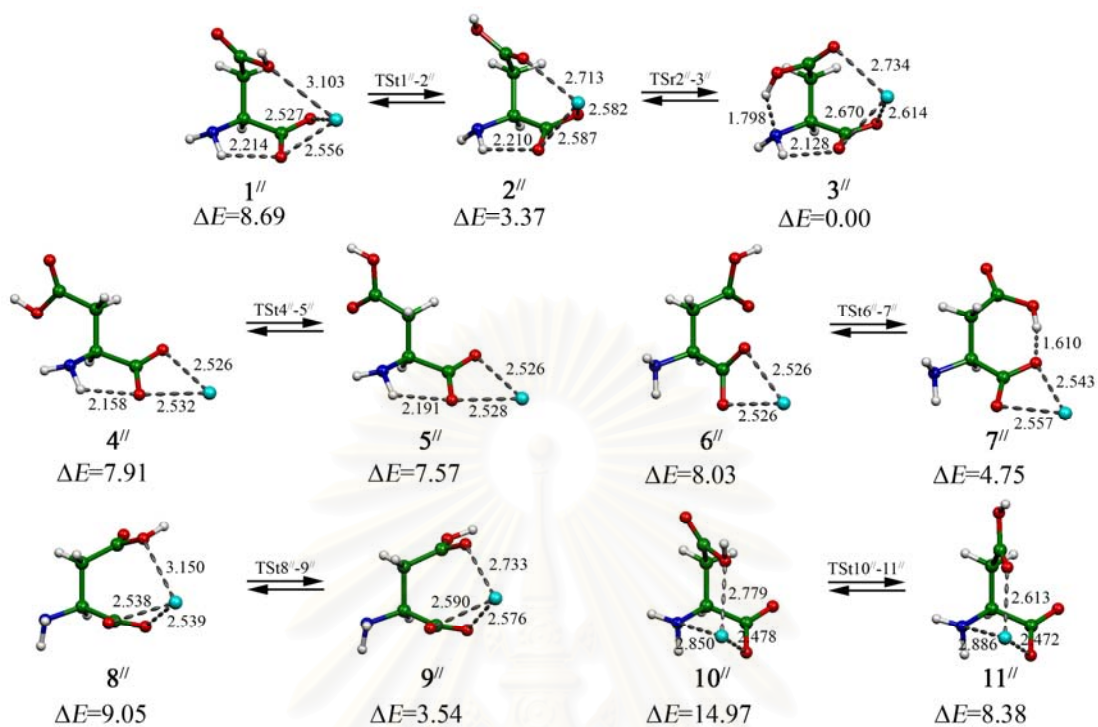


Figure A25: The B3LYP/6-311++G(d,p)-optimized structures of α -[Hasp-K] complexes. Bond distances are in Å.

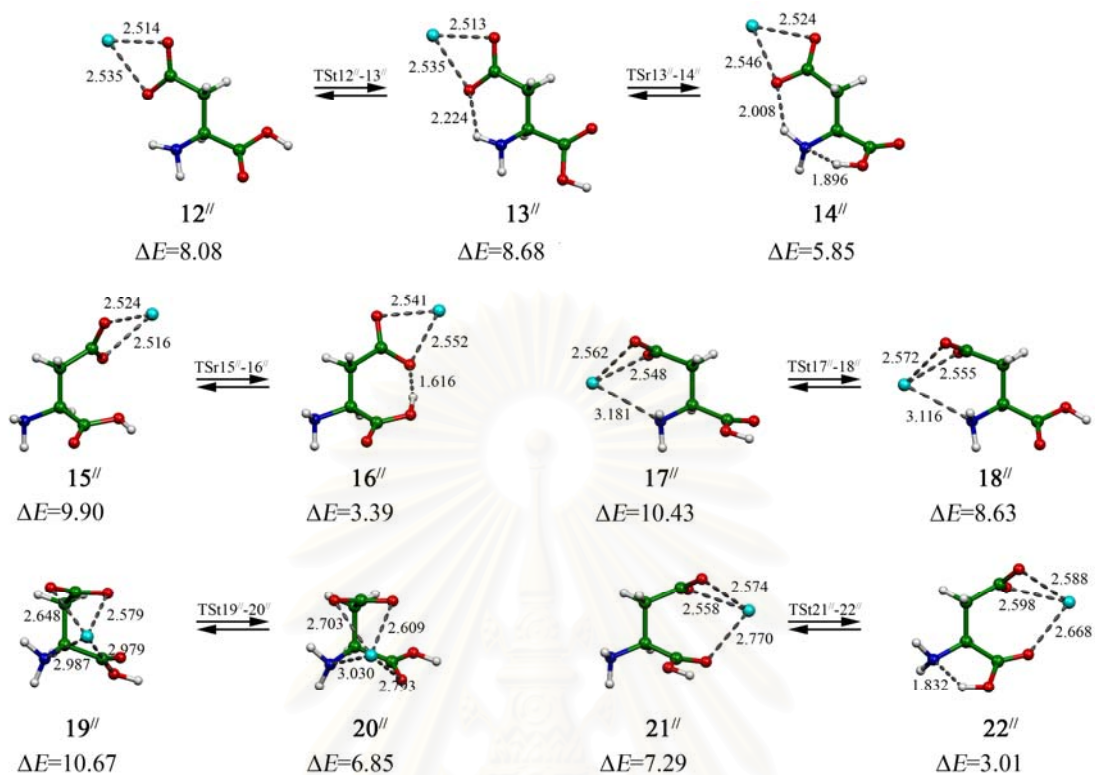


Figure A26: The B3LYP/6-311++G(d,p)-optimized structures of β -[Hasp-K] complexes. Bond distances are in Å.

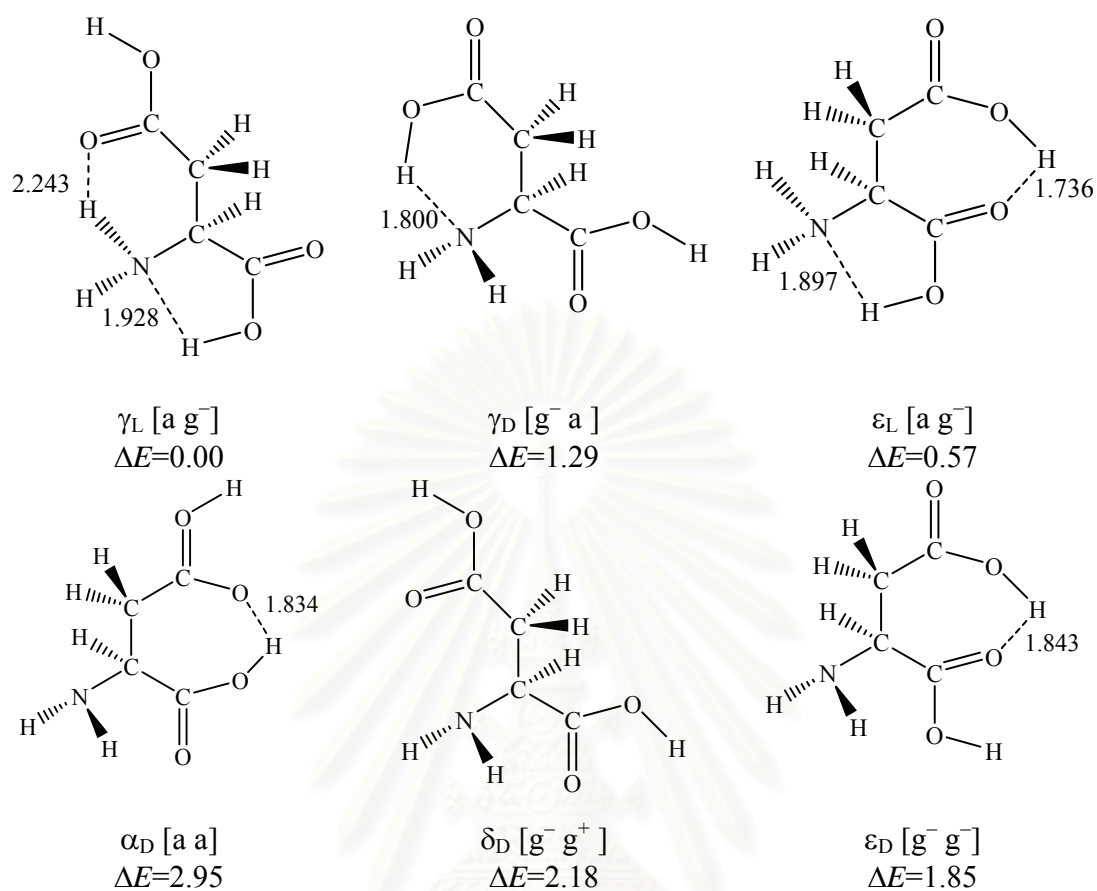


Figure A27: The B3LYP/6-311++G(d,p)-optimized structures of H₂asp ligand. Bond distances are in Å.

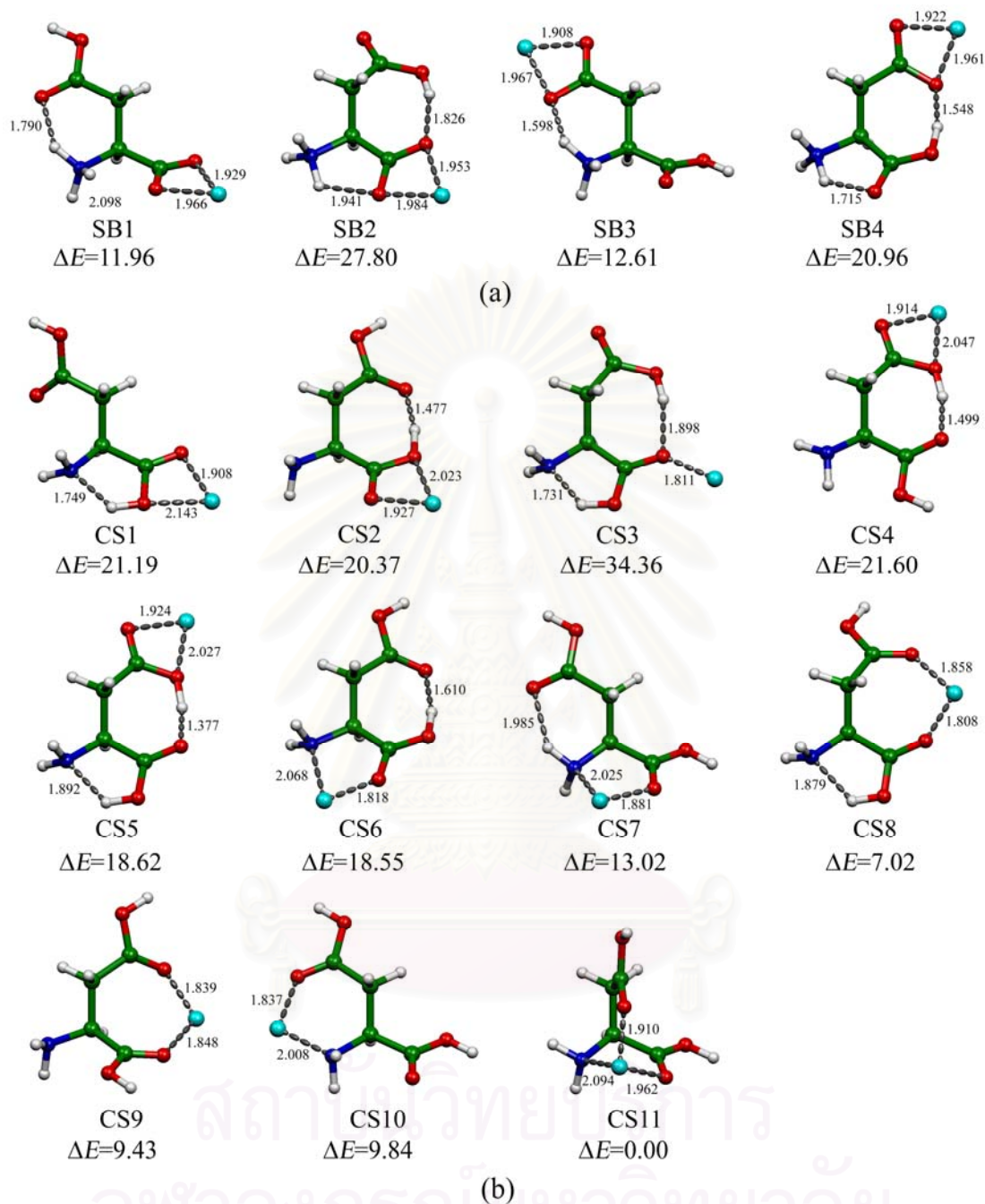


Figure A28: The B3LYP/6-311++G(d,p)-optimized structures of $[\text{H}_2\text{asp-Li}]^+$ complexes. Bond distances are in Å.

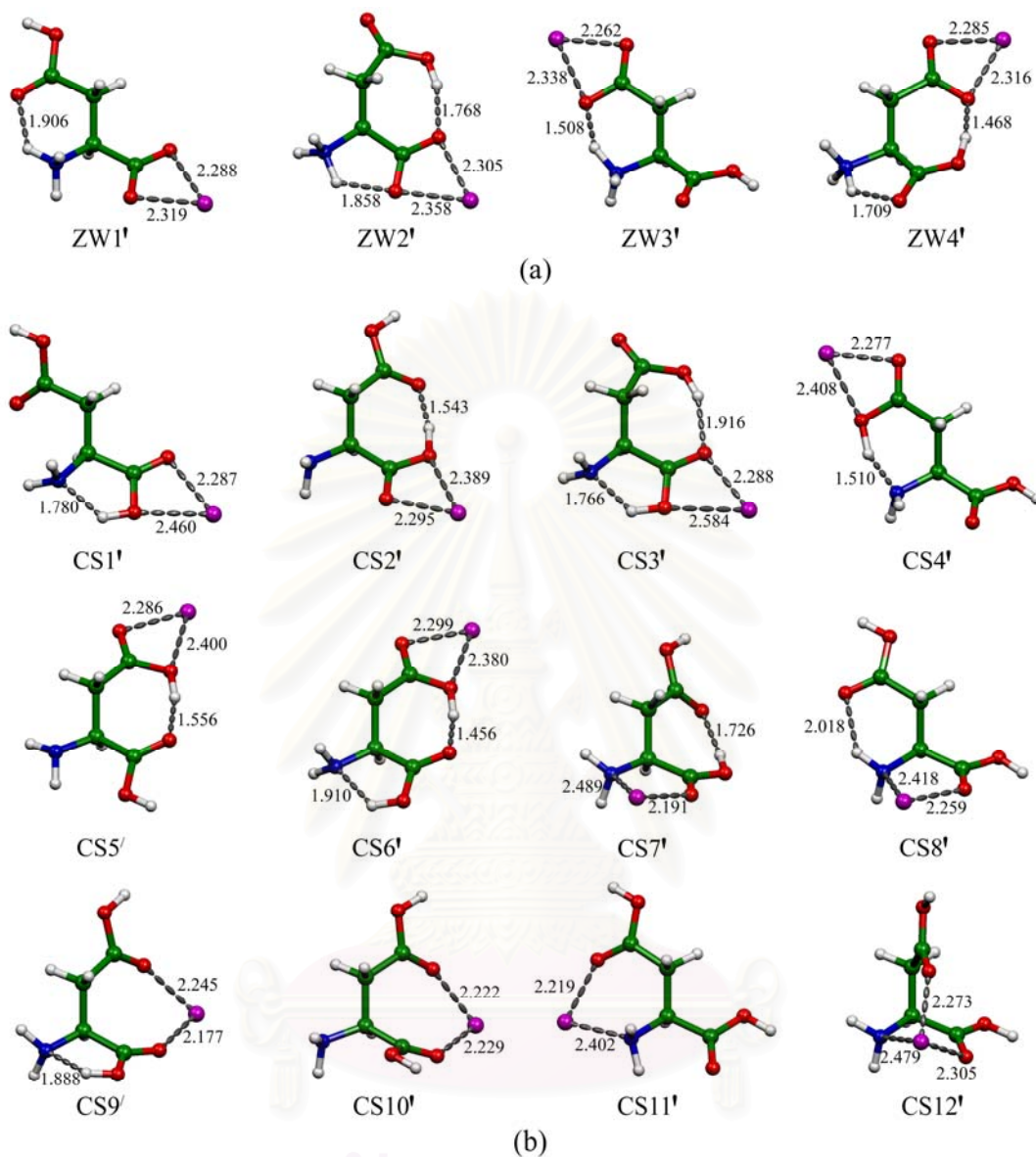


Figure A29: The B3LYP/6-311++G(d,p)-optimized structures of $[\text{H}_2\text{asp-Na}]^+$ complexes. Bond distances are in Å.

จุฬาลงกรณ์มหาวิทยาลัย

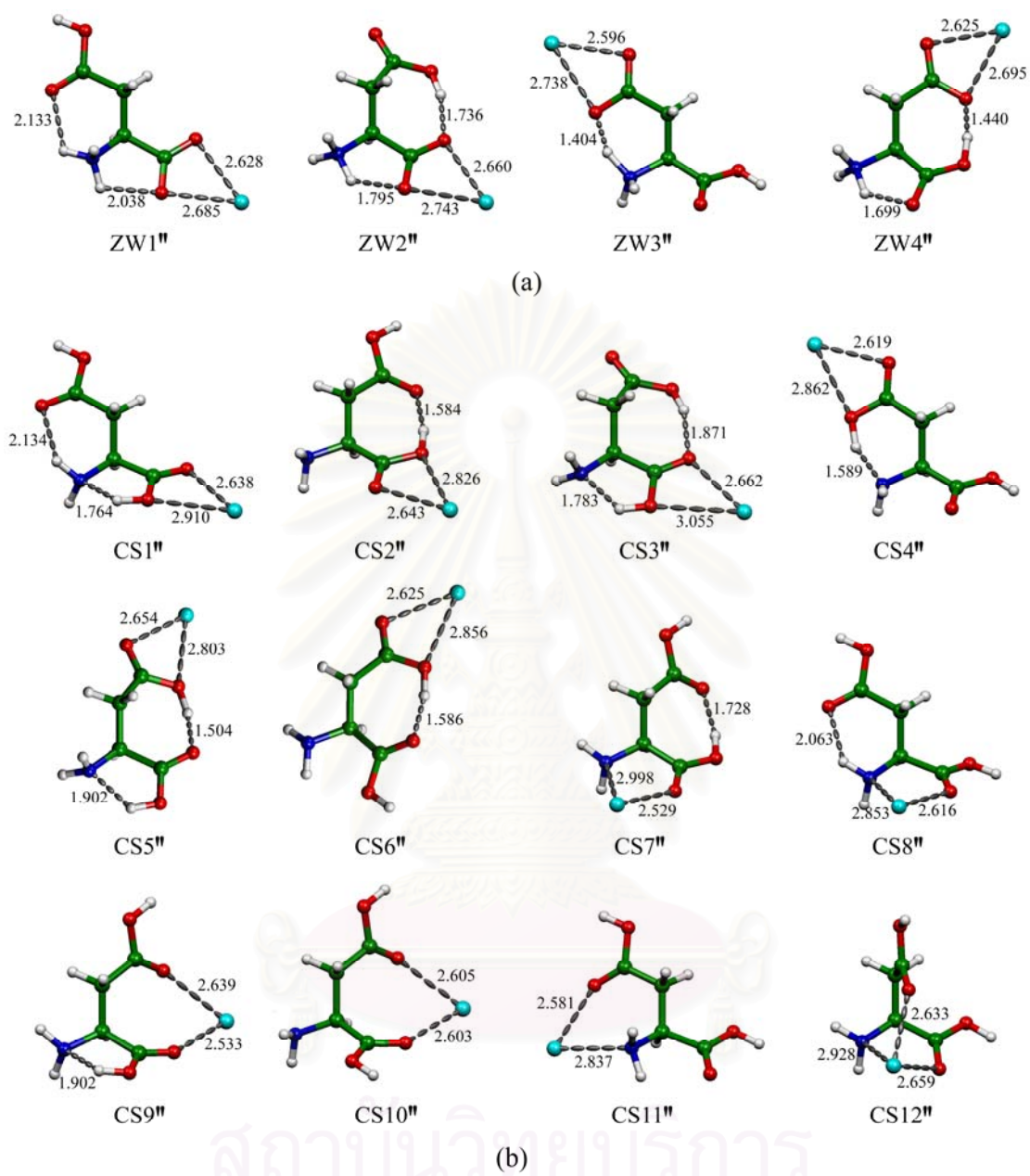
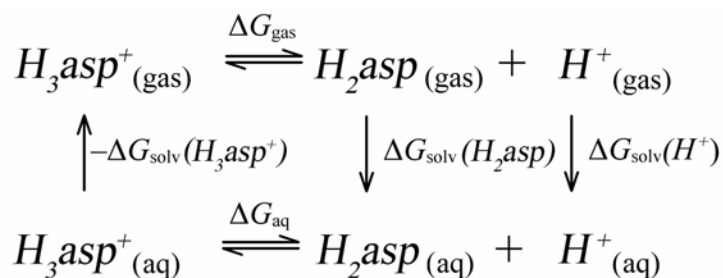
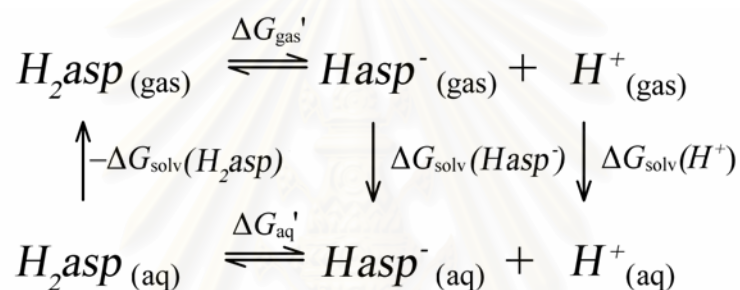


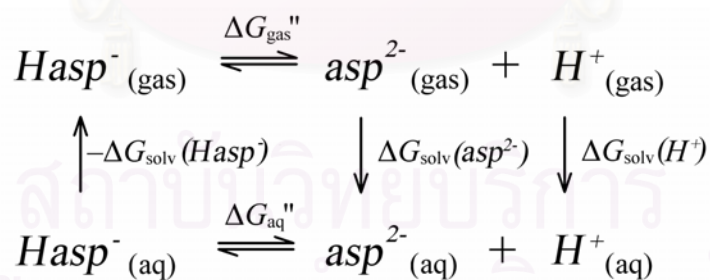
Figure A30: The B3LYP/6-311++G(d,p)-optimized structures of $[\text{H}_2\text{asp-K}]^+$ complexes. Bond distances are in Å.



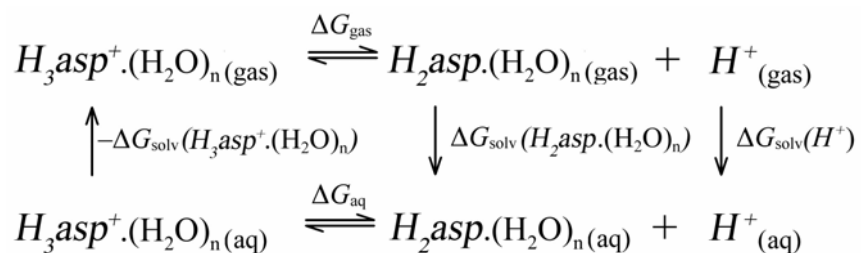
Scheme A-1. Thermodynamic cycles for calculation of the first pK_a corresponding to the deprotonation reaction of $H_3asp^+ \rightarrow H_2asp$ as bare structure.



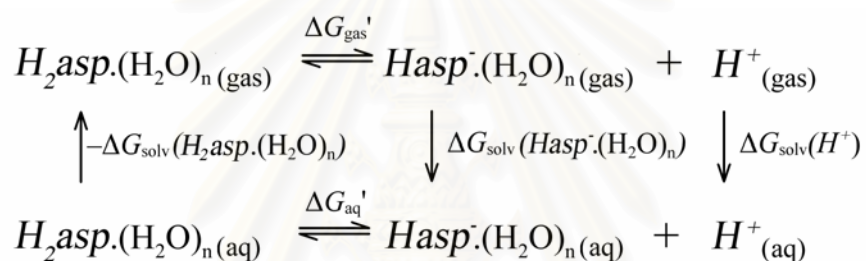
Scheme A-2. Thermodynamic cycles for calculation of the second pK_a corresponding to the deprotonation reaction of $H_2asp \rightarrow Hasp^-$ as bare structure.



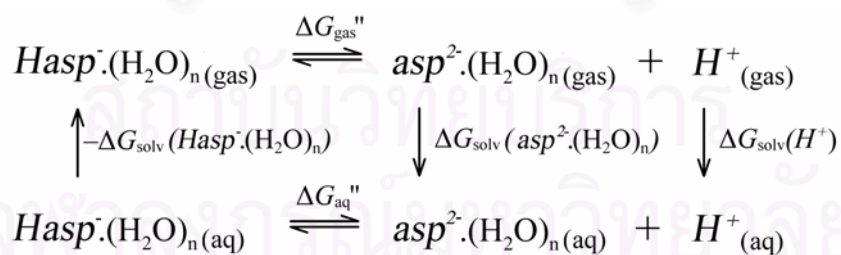
Scheme A-3. Thermodynamic cycles for calculation of the third pK_a corresponding to the deprotonation reaction of $Hasp^- \rightarrow asp^{2-}$ as bare structure.



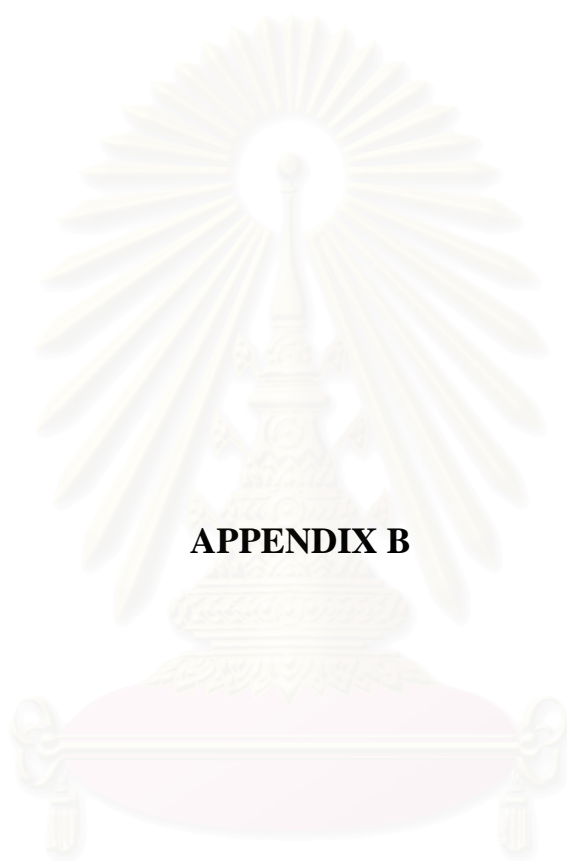
Scheme A-4. Thermodynamic cycles for calculation of the first pK_a corresponding to the deprotonation reaction of $H_3asp^+ \rightarrow H_2asp$ as n -hydrated structure.



Scheme A-5. Thermodynamic cycles for calculation of the second pK_a corresponding to the deprotonation reaction of $H_2asp \rightarrow Hasp^-$ as n -hydrated structure.



Scheme A-6. Thermodynamic cycles for calculation of the third pK_a corresponding to the deprotonation reaction of $Hasp^- \rightarrow asp^{2-}$ as n -hydrated structure.



APPENDIX B

สถาบันวิทยบริการ
จุฬาลงกรณ์มหาวิทยาลัย

Table B1 Optimized conformers of aspartic acid in H₃asp⁺-*endo*-*E* form for all stable backbone conformation computed at the B3LYP/6-31G(d) level of theory

Conformer	Optimized parameters						
	φ	ψ	χ^1	χ^2	χ^3	ω	$\Delta E(\text{kcal/mol})$
γ_D [a a] ^a	2.97	-0.34	159.02	-158.99	178.63	1.07	16.43
γ_D [g ⁻ a] ^b	24.01	-15.42	-67.08	-129.15	-176.66	3.41	16.53
γ_D [g ⁻ g ⁻] ^c	27.25	-29.94	-80.27	-70.85	178.22	-34.49	16.99
γ_D [g ⁻ g ⁺] ^c	21.35	-8.07	-50.44	33.94	-176.66	3.41	10.85
α_D [a g ⁺] ^d	119.52	0.65	166.60	20.86	-177.63	-2.03	9.55
α_D [g ⁺ a] ^d	86.18	18.17	64.26	131.91	176.27	7.41	16.27
α_D [g ⁺ g ⁻] ^c	83.25	19.11	51.99	-31.03	176.26	7.36	9.75
β_L [g ⁻ g ⁺] ^e	164.47	-127.29	-54.14	9.88	-178.86	17.04	17.45

^a Identical to δ_D [a a] and α_L [a a]. ^b Identical to δ_D [g⁻ a] and α_L [g⁻ a]. ^c Identical to δ_D [g⁻ g⁻] and α_L [g⁻ g⁻]. ^d Identical to δ_L [g⁺ a] and γ_L [g⁺ a]. ^e Identical to γ_L [g⁺ g⁺] and δ_L [g⁺ g⁺].

Table B2 Optimized conformers of aspartic acid in H₃asp⁺-*endo*-*Z* form for all stable backbone conformation computed at the B3LYP/6-31G(d) level of theory

Conformer	Optimized parameters						
	φ	ψ	χ^1	χ^2	χ^3	ω	$\Delta E(\text{kcal/mol})$
γ_D [a g ⁻] ^a	19.93	-12.31	150.77	-20.03	177.61	177.30	9.65
γ_D [g ⁻ a] ^b	26.96	-15.09	-62.81	-145.70	178.11	177.23	6.58
γ_D [g ⁻ g ⁺] ^c	27.92	-16.88	-50.95	26.53	-176.70	176.72	0.00
δ_D [a a] ^d	138.52	-9.51	167.57	141.50	177.61	177.32	12.25
ϵ_D [g ⁺ a] ^e	60.24	166.13	65.09	150.43	-178.60	-177.75	10.34
ϵ_D [g ⁺ g ⁻] ^f	64.94	164.28	54.33	-24.83	177.41	-177.73	3.05
ϵ_D [a g ⁻] ^g	44.84	150.33	154.72	-21.51	178.54	-176.68	13.40
ϵ_D [g ⁻ g ⁺] ^h	41.12	149.06	-53.97	23.78	-177.88	-177.92	2.54
ϵ_D [g ⁻ a] ⁱ	42.91	152.13	-63.49	-155.98	179.13	-177.17	9.95
ϵ_L [a a] ^j	-72.93	153.12	168.10	148.72	-178.64	-177.10	16.13
α_D [a g ⁺] ^k	79.57	36.05	-165.99	43.33	-176.15	-174.98	9.65
α_D [g ⁺ a] ^k	83.72	14.49	63.87	136.94	-177.43	-177.73	6.82
α_D [g ⁺ g ⁻] ^l	80.96	13.06	51.94	-30.06	176.66	-178.08	0.00

^a Identical to δ_D [a g⁻] and α_L [a g⁻]. ^b Identical to δ_D [g⁻ a] and α_L [g⁻ a]. ^c Identical to δ_D [g⁻ g⁺], the most stable form of H₃asp⁺. ^d Identical to α_L [a a]. ^e Identical to ϵ_L [g⁺ a] and β_L [g⁺ a]. ^f Identical to β_L [g⁺ g⁻] and ϵ_L [g⁺ g⁻]. ^g Identical to ϵ_L [a g⁻]. ^h Identical to β_L [g⁻ g⁺] and ϵ_L [g⁻ g⁺]. ⁱ Identical to β_L [a a]. ^j Identical to δ_L [a a]. ^k Identical to δ_L [g⁺ a] and γ_L [g⁺ a]. ^l Identical to δ_L [g⁺ g⁻] and γ_L [g⁺ g⁻], the most stable form of H₃asp⁺.

Table B3 Optimized conformers of aspartic acid in H₃asp⁺-*exo*-*E* form for all stable backbone conformation computed at the B3LYP/6-31G(d) level of theory

Conformer	Optimized parameters						$\Delta E(\text{kcal/mol})$
	φ	ψ	χ^1	χ^2	χ^3	ω	
$\gamma_D [\text{g}^- \text{g}^+]^a$	20.00	-4.02	-47.03	29.43	3.68	9.25	7.27
$\varepsilon_D [\text{g}^- \text{g}^+]$	43.02	-128.70	-53.95	10.72	0.69	-3.58	9.24
$\alpha_D [\text{g}^+ \text{a}]^b$	59.00	34.67	-33.70	140.69	5.06	8.34	7.27
$\gamma_D [\text{g}^+ \text{g}^-]^c$	81.64	22.12	51.83	-26.50	2.35	3.87	7.44
$\varepsilon_D [\text{a g}^+]^d$	-120.68	3.59	166.81	14.97	-2.33	9.84	18.27

^a Identical to $\delta_D [\text{g}^- \text{g}^+]$ and $\alpha_L [\text{g}^- \text{g}^+]$. ^b Identical to $\delta_L [\text{g}^- \text{a}]$ and $\gamma_L [\text{g}^- \text{a}]$. ^c Identical to $\delta_L [\text{g}^+ \text{g}^-]$ and $\gamma_L [\text{g}^+ \text{g}^-]$. ^d Identical to $\gamma_L [\text{a g}^+]$.

Table B4 Optimized conformers of aspartic acid in H₃asp⁺-*exo*-*Z* form for all stable backbone conformation computed at the B3LYP/6-31G(d) level of theory

Conformer	Optimized parameters						$\Delta E(\text{kcal/mol})$
	φ	ψ	χ^1	χ^2	χ^3	ω	
$\gamma_D [\text{a g}^-]^a$	20.50	-13.05	146.66	-19.49	2.98	-178.05	18.16
$\gamma_D [\text{g}^- \text{g}^+]^b$	29.44	-19.30	-52.13	25.46	3.69	178.28	7.27
$\delta_D [\text{g}^+ \text{g}^-]$	-159.82	-12.12	51.69	-28.28	-3.46	-178.62	7.44
$\varepsilon_D [\text{a g}^-]^c$	45.57	150.25	148.23	-24.62	-6.02	-176.26	18.16
$\varepsilon_D [\text{g}^- \text{g}^+]^d$	39.89	149.35	-54.31	26.65	5.98	-178.33	24.24
$\beta_L [\text{g}^+ \text{g}^-]^e$	-173.41	162.62	54.13	-24.05	-3.62	-177.65	9.97
$\alpha_D [\text{g}^- \text{a}]^f$	54.91	34.67	-33.70	140.69	-5.09	-178.26	32.37
$\alpha_D [\text{g}^+ \text{g}^-]^g$	80.45	22.12	51.82	-26.50	6.89	-178.57	17.72

^a Identical to $\delta_D [\text{a g}^-]$ and $\varepsilon_D [\text{a g}^-]$. ^b Identical to $\delta_D [\text{g}^- \text{g}^+]$ and $\alpha_L [\text{g}^- \text{g}^+]$. ^c Identical to $\beta_L [\text{a g}^-]$ and $\varepsilon_L [\text{a g}^-]$. ^d Identical to $\beta_L [\text{g}^- \text{g}^+]$ and $\varepsilon_L [\text{g}^- \text{g}^+]$. ^e Identical to $\varepsilon_L [\text{g}^+ \text{g}^-]$. ^f Identical to $\delta_L [\text{g}^- \text{a}]$ and $\gamma_L [\text{g}^- \text{a}]$. ^g Identical to $\gamma_L [\text{g}^+ \text{g}^-]$.

Table B5 Optimized conformers of aspartic acid in H₂asp-*endo* form for all stable backbone conformation computed at the B3LYP/6-31G(d) level of theory

Conformer	Optimized parameters					$\Delta E(\text{kcal/mol})$
	φ	ψ	χ^1	χ^2	χ^3	
$\varepsilon_D [\text{g}^+ \text{g}^-]$	33.81	149.84	80.09	-40.46	179.71	0.66
$\alpha_D [\text{g}^+ \text{g}^-]$	115.95	5.40	64.95	-89.23	179.15	17.72
$\delta_D [\text{g}^+ \text{g}^-]$	128.80	-8.71	75.46	-6.27	179.48	13.47
$\varepsilon_L [\text{g}^- \text{g}^+]$	-50.78	167.60	-53.17	76.60	179.48	0.26

Table B6 Optimized conformers of aspartic acid in H₂asp-*exo* form for all stable backbone conformation computed at the B3LYP/6-31G(d) level of theory

Conformer	Optimized parameters					$\Delta E(\text{kcal/mol})$
	φ	ψ	χ^1	χ^2	χ^3	
$\epsilon_D [g^+ a]$	78.19	-165.00	57.60	-136.90	7.64	89.29
$\epsilon_D [g^+ g^-]$	33.96	149.12	79.25	-9.13	-2.07	4.67
$\epsilon_D [a g^-]$	54.79	174.48	135.55	-108.10	-7.62	9.35
$\epsilon_D [g^- g^+]$	3.27	170.30	-77.09	111.62	11.56	12.17
$\delta_D [g^+ g^-]^a$	128.95	-9.57	61.49	-4.86	-2.31	16.70
$\gamma_L [g^+ g^-]$	-0.10	5.15	66.52	-84.32	4.97	22.09
$\alpha_L [a g^-]^b$	-71.08	-19.73	144.52	-105.19	-8.35	0.00

^a Identical to $\alpha_L [g^+ g^-]$. ^b The most stable form of H₂asp.

Table B7 Optimized conformers of aspartic acid in Hasp⁻ form for all stable backbone conformation computed at the B3LYP/6-31G(d) level of theory

Conformer	Optimized parameters				$\Delta E(\text{kcal/mol})$
	φ	ψ	χ^1	χ^2	
$\alpha_D [g^+ a]^a$	85.88	32.23	49.40	135.30	3.26
$\delta_D [a g^-]$	157.67	-23.35	128.43	-49.75	3.07
$\epsilon_D [g^+ g^+]^b$	49.57	-168.87	33.90	24.53	15.14
$\epsilon_D [g^+ a]$	62.60	-170.82	43.36	162.08	10.78
$\epsilon_D [g^- g^+]$	14.86	168.32	-35.69	21.30	10.40
$\gamma_L [g^+ g^+]^c$	-51.39	58.53	37.37	9.19	6.64
$\gamma_L [g^- g^+]$	-11.67	21.36	-17.52	33.47	17.17
$\epsilon_L [g^+ a]^d$	-42.27	-134.08	49.61	134.99	0.00
$\epsilon_L [g^+ g^-]$	-50.95	-167.48	56.36	-54.84	13.20

^a Identical to $\gamma_L [g^+ a]$. ^b Identical to $\beta_L [g^+ g^-]$. ^c Identical to $\delta_L [g^+ g^+]$. ^d The most stable form of Hasp⁻, identical to $\beta_L [g^+ g^-]$.

Table B8 Optimized conformers of aspartic acid in asp²⁻ form for all stable backbone conformation computed at the B3LYP/6-31G(d) level of theory

Conformer	Optimized parameters				$\Delta E(\text{kcal/mol})$
	φ	ψ	χ^1	χ^2	
$\gamma_D [g^+ a]^a$	43.85	-32.57	65.94	175.46	3.50
$\alpha_L [g^- g^+]^b$	-98.65	-6.80	-44.81	19.96	5.10
$\beta_L [g^+ a]^c,d$	-145.52	-151.20	55.81	123.71	0.00

^a Identical to $\gamma_D [g^+ g^-]$, $\epsilon_D [g^+ a]$ and $\epsilon_D [g^+ g^-]$. ^b Identical to $\alpha_L [g^- a]$, $\epsilon_L [g^- g^+]$ and $\epsilon_L [g^- a]$. ^c Identical to $\beta_L [g^+ g^-]$, $\delta_L [g^+ a]$ and $\delta_L [g^+ g^-]$. ^d The most stable form of asp²⁻.

Table B9 Fitted linear equations of acid dissociation constants, pK_{a1} , pK_{a2} and pK_{a3} of aspartic acid and their correlation coefficients based on different solvent effect models against the experimental data

Structure model	CPCM ^a		IEFPCM ^a	
	Equation	r^2	Equation	r^2
Model I^b				
Bare structure of free form	$y=0.8280x-0.0165$ ($y=1.2435x-1.3611$)	0.9972 (0.9205)	$y=0.8295x+0.0002$ ($y=1.2397x-1.3012$)	0.9970 (0.9190)
Model II^c				
Bare structure of tri-hydrated form	$y=0.5876x+1.3971$ ($y=0.5003x+2.4112$)	0.9890 (0.9992)	$y=0.5667x+1.6926$ ($y=0.4778x+2.7539$)	0.9784 (0.9987)
Bare structure of tetra-hydrated form	$y=0.5317x+1.7616$ ($y=0.4457x+2.7892$)	0.9936 (0.9995)	$y=0.5392x+1.7309$ ($y=0.4511x+2.7747$)	0.9931 (0.9996)
Bare structure of penta-hydrated form	$y=0.3366x+3.1986$ ($y=0.2951x+3.7535$)	0.9876 (0.9780)	$y=0.3391x+3.1967$ ($y=0.2971x+3.7559$)	0.9875 (0.9780)
Bare structure of hexa-hydrated form	$y=0.3358x+3.1589$ ($y=0.2924x+3.7221$)	0.9794 (0.9703)	$y=0.3390x+3.1523$ ($y=0.2947x+3.7211$)	0.9790 (0.9698)
Model III^d				
Tri-hydrated structure	$y=0.8025x+4.3376$ ($y=1.0091x+2.6183$)	0.5834 (0.5567)	$y=0.7791x+4.4069$ ($y=0.9990x+2.6516$)	0.5748 (0.5560)
Tetra-hydrated structure	$y=0.5540x+5.6246$ ($y=0.7610x+3.6442$)	0.8840 (0.8819)	$y=0.5410x+5.6639$ ($y=0.7463x+3.6945$)	0.8790 (0.8788)
Penta-hydrated structure	$y=1.8214x-2.6692$ ($y=1.9558x-3.8694$)	0.9676 (0.9425)	$y=1.8104x-2.6285$ ($y=1.9428x-3.8135$)	0.9670 (0.9422)
Hexa-hydrated structure	$y=1.5741x-0.2849$ ($y=1.8040x-2.0663$)	0.9195 (0.8820)	$y=1.5636x-0.2495$ ($y=1.7916x-2.0230$)	0.9204 (0.8835)

^a The PCMs with UAKS and UAHF (in parenthesis) cavity models. ^b No water molecule is associated. ^c Based on single-point calculation of bare structures of n -hydrated forms. ^d Based on single-point calculation of n -hydrated structures.

VITA

Name: Mr. Wichien SANG-AROON.

Date of Birth: February 27, 1979.

Birth place: Burirum, Thailand.

Educations:

2002-2008: Ph.D (chemistry), Chulalongkorn University, Thailand.

1998-2002: B.Sc (chemistry), Mahasarakham University, Thailand.

Award:

2002-2007: Royal Golden Jubilee (RGJ-Ph.D) grant no. PHD46K0087
from the Thailand Research Fund.

Publications:

1. **W. Sang–aroon**, V. Ruangpornvisuti, *Conformational analysis of alkali metal complexes of zwitterionic species of aspartic acid, their reaction and deprotonation: A DFT investigation*, J. Phys. Org. Chem, Revised.
2. **W. Sang–aroon**, V. Ruangpornvisuti, *Determination of aqueous-dissociation constant of aspartic acid using PCM/DFT method*, Int. J. Quant. Chem, **2008**, 108, 1181–1188.
3. **W. Sang–aroon**, V. Ruangpornvisuti, *Conformational analysis of alkali metal complexes of anionic species of aspartic acid, their interconversion and deprotonation: A DFT investigation*, J. Mol. Graph. Model, **2007**, 26, 982–990.
4. **W. Sang–aroon**, V. Ruangpornvisuti, *Conformational analysis of alkali metal complexes of aspartate dianion and their interactions in gas phase*, J. Mol. Graph. Model, **2007**, 26, 342-351.
5. **W. Sang–aroon**, V. Ruangpornvisuti, *Conformational study of cationic, zwitterionic, anionic species of aspartic acid, water-added forms and their protonation. A DFT method*, J. Mol. Struct (Theochem) **2006**, 758, 181-187.
6. B. Wannoo, **W. Sang–aroon**, T. Tuntulani, B. Polpoka and V. Ruangpornvisuti, *Conformational and energetical structures of sulfonylcalix[4]arene, p-tert-butylsulfonylcalix[4]arene and their zinc complexes*, J. Mol. Struct (Theochem) **2003**, 629, 137-150.